REVISTA PORTUGUESA DE QUÍMICA

REVISTA PORTUGUESA DE QUÍMICA

Os artigos publicados são da exclusiva responsabilidade dos seus autores.

índice
de
autores

índice
por
assuntos

REVISTA PORTUGUESA DE
QUĪMICA

Os artigos publicados são de exclusiva responsabilidade dos seus autores.

índice

A. M. LOBO*

S. PRABHAKAR

Centro de Química Estrutural,

Complexo I,

I.S.T., 1096 Lisboa Codex

and Department of Chemistry,

F.C.T., U.N.L., Lisboa

A. M. BENITO-RODRIGUEZ

Faculdade de Farmácia,

Av. das Forças Armadas,

Lisboa

THE ALKALOIDS OF THE PORTUGUESE ERGOT *

The alkaloid content of portuguese ergot collected in Trás-os-Montes were determined by t.l.c. and u.v. spectroscopy. Ergotoxine complex was found to predominate and for the first time the presence of N—[N—(D—lysergyl)—L—valyl]—cyclo (L—phenyl—alanyl—D—propyl) was detected in the crude extract.

1 — INTRODUCTION

The ergot alkaloids are the metabolic products of various species of a parasitic fungus *Claviceps* (Clavicipitales) which frequently contaminate rye. The interest in this class of compounds continues unabated due to the many pharmacological properties, such as induction of uterin contraction, adrenolytic and vaso-constrictor action and central nervous effects, that these alkaloids possess [1].

Chemically all ergot alkaloids can be formally derived from ergoline (I).
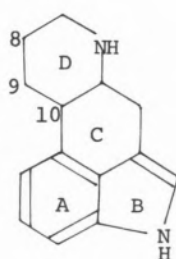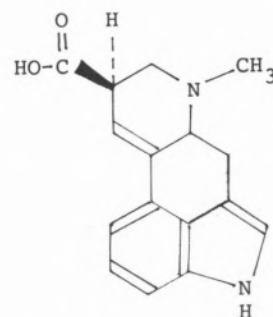
I: Ergoline   II:(+)—Lysergic acid

Among the most important ergot alkaloids are the peptide derivatives of lysergic acid (II), which are listed in Table 1, and all are characterized by the presence of a modified tripeptide containing proline and an α—hydroxy—α—amino acid which has undergone cyclol formation.

Other simpler alkaloids co-occur with the peptide ergot alkaloids and these are listed in Table 2 [2].

2 — DISCUSSION OF RESULTS

The examination of the alkaloid content of Portuguese ergot, collected in Trás-os-Montes, was carried out using thin layer chromatography (t.l.c.) and compared against authentic samples of the alkaloids (Table 3). The solvent system that gave the best separation for the peptide alkaloids was chloroform: ethanol (95:5) on a silica gel GF_{254} support. T.l.c. analysis of the total extract showed the presence of the ergotoxine complex (ergocornine, ergokriptine and ergocristine), ergotamine, ergobasine, ergosine, N—[N—(D—lysergyl)—L—valyl]—cy-

Table 1
Peptide ergot alkaloids [a)]

R₁ R₂ \ R₃	$CH_2C_6H_5$	$C{<}^{H_3}_{H}{\,}^{CH_3}$	$CH_2{-}CH{<}^{CH_3}_{CH_3}$	$CH_2\,CH_2CH{<}^{CH_3}_{CH_3}$	$CH{<}^{CH_3}_{CH_2{-}CH_3}$
H H	ergotamine	[ergovaline][b)]	ergosine	ergohexine[c)]	—
CH₃ CH₃	ergocristine	ergocornine	α-ergokriptine	ergoheptine[c)]	β-ergokriptine
H CH₃	ergostine	—	—	—	—

a) See reference [2]

b) Synthetic; not yet found in natural sources.

c) Recently isolated by S. OHMOMO and M. ABE, *Nippon Nogei Kagaku,* **50,** 543 (1976) [CA:**86,**190 303].

clo (L—phenyl—alanyl—D—prolyl), and varying amounts of their respective C—8 epimers.

The total extract was also analysed by paper chromatography and identical results were obtained (Table 4).

Quantitative analysis of the alkaloids present in the total extract, and in the ergot, was carried out by ultraviolet spectroscopy, after separating the alkaloids by preparative layer chromatography (see Experimental) (Table 5). It is of interest to note that Portuguese ergot is particularly rich in the ergotoxine complex, the second most abundant alkaloid being ergotamine. It also contains ergobasine, and traces of ergosine and N—[N—(D—lysergyl)—L—valyl]—cyclo (L—phenyl—alanyl—D—prolyl). The presence of the last alkaloid, isolated for the first time from wild Czech ergot [3], is of biogenetic interest since it could be a possible precursor of ergocristine [2].

The relatively high percentage of the peptide alkaloids isomeric at C-8, and known to be devoid of any useful pharmaceutical interest deserves comment. It is well known that epimerisation at C-8, a particularly facile reaction, catalysed by either acids or bases, proceeds, according to the mechanism proposed by Woodward, *via* an·achiral intermediate (Scheme 1) [4].

Either due to an aging process occurring during storage or extraction, the C-8 epimers of all ergot alkaloids were detected in varying amounts in the extracts analysed, and their concentrations found to increase with the time of contact with bases.

The isolation of the individual alkaloids in pure state could be carried out in a small scale using preparative thin layer chromatography, and. when coupled with ultraviolet analysis gave the best results. However, for larger scale this method proved cumbersome and it was decided to use

Table 2

Non-peptide ergot alkaloids [a]
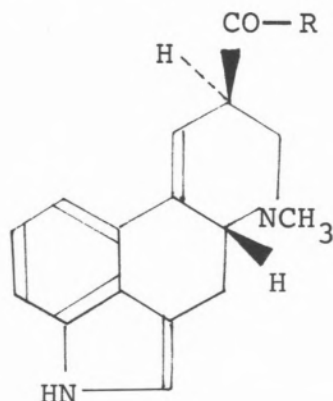
Name	R
Ergobasine (ergonovine, ergometrine)	NH—C(CH₃)(H)—CH₂OH $\mathrm{NH-\underset{\underset{CH_2OH}{|}}{\overset{\overset{CH_3}{|}}{C}}-H}$
Lysergic acid α-hydroxyethylamide	$\mathrm{NH-\underset{}{\overset{\overset{CH_3}{|}}{CH}}-OH}$
Lysergic acid amide (ergine)	NH_2
Lysergic acid	OH
$\Delta^{8,9}$-Lysergic acid (paspalic acid)	OH

a) See reference [2].

column chromatography for a preliminary separation of the various groups of alkaloids. On these alkaloid enriched fractions, several precipitating agents were then tried (Table 6). By far the best results were obtained using phosphoric acid which gave a reasonably pure crystalline phosphate of ergotoxine in 30% yield. (+)—Tartaric acid also proved an effective precipitating agent for the ergotamine-ergotaminine pair, which could thus be separated from other alkaloids (enriched fraction) in a state of high purity.

3 — EXPERIMENTAL

U.v. spectra were recorded on a Perkin-Elmer 124 instrument. Thin layer chromatography was carried

Table 3

Alkaloids	R_f [a]
Ergobasine	0.02
Ergobasinine	0.06
Ergotamine	0.13
Ergotaminine	0.42
Ergosine	0.13
Ergosinine	0.41
Ergostine	0.22
Ergostinine	0.57
N-[N-(D-lysergyl)--L-valyl]-cyclo(L-phenylalanyl-D-prolyl)	0.29
Isomer in C-8	0.55
Ergocristine	0.35
Ergocristinine	0.58
Ergokriptine	0.36
Ergokriptinine	0.58
Ergocornine	0.36
Ergocorninine	0.58

a) System used CHCl₃:EtOH (95:5) support: SiO₂ gel GF₂₅₄.

Table 4

Alkaloids	R_f [a]	
	Paper [b] Schuell-2043 A	Paper [c] Schuell-2045 A
Ergocornine	0.72	0.67
Ergokriptine	0.53	0.57
Ergocristine	0.34	0.26
Ergokriptinine	0.21	—
Ergocristinine	0.09	—
Ergostine [d]	0.65	0.57
Ergotamine	0.69	0.61
Ergosine	0.79	0.73
Ergobasine	0.75	0.71
N-[N-(D-lysergyl)--L-valyl]-cyclo(L--phenylalanyl-D-prolyl)	0.71	0.63
Lysergic acid [d]	0.52	—

a) Stationary phase: 10% dimethyl phthalate in chloroform.
   Mobile phase: 20% formamide, 80% of a citrate buffer 0.065M, saturated with a solution of dimethyl phthalate and acidified with hydrochloric acid 4N to pH 3.2.
b) Elution time 3h30'.
c) Elution time 5h30'.
d) Alkaloids not detected in the total extract.

ALKALOIDS	Total Extract (%)	Ergot (%)
C-8 isomers of Ergotoxine	2.20	0.014
Ergotoxine	4.65	0.029
Ergotamine	2.60	0.016
Ergobasine	1.91	0.012
Ergobasinine	0.89	0.005
Ergosine	traces	traces
N-[N-(D-lysergyl)-L-valyl]-cyclo(L-phenylalanyl--D-prolyl)	traces	traces

extracted with chloroform (5×100 ml), the chloroform extracts were dried (Mg SO$_4$), and the solvent was evaporated under reduced pressure yielding a yellow-brown residue, which was dried (24 hr) under high vacuum (over P$_2$O$_5$). The composition of the alkaloid residue was done using t.l.c. on alumina or silica gel GF$_{254}$ and several solvent systems.

3.2 — T.L.C. SYSTEMS FOR ANALYSIS OF THE ERGOT EXTRACT

The following systems were used to determine the composition of the alkaloid content of the ergot extract:

II   achiral intermediate
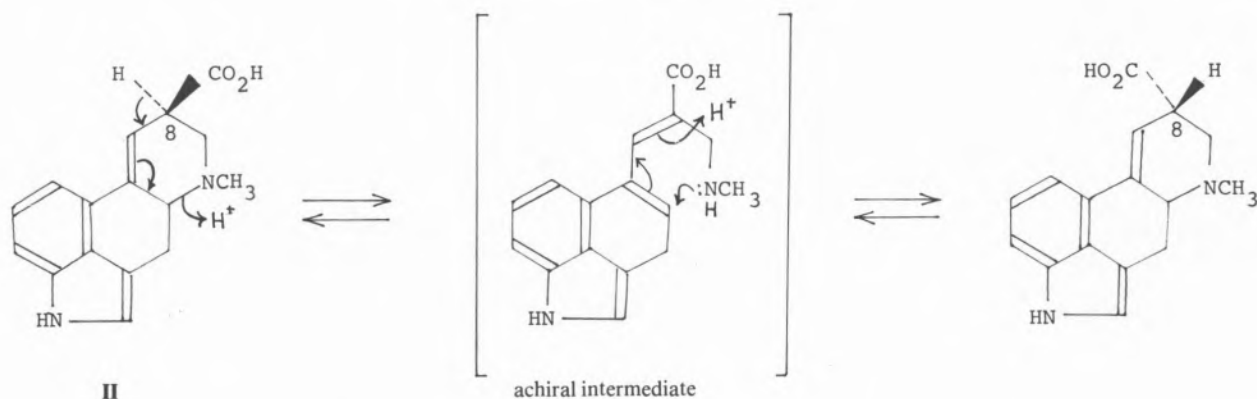
Scheme 1

out on silica gel GF$_{254}$ (Merck) plates, 0.30 mm thick. For preparative work these were 0.5 mm thick. Column chromatography was carried out on alumina, grade II (BDH).

The visualization of the alkaloids on the t.l.c. plates was carried out by direct irradiation of the plates with an ultraviolet lamp at 254 and 366 nm, or by spraying the plates with Van Urk's [5a], Salkowski's [6] or Dragendorff's [5b] reagent.

The anhydride of (—)-di—O—p—toluyltartaric acid and this acid were synthesized by the method of STOLL and HOFMANN [7].

3.1 — ALKALOID EXTRACTION

The ergot (1 Kg), powdered in a Starmix for 5 minutes, was macerated during 24 hours at room temperature, with a solution of citric acid (100 g) in aqueous methanol (1:1, 4 1).

The extract was filtered through Celite, the filtrate basified with aqueous sodium bicarbonate to pH 8. The basic solution in portions (of 500 ml each) was

a) Al$_2$O$_3$; CHCl$_3$:
b) Al$_2$O$_3$; CHCl$_3$; MeOH (95:5)
c) Al$_2$O$_3$; CHCl$_3$: EtOH (95:1)
d) Al$_2$O$_3$; CHCl$_3$: petroleum ether (40:60)
e) Al$_2$O$_3$; CHCl$_3$: petroleum ether (10:90)
f) SiO$_2$; CHCl$_3$: MeOH (95:5)
g) SiO$_2$; CHCl$_3$: EtOH (95:5)
h) SiO$_2$; CHCl$_3$: EtOH (95:1)
i) SiO$_2$; CHCl$_3$: EtOH (95:0.5)
j) SiO$_2$; C$_6$H$_6$: CHCl$_3$:EtOH (28.5:57:14.5)
l) SiO$_2$; C$_6$H$_6$: CHCl$_3$:EtOH (28.5:57:10)
m) SiO$_2$; C$_6$H$_6$: CHCl$_3$:EtOH (15:75:10)
n) SiO$_2$; C$_6$H$_6$: DMF (86.5:13.5)
o) SiO$_2$; diisopropyl ether: THF: toluene: diethylamine (70:15:15:0.1).

The system that gave best separation of the alkaloids was g).

3.3 — COLUMN CHROMATOGRAPHY OF THE CRUDE EXTRACT

A column (3 cm of internal diameter and 35 cm

Table 6

FRACTION COMPOSITION[a]	PRECIPITATING AGENT	YIELD OF ALKALOID SALT [b]	OBSERVATION
Total alkaloid extract	(—)-di-*p*-totuyltartaric acid	33%	precipitation but no separation of the individual alkaloids
Rich in ergotoxine	»	—	viscous oil obtained
Total alkaloid extract	picric acid	—	no crystalline precipitate
Rich in ergotoxine	»	—	»
Rich in ergotoxine	phosphoric acid	30%	crystalline precipitate showing appreciable purification
Rich in ergotoxine and ergotamine	»	—	no purification
Rich in ergotoxine	(+)-tartaric acid	55%	precipitation but no purification from C-8 isomers
Rich in ergotamine and ergotaminine	»	50%	purification of the extract but coprecipitation of ergotamine and ergotaminine tartrates
Rich in ergotoxine	sulphuric acid	—	No crystalline precipitate
Rich in ergotoxine	methyl iodide	—	»

a) As analysed by t.l.c.
b) For details see the experimental section.

high) was filled with a slurry of alumina (198 g) in chloroform. The alkaloid extract (2.5 g) absorbed on alumina (2 g) was deposited on the top. The column was then eluted with chloroform-methanol (100:0.1), and the polarity of the eluant being progressively increased. The last fraction to be eluted involved the use of chloroform-methanol (100:2). Each fraction was analysed by t.l.c. and fractions with identical composition (t.l.c. control) were pooled together, the solvents evaporated under reduced pressure and dried under vacuum over P_2O_5.

The composition of the fractions obtained by order of elution was:

ergotoxine and C-8 epimers (810 mg);
ergotoxine and traces of C-8 epimers (40 mg);

ergotoxine and traces of ergotamine (50 mg);
ergotamine and traces of ergobasine (160 mg);
ergobasine and traces of ergotamine (70 mg).

Other ergot alkaloids were also present but only in trace quantities.

3.4 — ULTRAVIOLET ANALYSIS OF THE TOTAL ALKALOID EXTRACT

The total alkaloid extract (50 mg) from powdered ergot (8 g) was applied to a preparative silica gel layer chromatoplate (0.5 mm thick) and eluted with chloroform: methanol (95:5). The bands corresponding to the alkaloids, after identification against standard samples, were immediately removed, diluted with methanol and their ultraviolet spectra

taken [at 312 nm (ε 8500), a band present in them all]. The concentration of individual alkaloids in the extract was then obtained applying the Beer-Lambert law.

3.5 — ALKALOID PRECIPITATION

3.5.1 — OF AN ENRICHED EXTRACT IN ERGOTOXINE (adapted from [8])

An alkaloid extract (100 mg) enriched in ergotoxine was dissolved in methanol (0.25 ml) and diethyl ether (3 ml) added. After leaving it for 24 hr at 0-5°C, the mixture was filtered and to the filtrate a solution of (+)-tartaric acid (25 mg in 0.15 ml of ethanol and 0.3 ml of ether) was added. This solution was allowed to stand for 24 hr at 0-5°C, the precipitate was collected by filtration, washed with ether, redissolved in ethanol (0.4 ml) and treated with phosphoric acid (24 mg) in ethanol (0.2 ml). The white crystals of the phosphate that separated were collected by filtration, washed with cold ethanol and diethyl ether, and dried (P_2O_5), (yield 30%).

3.5.2 — OF AN ENRICHED EXTRACT IN ERGOTAMINE (adapted from [8])

An alkaloid extract (100 mg) enriched in ergotamine and its C-8 epimer, ergotaminine, was dissolved in ethanol (0.25 ml) and diluted with diethyl ether (3 ml). After 24 hr at 0-5°C, the solution was filtered and to the filtrate (+)-tartaric acid (25 mg) in a mixture of ethanol (0.15 ml) and diethyl ether (0.3 ml) was added. The precipitate that separated (yield 50%) was collected, dried and shown by t.l.c. to be a mixture of tartrates of ergotamine and ergotaminine.

REFERENCES

[1] A. STOLL, A. HOFMANN, «The Alkaloids», vol. VIII, R. F. F. Manske (ed.), Academic Press, London, 1968, p. 725.
[2] H. G. FLOSS, *Tetrahedron, 32*, 873 (1976).
[3] A. CERNY, A. KRAJICEK, J. SPACIL, M. BERAN, B. KAKAC, M. SEMONSKY, *Coll. Czech. Chem. Comm., 41*, 3415 (1976).
[4] V. W. ARMSTRONG, S. COULTON, R. RAMAGE, *Tetrahedron Letters*, 4311 (1976).
[5] a) E. STAHL, «Thin Layer Chromatography», Verlag, Berlin, 1967, p. 869;
    b) *ibid.*, p. 873.
[6] A. F. COSTA, «Farmacognosia», 2.º vol., Fundação Calouste Gulbenkian, Lisboa, 1967, p. 610.
[7] A. STOLL, A. HOFMANN, *Helv. Chim. Acta, 26*, 925 (1943).
[8] J. PITRA, V. SAPARA, S. KORISTEK, Czech. Pat. 86,237 (1957) [CA:52, 1560 (1958)].

RESUMO

Os alcalóides do ergot português.

O conteúdo alcaloídico do ergot português recolhido em Trás-os-Montes foi analisado por c.c.f. e espectroscopia no u.v. Verificou-se o predomínio do complexo ergotoxímico e detectou-se pela primeira vez a presença de N—[N—(D—lisergil)—L—valil]—ciclo(L—fenilalanil—D—propil) no extracto cru.

A.J.F. MENDONÇA
C.A. NIETO DE CASTRO *
Centro de Química Estrutural,
Complexo I, Instituto Superior Técnico,
1096 Lisboa Codex, Portugal

M.J. ASSAEL
W.A. WAKEHAM
Department of Chemical Engineering
and Chemical Technology,
Imperial College, London SW7 2BY,
United Kingdom

THE ECONOMIC ADVANTAGES OF ACCURATE TRANSPORT PROPERTY DATA FOR HEAT TRANSFER EQUIPMENT DESIGN

The technical and economic consequences of the uncertainties in the estimation methods currently used in Chemical Engineering for transport properties of fluids to process plant design and operation are acessed.
This assignment is carried out by means of specific examples of one heat exchanger and one condenser design.
It is shown that the uncertainties in the transport coefficients which result from commonly used estimation procedures have a significant effect upon the overall technical design of heat exchange equipment. In turn these effects contribute to the necessary capital expenditures on the items of plant. It is demonstrated that such expenditure would be considerably reduced by more reliable estimation procedures based upon accurate experimental data for the transport coefficients of fluids.

1 — INTRODUCTION

We have shown in previous work that at present the transport properties of many fluids must be estimated by methods which depart considerably from the ideal and that therefore the data generated are burdened with large uncertainties [1]. We have also shown that the uncertainties in the transport coefficients which result from commonly-used estimation procedures have a significant effect upon the overall technical design of heat exchange equipment and may result in unnecessary capital expenditure [2]. Although many workers in the field of transport properties have already noted that a knowledge of these properties is significant for process plant design [3-6], there seems to have been no systematic discussion of how significant accurate values of these properties are in quantitative technical and economic terms. This paper is devoted to a study of this type in order to illustrate the need for improved estimation techniques and more accurate experimental measurements. In order to carry out this program we have chosen to study the effect of uncertainties in fluid properties upon the design of heat exchange equipment. In a preliminary paper [2], we discussed two types of heat exchanger (shell and tube and double pipe). Here, we extend our treatment to condensers. In the interests of brevity we report here only the results obtained for one heat exchanger and one condenser since those results obtained for any particular item of equipment are qualitatively similar.

2 — THE METHODOLOGY

The aim of our calculations will be to evaluate the changes in the design parameters of a heat exchanger or a condenser which arise solely from changes made in the transport coefficients of the fluids involved in the process. We then identify these changes in the transport coefficients with possible uncertainties in the values employed for a design. The degrees of freedom of a heat exchanger and condenser may be reduced to two by selecting a specific type of device and by prescribing its duty to satisfy the external constraints of a particular process. We are then left with the heat transfer area and the pressure drop across the fluid ducts. Because this last effect is not usually a major factor

in the design of a heat exchanger or condenser, we shall adopt the heat transfer area as the sole factor that reflects the changes in the design arising from the changes in the transport coefficients of the process streams. The reduction of the numbers of parameters necessary to define the design in this way has the added advantage that the economic consequences of changes in the design are readily estimated.

A second simplification is afforded by the adoption of a standard methodology for the evaluation of the heat exchange area. Since any reasonable design incorporates the physical properties of the fluid streams into correlations for the heat transfer coefficients we are free to use any one of them [3]. In accord with the aims of this paper we adopt one of the simplest.

In the case of shell and tube exchangers we employ the correlation of SIEDER and TATE [7] for the heat transfer coefficient on the inside of the heat exchanger tubes. Denoting this coefficient, referred to the inside tube area, by h_i the correlation reads

$$\frac{h_i D_i}{\lambda} = 0.027 \, Re^{0.8} Pr^{1/3} (\frac{\mu}{\mu_w})^{0.14} \tag{1}$$

where the Reynolds number, Re, is $D_i G/\mu$ and the Prandtl number, Pr, is $\mu C_p/\lambda$. Here, D_i represents the internal diameter of the tubes, λ the thermal conductivity of the fluid, μ its viscosity and C_p its heat capacity, all evaluated at the mean bulk temperature of the fluid. G represents the mass flux in the heat exchanger tubes and μ_w the fluid viscosity at the temperature of the wall.

The heat transfer coefficients on the shell side of the heat exchanger tubes, referred to the outside tube area, h_o, is given by the correlation

$$\frac{h_o D_e}{\lambda} = 0.36 \, Re^{0.55} Pr^{1/3} (\frac{\mu}{\mu_w})^{0.14} \tag{2}$$

D_e being the equivalent diameter for the shell (D.Q. Kern, 1950).

For horizontal condensers, the average heat transfer coefficients can be evaluated from the correlation [8]

$$h = 1.5 \left(\frac{4G'}{\mu_f}\right)^{-1/3} \quad \left(\frac{\mu_f^2}{\lambda_f^3 \varrho_f^2 g}\right)^{-1/3} \tag{3}$$

where the subscript f refers condensate properties evaluated at the temperature of the film formed, g is the acceleration due to gravity and G' is the condensate loading.

The overall heat transfer coefficient, U_o, referred to the outside tube area for the heat exchanger and to the total surface area required for the condenser, is then calculated from the equation

$$\frac{1}{U_o} = \frac{D_o}{h_i D_i} + \frac{1}{h_o} + R \tag{4}$$

where D_o is the outside tube diameter and R represents the combined resistance of the tube wall and any scale.

Finally, the heat transfer area, A_o, is obtained from the prescribed duty of the exchanger Q, according to the equation

$$Q = U_o A_o (\Delta T)_{lm} \tag{5}$$

where $(\Delta T)_{lm}$ is the corrected logarithmic mean temperature difference for the process streams.

Equations (1) to (5) demonstrate how the transport properties of the fluids will influence the calculated heat exchanger area and so the length of the heat exchanger. It is clear that of the fluid properties is is the thermal conductivity which is the dominant factor in the determination of the heat transfer area. It is noteworthy, that it is just this property which is the most difficult to estimate accurately [1].

SAMPLE CALCULATIONS

We consider here two examples from our calculations; first a gas-liquid heat exchanger, and secondly a horizontal condenser for a mixture of gases. The heat exchanger involves the cooling of dry ammonia gas from a compressor with water before passage to a reactor. The exchanger selected is of the baffled shell and tube type, with one shell pass and eight tube passes, and contains 364 tubes (2.44 m long, OD = ¾ inch, 16 BWG) mounted in a triangular arrangement. The condenser involves liquefaction of a five component vapour mixture of light hydro-

carbons taken from a distillation column. Again the coolant employed is water. The horizontal condenser chosen has one pass in the shell side and four tube passes and contains 774 tubes (4.88 m long, OD = ¾ inch, 16 BWG) mounted in a triangular arrangement.

For each of these exchangers the transport properties of the fluid streams have first been assigned reasonable reference values. Subsequently the reference heat transfer area for each exchanger has been evaluated. The results obtained were $(A_o)_r = 53.79$ m² for the heat exchanger and $(A_o)_r = 137.22$ m² for the condenser (condensation + subcooling). It should be emphasized that these figures constitute our arbitrary reference values for subsequent calculations, rather than any optimized design.

The next stage in our calculation involves the perturbation of the assumed values for the transport coefficients of the fluids, about their reference values by amounts corresponding to likely uncertainties in the data [1]. The changes in the calculated heat transfer area from the corresponding reference area have been determined as functions of the changes in the transport coefficients for both items of equipment. The value of R has been assumed constant throughout and equal to the equipment design requirements (R = 0.007 and R = 0.004 respectively). Furthermore, the properties of water have not been perturbed since they have been assumed to be known exactly.

RESULTS AND DISCUSSION

Fig. 1 contains plots of the deviation of the calculated heat transfer coefficients $(h)_c$ from the reference condition $(h)_r$ for the shell side of the exchanger. The change in the thermal conductivity is plotted along the abcissa whereas the change in the viscosity is shown as a parameter of the curves. Fig. 2 contains a plot of the deviations of the calculated area of the heat exchanger $(A_o)_c$ from the reference one $(A_o)_r$ as a result of variation of the heat transfer coefficient of the ammonia. These two figures together allow us to determine the variation in the design area of the heat exchanger as a result of variation in the transport properties of the ammonia. As an example of the use of these diagrams we take the situation when the viscosity of the ammonia exceeds the reference value by 10%
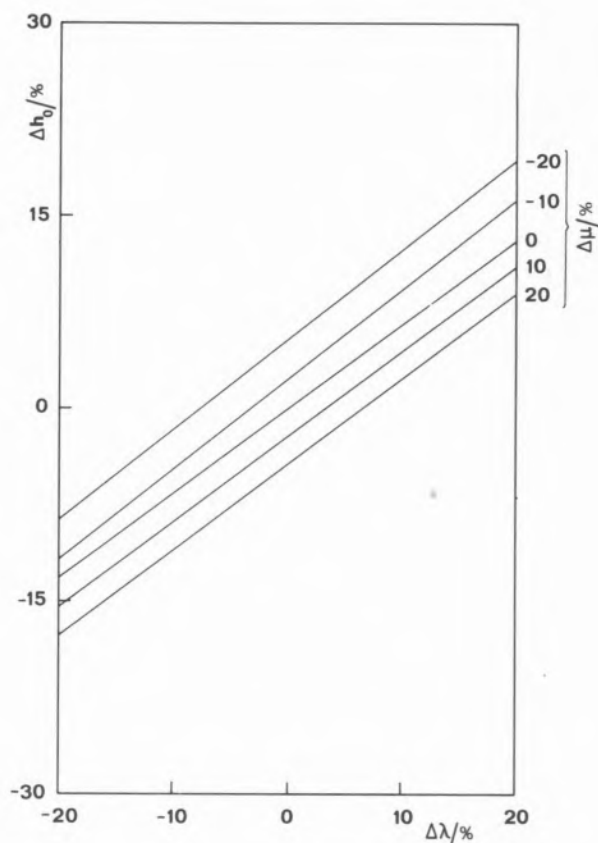
Fig. 1

The influence of the fluid transport coefficients upon the outside film heat transfer coefficient, for the heat exchanger.

$$\Delta h_o = \frac{(h_o)_c - (h_o)_r}{(h_o)_r} \times 100\%$$

$$\Delta\mu = (\frac{\mu - \mu_r}{\mu_r}) \times 100\%$$

$$\Delta\lambda = (\frac{\lambda - \lambda_r}{\lambda_r}) \times 100\%$$

The subscript r denotes reference conditions

and the thermal conductivity is 15% below its reference value. Then it follows from fig. 1 that Δh_o is about −15% and from fig. 2 that ΔA_o is +14%.

Thus as a result of these errors in the transport coefficients alone, the heat exchanger area is overestimated by some 14%. The results for the condenser are qualitatively the same with a variation in the area of −14% to +26%, as can be seen from fig. 3 and 4.
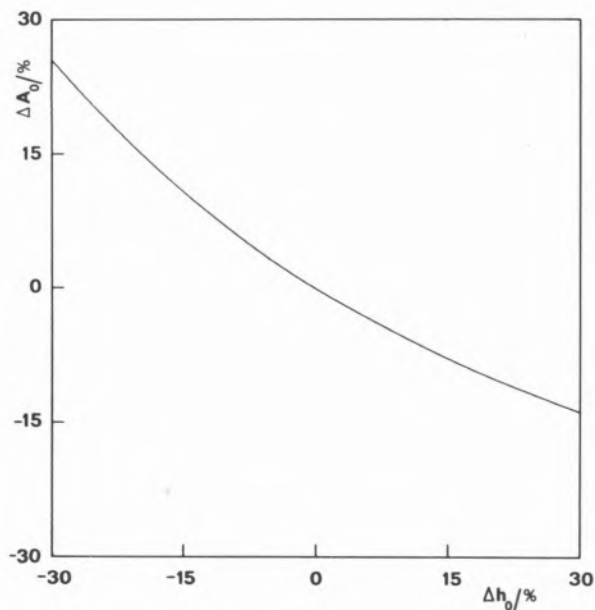
Fig. 2

The influence of the outside film heat transfer coefficient upon the heat transfer area for the heat exchanger

$$A_o = \left\{ \frac{A - (A_o)_r}{(A_o)_r} \right\} \times 100\%$$

The remainder of the legend is the same as for fig. 1

In an earlier paper [1] it was shown that for many fluids or fluid mixtures it is at present impossible to estimate their transport properties to within $\pm 20\%$. Here we have shown that because of such uncertainties alone it is possible to over- or under- estimate the heat transfer area for a heat exchanger or a condenser to fulfil a particular need by as much as 25%. Of course it must also be recognised that any methodology for heat exchanger design such as that given here has an inherent uncertainty by virtue of its empirical nature. Generally, this latter uncertainty is accommodated into a practical design by increasing the design heat transfer area by a multiplicative safety factor. The results of our calculations might therefore be interpreted as a demonstration that the safety factor should be increased to allow for the effect of uncertainty in the fluid transport properties. For example, if in the condenser we evaluate a hypothetical fouling factor R', which represents the effective additional resistance to fluid property uncertainties, we obtain values that range

from -0.003 to $+0.001$. Such values are comparable with the value of R employed in the reference design. If this argument is pursued then merely because of $\Delta\lambda$ and $\Delta\mu$ heat exchangers or condensers may be manufactured 25% larger than necessary at a typical incremental cost of some 23%. Although this increase represents a small fraction of the total capital expenditure on a particular chemical plant the total extra expenditure, taken over a series of plants and a number of years, represents a considerable extra expenditure. It must be stressed that these increased costs are in addition to, and not a part of, the costs incurred by faults in design procedures.

An alternative interpretation of the results of our calculations is, however, possible. If the uncertainties in the estimation of the transport coefficients of fluids could be reduced to a few percent from their present high values, then the over-design of heat exchange equipment could be similarly reduced. Such a reduction could be
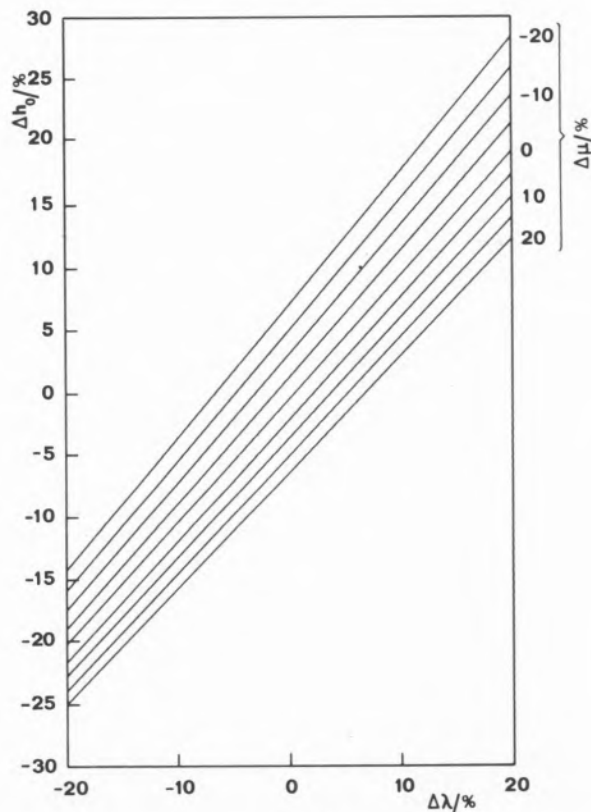
Fig. 3

The influence of the fluid mixture transport coefficients upon the outside film heat transfer coefficient, for the condenser
The legend is the same as for fig. 1
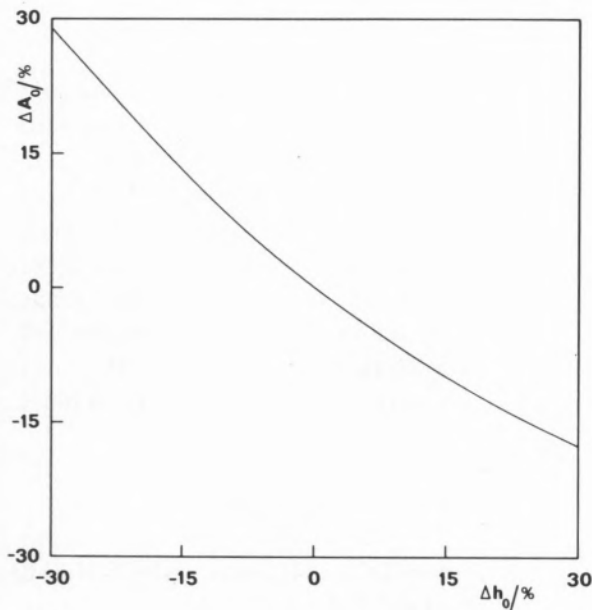
Fig. 4

*The influence of the outside film heat transfer coefficient upon the heat transfer area for the condenser
The legend is the same as for fig. 2*

achieved by a series of accurate measurements on carefully chosen systems, supported by the development of fundamental theories and subsequently estimation schemes. The incremental costs of only three items of plant equipment (about 40,000 US dollars) would provide a significant contribution to such a research effort with the corresponding savings rapidly justifying the initial expenditure.

In summary, research effort in the field of the transport properties of fluids has been shown to have a quantitatively important technical and economic role in the optimum design of at least some items of chemical process plant.

REFERENCES

[1] C. A. NIETO DE CASTRO, W. A. WAKEHAM, *Proceedings of Chempor 78,* paper 15, Braga, Portugal (1978).

[2] M. J. ASSAEL, C. A. NIETO DE CASTRO, W. A. WAKEHAM, *Proceedings of Chempor 78,* paper 16, Braga, Portugal (1978).

[3] L. B. COUSINS, D. BUTTERWORTH, Symposium on Transport Properties of Fluids and Fluid Mixtures, Glasgow, U. K. (1979).

[4] R.S.H. MAH, *Computers and Chemical Enginnering,* **1,** 183 (1977).

[5] J. M. PRAUSNITZ, *Science,* **205,** 759 (1979).

[6] C. C. WILLIAMS, M. A. ALBRIGHT, *Hydrocarbon Processing,* 115, May (1976).

[7] E. N. SIEDER, G. E. TATE, *Ind. Eng. Chem.,* **28,** 1429 (1936).

[8] D. Q. KERN, «Process Heat Transfer», McGraw Hill Book Comp., New York, 1950.

RESUMO

Analisa-se a influência que a utilização de técnicas de estimativa normalmente utilizadas em engenharia química têm no projecto e operação de unidade de transferência de calor presentes em instalações químicas correntes.

Utilizam-se como exemplos um permutador de calor e um condensador. Mostra-se que as incertezas nos coeficientes de transporte resultantes de métodos correntes de estimativa de propriedades têm um efeito significativo no projecto tecnológico global do equipamento de transferência de calor, contribuindo para um aumento de gastos de capital.

Demonstra-se ser possível reduzir estes gastos adicionais pelo desenvolvimento de métodos de estimativa mais correctos, baseados em dados experimentais das propriedades de transporte de fluídos com maior exactidão.

MARIA J. CALHORDA
ALBERTO R. DIAS*

Centro de Quimica Estrutural
Complexo I
Instituto Superior Técnico
1096 Lisboa Codex, Portugal

METAL COMPLEXES WITH DIAZINES AND 4,4' — BIPYRIDYL LIGANDS

Complexes $[M(\eta^5-C_5H_5)_2X_2]$ (M = Mo, W; X = halogen) and $[Mo(\eta^5-C_5H_5)_2HI]$ react with nitrogen donor atom ligands pyridazine, pyrimidine, pyrazine and 4,4'— bipyridyl to give new complexes which were fully characterized.

1 — INTRODUCTION

We have been interested for some time in the coordination of nitrogen donor atom ligands and nitrogen and oxygen donor atom ligands to the early transition metals. In previous articles [1] we have described the synthesis, characterization and reactivity of new complexes containing the $M(\eta^5-C_5H_5)_2$ (M = Ti,Mo,W) moiety and some of these ligands. We now report the results of related studies with ligands pyridazine (**I**, pyrd), pyrimidine (**II**, pyrm), pyrazine (**III**, pyrz) and 4,4'-bipyridyl (**IV**, 4-bipy).

2 — RESULTS AND DISCUSSION

The compounds $[M(\eta-C_5H_5)_2Br_2]$, $[M(\eta-C_5H_5)_2HI]$ and $[M(\eta-C_5H_5)_2H_3]$ $[PF_6]$ (M = Mo and, sometimes, W) reacted under various conditions with the nitrogen donor atom ligands pyridazine (**I**, pyrd), pyrimidine (**II**, pyrm), pyrazine (**III**, pyrz) and 4,4'— bipyridyl (**IV**, 4-bipy) to give the new compounds shown in fig. 1. The analytical and conductimetric evidence for the formulae proposed is given in Table 1, the ^1H nmr spectra are described in Table 2 and the ir assignments are given in Tables 3-5.

Reaction of $[Mo(\eta-C_5H_5)_2Br_2]$ with pyridazine in refluxing acetone in the presence of one equivalent of $T1[PF_6]$ gave an air stable dark brown crystalline compound. The elemental and conductimetric data (Table 1) together with the ^1H nmr spectrum (three triplets and one singlet with relative areas 1:1:2:10) (Table 2), and the infrared spectrum (showing bands characteristic of the $\eta^5-C_5H_5$ ring, $[PF_6]$ anion and bands characteristic of the ligands, some of which shifted in relation to the free ligand) (Table 3), support the formula $[Mo(\eta-C_5H_5)_2Br(pyrd)]$ $[PF_6]$ (**Ia**). The analogous tungsten complex was prepared in the same way and was characterized in a similar fashion although the results of elemental analysis were not good even after repeated recrystallisations. Compound **Ia** reacts with $[NO][PF_6]$ in acetonitrile solution to give red crystals which were identified as being the known compounds $[Mo(\eta-C_5H_5)_2Br(MeCN)]$ $[PF_6]_2$ [2] by comparison of its ir spectrum with that of an authentic sample. When the reaction of **Ia** with $[NO][PF_6]$ was repeated in dry CH_2Cl_2 a dark blue compound was obtained.
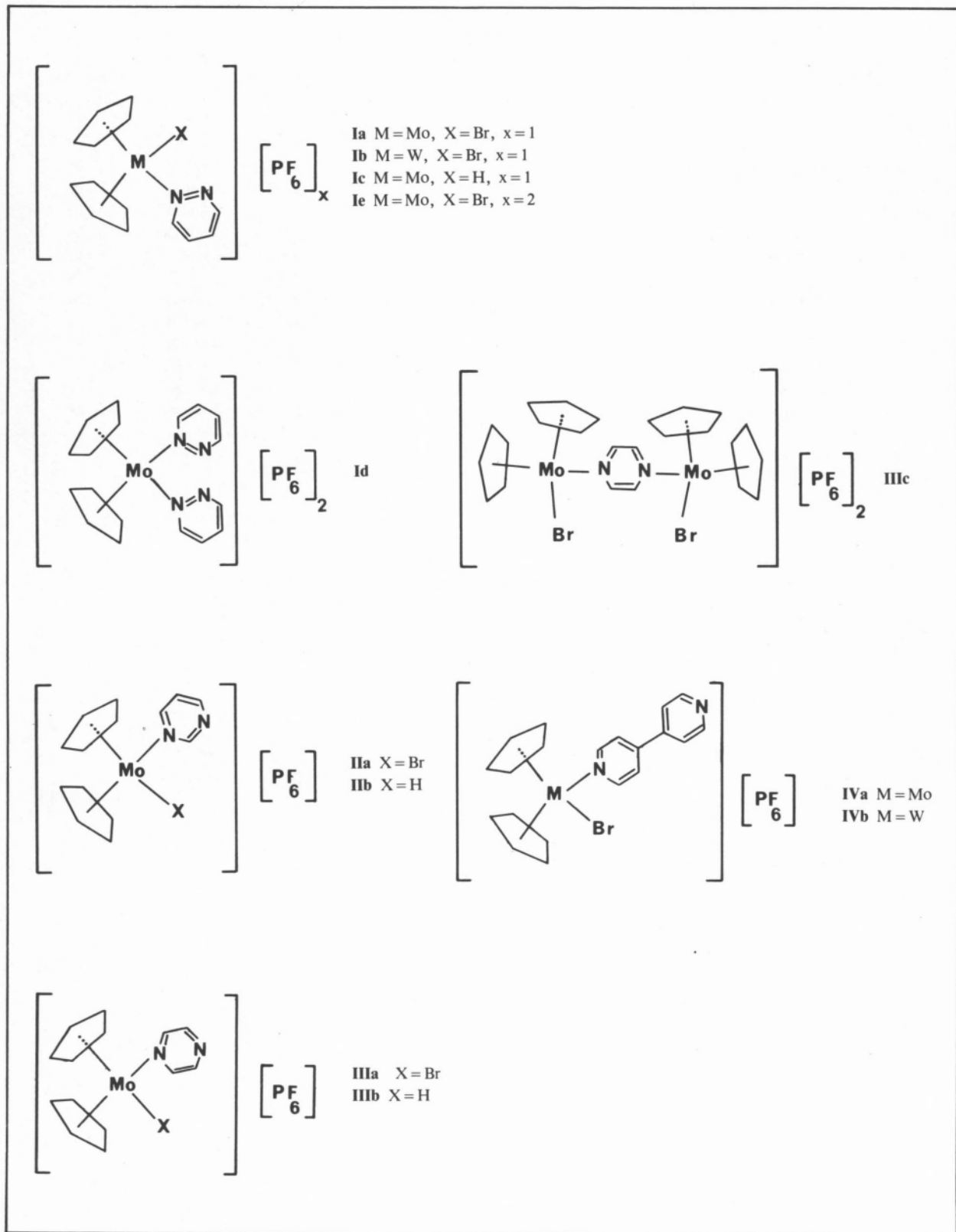
Fig. 1
Structural formulae of compounds I-IV

Table 1
Analytical and conductimetric data

COMPOUND	COLOUR	DEC/°C	ANALYSIS found (req)			MOLAR CONDUCTIVITY[a]
			C	H	N	
Ia $[Mo(\eta\text{-}C_5H_5)_2Br(pyrd)][PF_6]$	brown	—	32.2(31.7)	2.7(2.7)	5.6(5.3)	91
Ib $[W(\eta\text{-}C_5H_5)_2Br(pyrd)][PF_6]$	red	180	28.3(27.2)	2.6(2.3)	4.8(4.3)	100
Ic $[Mo(\eta\text{-}C_5H_5)_2H(pyrd)][PF_6]$	red	140	37.15(37.2)	3.5(3.3)	6.1(6.2)	106
Id $[Mo(\eta\text{-}C_5H_5)_2(pyrd)_2][PF_6]_2$	red	180	32.6(32.0)	2.9(2.7)	7.8(8.3)	206
Ie $[Mo(\eta\text{-}C_5H_5)_2Br(pyrd)][PF_6]_2$	dark blue	—	25.9(24.9)	2.4(2.1)	4.35(4.1)	440[b]
IIa $[Mo(\eta\text{-}C_5H_5)_2Br(pyrm)][PF_6]$	green	190	31.8(31.7)	2.6(2.7)	5.4(5.3)	76
IIb $[Mo(\eta\text{-}C_5H_5)_2H(pyrm)][PF_6]$	orange	140	37.2(37.2)	3.7(3.3)	5.4(6.2)	84
IIIa $[Mo(\eta\text{-}C_5H_5)_2Br(pyrz)][PF_6]$	green	230	31.7(31.7)	2.8(2.7)	5.6(5.3)	80
IIIb $[Mo(\eta\text{-}C_5H_5)_2H(pyrz)][PF_6]$	purplish-pink	130	37.0(37.2)	3.4(3.3)	4.7(6.2)	95
IIIc $[Mo(\text{-}C_5H_5)_2Br_2(pyrz)][PF_6]_2$	light-green	210	30.2(29.35)	2.6(2.5)	2.3(2.85)	—
IVa $[Mo(\eta\text{-}C_5H_5)_2Br(4\text{-}bipy)][PF_6]$	dark green	200	39.5(39.6)	3.2(3.0)	4.5(4.6)	—
IVb $[W(\eta\text{-}C_5H_5)_2Br(4\text{-}bipy)][PF_6]$	dark brown	190	34.2(34.6)	2.8(2.6)	3.4(4.0)	88

a) $\Lambda_M/ohm^{-1} cm^2 mol.^{-1}$ in CH_3NO_2; b) in CH_3CN.

Table 2
^1H nmr Data $^{a)}$

Compound	τ(multiplicity $^{b)}$, relative intensity)					
4 5 / 3 ⟨ ⟩ 6 / N=N	3	4	5	6	$\eta^5\text{-}C_5H_5$	H⁻
	0.72(T,2)$^{c)}$	2.30(T,2)				
Ia	−0.47(T,1)	1.96(T,2)		0.92(T,1)	3.99(S,10)	
Ib	−0.34(br,1)	1.89(br,2)		0.84(br,1)	4.04(S,10)	
Ic	0.25(C,1)	2.20(C,2)		0.98(C,1)	4.63(S,10)	19.00(S,1)
Id	0.72(C,4)$^{c)}$	1.97(C,4)			3.57(S,10)	
5 / 6 ⟨ ⟩ 4 / N ⟍ N / 2	2	4	5	6	$\eta^5\text{-}C_5H_5$	H⁻
	0.79(S,1)	1.17(D,2)^c	2.47(T,1)			
IIa	0.41(C,2)^C	0.94(D,2)	2.28(T,1)		3.86(S,10)	
IIb	0.53(S,1)	1.12(D,2)	2.51(T,1)	0.84(D,1)	4.49(S,10)	19.04(S,1)
6 5 / N ⟨ ⟩ N / 2 3	2	3	5	6	$\eta^5\text{-}C_5H_5$	
	1.35(S)^d					
IIIa	0.81(D,2)	1.24(D,2)			3.88(S,10)	
IIIb	1.12(D,2)	1.40(D,2)			4.49(S,10)	19.17(S,1)
IIIc	1.20(S)^{d,e}				4.21(S)	
3 2 2' 3' / N⟨ ⟩—⟨ ⟩N	3	3'	2,2'		$\eta^5\text{-}C_5H_5$	
	1.21(D,2)		2,20(C,4)			
IVa	0.68(D,2)	1.12(D,2)	2.13(C,4)		3.91(S,10)	
IVb	0.37(br,2)	1.12(br,2)	2.07(br,4)		3.95(S,10)	
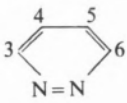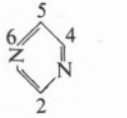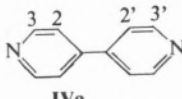
a) solvente acetone-d^6 except where stated otherwise, internal reference TMS; b) S singlet, D doublet, T triplet, C complex; br broad;
c) includes proton 6; d) includes all the ligand protons; e) solvent DMSO-d_6.

Table 3
Frequencies of some of the vibrational modes of pyridazine and its complexes *

Vibrational mode	Description [4]	Pyridazine [PF$_6$]	[MoCp$_2$Br(pyrd)] [PF$_6$]	[WCp$_2$Br(pyrd)] [PF$_6$]	[MoCp$_2$H(pyrd)] [PF$_6$]	[MoCp$_2$(pyrd)$_2$] [PF$_6$]$_2$
8a	Ring	1575	1590	1590	1580 (shoulder)	1590
8b	Ring	1565	1575	1575	1570	1575
19a	Ring	1445	1450	1450	1450	1450
19b	Ring	1415	1425	1425	1425	1425
14	Ring	1285	—	—	—	—
9a		1160	1155	1155	—	—
15	Bending CH	1065	1065	1065	1065	1065
1	Ring	965	960	955	975	960,975
10a	Deformation CH	775	775	775	780	770
6a	Ring	620	640	645	640	640
6b	Ring	665	675	675	675	675
16b	Ring	375	395	—	400	395

* Cp = η^5—C$_5$H$_5$

Although its complete characterization was not satisfactory due to its decomposition in solution, the data available support the formulation [Mo(η-C$_5$H$_5$)$_2$Br(pyrd)] [PF$_6$]$_2$ (Ie).

Refluxing Ia in acetone for 25 hrs in the presence of excess pyridazine and thalium hexafluorophosphate yielded a red crystalline compound. Its ir spectrum is very similar to that of complex Ia and the molar conductivity is characteristic of a 2:1 electrolite. Together with elemental analysis results these data are compatible with the formulation [Mo(η-C$_5$H$_5$)$_2$ (pyrd)$_2$] [PF$_6$]$_2$(Id).

The ^{1}H nmr spectrum is puzzling: it shows three peaks with the relative areas 4:4:10; although the presence of only two peaks assignable to the pyridazine ligand seems to suggest a dimeric structure, the relative areas (pyridazine and η-C$_5$H$_5$) favour the monomeric structure Id in agreement with the elemental analysis results. No change was observed in the ^{1}H nmr spectrum on lowering the temperature down to −70°C. The equivalence of protons 3 and 6 (see Table 2) in the nmr spectrum may be due either to fluxional behaviour (coordination of the ligand to the metal changing from one nitrogen atom to the other) or to coordination through the N = N double bond. Further clarification of this problem must wait for an X-ray molecular structure determination. Under similar reaction conditions a very small amount of a reddish-brown crystalline compound was obtained from [W(η-C$_5$H$_5$)$_2$Br$_2$]; its characterization was not complete but the data

available suggest a structure similar to that of complex Id. The use of complexes [M(η-C$_5$H$_5$)$_2$ (SR)$_2$] (M = Mo,W,Ta, Nb) as bidentate chelating ligands is well established [3]. Preliminary studies on the behaviour of complex Id as a bidentate ligand to transition metals proved promising and will be further investigated in the near future.

Reaction of [Mo(η-C$_5$H$_5$)$_2$H$_3$] [PF$_6$] with pyridazine in refluxing acetone or of [Mo(η-C$_5$H$_5$)$_2$HI] with the same ligand and in the same solvent but in the presence of Tl[PF$_6$] gave red crystals which were fully characterized as being the new hydride complex [Mo(η-C$_5$H$_5$)$_2$H(pyrd)] [PF$_6$] (Ic). This complex reacts with CHBr$_3$ in acetone to give complex (Ia) identified by comparison of its infrared spectrum with that of an authentic sample. Reaction of [Mo(η-C$_5$H$_5$)$_2$Br$_2$] with pyrimidine in refluxing acetone in the presence of one equivalent of Tl[PF$_6$] gave green crystals which were fully characterized as being the complex [Mo(η-C$_5$H$_5$)$_2$Br (pyrm)] [PF$_6$] (IIa). Starting from the complex [Mo(η-C$_5$H$_5$)$_2$HI] and working under the same conditions the related hydride complex [Mo(η-C$_5$H$_5$)$_2$H (pyrm)] [PF$_6$] (IIb) was obtained.

Reaction of [Mo(η-C$_5$H$_5$)$_2$Br$_2$] with pyrazine in the presence of Tl[PF$_6$] in refluxing acetone during one hour gave a brownish-green crystalline compound which, on the basis of the evidence available, was formulated as being the complex [Mo(η-C$_5$H$_5$)$_2$Br (pyrz)] [PF$_6$] (IIIa). It was also observed that the results of elemental analysis became worse with

successive recrystallisations. When a larger reaction time was used, a light-green crystalline compound formed which was insoluble in all the common solvents except DMSO. The ir spectrum shows the presence of the anions η-$C_5H_5^-$ and FP_6^-, as well as the peaks characteristic of the coordinated pyrazine. The ^1H nmr spectrum in DMSO-d_6 is not clean and suggests the presence of two compounds. After some time two of the peaks increased in area; based on their position and relative intensities we can assign one of them to four equivalent protons of one heterocycle and the other one to twenty protons of four η-C_5H_5 rings. Together with the values of elemental analysis we propose for this complex the formula [{Mo(η-C_5H_5)$_2$Br}$_2$pyrz] [PF_6] (IIIc) where the pyrazine is a bridging ligand, its favourite coordination mode [5]. The observations described suggest that the first product of the reaction of [Mo(η-C_5H_5)$_2$Br$_2$] with pyrazine is the mononuclear complex (IIIa) which slowly decomposes in solution to give the dinuclear complex (IIIc)

$$2[Mo(\eta\text{-}C_5H_5)_2Br(pyrz)]\ [PF_6] \xrightarrow[\text{soln.}]{}$$
$$\longrightarrow [\,|\,Mo(\eta\text{-}C_5H_5)_2Br\,|\,_2(pyrz)]\ [PF_6]_2 + pyrz$$
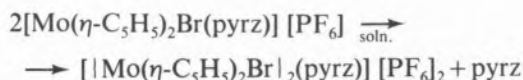
Pyrazine also reacts with [Mo(η-C_5H_5)$_2$HI] in refluxing acetone and in the presence of Tl[PF_6] to give a reddish-pink crystalline compound which we tentatively identified as the hydride complex. [Mo(η-C_5H_5)$_2$H(pyrz)] [PF_6] IIIb; the analytical results are not very good as recrystallisation gives an

insoluble product probably a dimeric species equivalent to IIIc.

[M(η-C_5H_5)$_2$Br$_2$] (M = Mo, W) reacts with 4,4'-bipyridyl in refluxing acetone to give crystalline compounds identified as [M(η-C_5H_5)$_2$Br(4-bipy)] [PF_6] (M = Mo (IVa); M = W (IVb), the tungsten compound being obtained only in very small yield. The formation of dimeric species was not observed even after 20 hrs reflux and a 2:1 metal/ligand ratio.

INFRARED SPECTRA The infrared and Raman spectra of ligands pyridazine, pyrimidine and pyrazine are described in the literature [4]. A complete study of the vibrational modes of 4,4'-bipyridyl has not been found.

Table 3 describes the frequencies of several vibrational modes of the free pyridazine [4] and of the coordinated ligand in complexes (Ia-d). Small shifts to higher frequencies in the bands corresponding to vibrational modes of the ring were observed. As in other cases where the ligand acts as monodentate [6,7], the band corresponding to stretching mode C-H was not observed as it comes under the corresponding mode of the cyclopentadienyl ring. Table 4 describes the frequencies of the free pyrimidine [4] and of the ligand in complexes (IIa-b). It was observed that the frequencies of the several vibrational modes are not much affected upon coordination to the metal. The largest shift was observed for the band corresponding to the vibrational modes 8a and 8b of the ring, which is

Table 4
*Frequencies of some of the vibrational modes of pyrimidine and its complexes**

Vibrational mode	Description [4]	Pyrimidine	[MoCp$_2$Br(pyrm)] [PF_6]	[MoCp$_2$H(pyrm)] [PF_6]
2,13	Stretching C-H	3040	3090	3100
8a,8b	Ring	1570	1595,1560	1595
19a	Ring	1470	1470	1470
19b	Ring	1400	1410	1410
3	Deformation C-H	1230	1230	1235
15	Deformation C-H	1160	1180	1180
9a	Deformation C-H	1140	1135	1140
12	Ring	1075	1070	1070
1,5	Ring	995	995	—
11	Deformation C-H	815	—	825(?)
10b	Deformation C-H	720	705	710
4	Ring	680	685	690
6a	Ring	625	645	645
16b	Ring	350	390	400

* Cp = η^5-C_5H_5

shifted from 1575 cm^{-1} in the free ligand to near 1600 cm^{-1} in **IIa** and split into two bands at 1599 and 1560 cm^{-1} in **IIb**. The band at 1400 cm^{-1} in the free ligand is shifted to higer frequencies upon coordination. These results are in agreement with those described in the literature for pyrimidine complexes of metals of the first transition series [7].

Table 5 describes the frequencies of the free pyrazine [4] and of the ligand in its complexes (**IIIa-c**). A new band at 950-1000 cm^{-1} was observed as it had been reported before [8] but it seems to be stronger in the case of bridging pyrazine.

Preparation of [Mo(η -C₅H₅)₂Br(pyrd)][PF₆]

560 mg (∼1.2 mmole) of [Mo(η-C₅H₅)₂Br₂] together with Tl[PF₆] (700 mg ∼2 mmole) and pyridazine (1 cm³) were refluxed in acetone (50 cm³) for 11 hrs. The brown mixture was filtered, the volume of the filtrate was reduced under vacuum and diethyl ether was added giving an oil. The solvent was decanted and the oil was taken to dryness under vacuum. Recrystallisation from acetone/ethanol gave dark brown crystals which were identified as being [Mo(η-C₅H₅)₂Br(pyrd)] [PF₆]. Yield *ca.* 80%.

Table 5
Frequencies of some of the vibrational modes of pyrazine and its complexes *

Vibrational mode	Description [4]	Pyrazine	[Mo(Cp₂Br)₂pyrz] [PF₆]₂	[(MoCp₂Br)₂pyrz] [PF₆]₂	[MoCp₂H(pyrz)] [PF₆]
2,13,20b	Stretching C-H	3060	3100,3040	3100,3050	—
8a	Ring	1585 [4]	1590	—	1590
19a	Ring	1495	1485	1480	1480
19b	Ring	1420	1415	1425(?)	1415
15	Deformation C-H	1145	1150	1150	1150
18a	Deformation C-H	1065	1050	1065	1050
1,12	Ring	1020	1020(?)	1025	1010(?)
11	Deformation C-H	790	—	—	780
16b	Ring	415	∼400	∼400	∼400

* Cp = η^5-C₅H₅

3 — EXPERIMENTAL

All preparations and further manipulation were carried out under dry nitrogen unless otherwise stated. The compouns [Mo(η-C₅H₅)₂H₃] [PF₆], [M(η-C₅H₅)₂Br₂] and [Mo(η-C₅H₅)₂HI] (M = Mo,W) were prepared by the reported methods [9-11] Pyridazine (Aldrich), pyrimidine (Merck), pyrazine (Fluka) and 4,4'-bipyridyl (Merck) were purchased and used without further purification.

¹H nmr spectra were determined on a JEOL JNM-PS-100 instrument. Infrared spectra were determined on a Perkin-Elmer 457 spectrophotometer in KBr pellets and were calibrated with polystyrene film. Conductivity measurements were made at 25°C using a Radiometer CDM 3 Conductivity Meter instrument calibrated with a standard KCl solution. C,H,N analyses were carried out in these laboratories.

The experimental conditions for some typical reactions are given below.

Preparation of [Mo(η -C₅H₅)₂(pyrd)₂][PF₆]₂

400 mg (≅ 1 mmole) of [Mo(η-C₅H₅)₂Br₂] together with excess Tl[PF₆] and pyridazine (2 cm³) were refluxed in acetone (30 cm³) for 10 hrs. The mixture was filtered, the volume of the filtrate was reduced and water was added. Removal of acetone under vacuum gave a red oil. This was crystallised from acetone/ethanol giving a mixture of brown and red crystals. This mixture was dissolved in acetone (40 cm³) and an excess of Tl[PF₆] and of pyridazine was added. The same mixture was refluxed for 25 hrs and then treated as above. Red crystals were obtained which were identified as being [Mo(η-C₅H₅)₂(pyrd)₂][PF₆]₂. Yield *ca.* 70%.

Preparation of [Mo(η -C₅H₅)₂H(pyrd)][PF₆]

450 mg (≅ 1.3 mmole) of [Mo(η-C₅H₅)₂HI] together with 470 mg (≅ 1.3 mmole) of Tl[PF₆] and 0.5 cm³ of pyridazine were refluxed in acetone (40 cm³) for 4 hrs. The mixture was filtered, the volume of the filtrate was reduced and chromatographed on an

alumina column, using acetone as eluent. A red solution was obtained; its volume was reduced under vacuum and slow addition of diethylether gave red crystals which were identified as being [Mo(η-C$_5$H$_5$)$_2$H(pyrd)][PF$_6$] yield *ca.* 70%.

Preparation of [Mo(η-C$_5$H$_5$)$_2$Br(pyrd)][PF$_6$]$_2$

[NO][PF$_6$] (90 mg$\cong$0.5 mmole) was added to a suspension of [Mo(η-C$_5$H$_5$)$_2$Br(pyrd)][PF$_6$] (160 mg$\cong$0.3 mmole) in dry CH$_2$Cl$_2$ (5 cm^3). The mixture was stirred during 4 hrs at room temperature and then filtered. The dark blue solid was washed several times with dry diethyl ether and then dried. It was identified as being [Mo(η-C$_5$H$_5$)$_2$Br(pyrd)][PF$_6$]$_2$. Yield *ca.* 50%.

Preparation of [|Mo(η-C$_5$H$_5$)$_2$Br|$_2$(pyrz)][PF$_6$]$_2$

[Mo(η-C$_5$H$_5$)$_2$Br$_2$] (400 mg$\cong$1 mmole), T1[PF$_6$] (350 mg$\cong$1 mmole) and pyrazine (10 mg$\cong$1.5 mmole) were refluxed in acetone (30 cm^3) during six hrs. The mixture was filtered, the volume of the green filtrate was reduced under vacuum and addition of diethyl ether gave a light green solid. This was insoluble in the common organic solvents except in DMSO where it decomposed.

The solid was identified as being
[|Mo(η-C$_5$H$_5$)$_2$Br|$_2$(pyrz)][PF$_6$]$_2$. Yield *ca.* 40%.

Preparation of [Mo(η-C$_5$H$_5$)$_2$Br(pyrz)][PF$_6$]

[Mo(η-C$_5$H$_5$)$_2$Br$_2$] (400 mg$\cong$1.2 mmole), pyrizine (180 mg$\cong$3 mmole) were refluxed in acetone (200 cm^3) for 1 hr. The mixture was filtered. The volume of the filtrate was reduced and water was added giving green crystals which were identified as being [Mo(η-C$_5$H$_5$)$_2$Br(pyrz)][PF$_6$]. Yield *ca.* 60%.

REFERENCES

[1] (a) — M. J. Calhorda, A. R. Dias, *Rev. Port. Quím.*, **20**, 77 (1978).
   (b) — idem, *J. Chem. Soc. Dalton,* 1443 (1980).
   (c) — idem, *J. Organometal. Chem.*, **197**, 291 (1980).
   (d) — ibid, **198**, 41 (1980).
[2] M. J. Calhorda, Doctoral Thesis, Lisbon (1980).
[3] See for instance (a) A. R. Dias, M. L. H. Green, *Rev. Port. Quím.*, **11**, 61 (1969).
   (b) — idem, *J. Chem. Soc. (A),* 195 (1971).
   (c) — ibid, 2807 (1971).
   (d) — P. S. Braterman, V. A. Wilson, K. K. Joshi, *J. Chem. Soc. (A),* 191 (1971).
   (e) — W. E. Douglas, M. L. H. Green, *J. Chem. Soc. Dalton,* 1976 (1972).
   (f) — C. Daren, K. Prout, A. de Ciam, M. L. H. Green, N. Singaporia, *J. Organometal. Chem.*, **136**, C4 (1974).
[4] R. C. Lord, A. L. Marston, F. A. Miller, *Spectrosc. Acta,* **9**, 113 (1957).
[5] W. M. Carmichael, D. A. Edwards — *J. Inorg. Nucl. Chem.*, **32**, 1199 (1970).
[6] M. Herberhold, M. Leonhard, *J. Organometal. Chem.*, **78**, 253 (1974).
[7] J. R. Ferrero, J. Zipper, W. Wozniak, *Appl. Spectrosc.* **23**, 160 (1969).
[8] W. M. Carmichael, D. A. Edwards, *J. Inorg. Nuch. Chem.*, **34**, 1181 (1972).
[9] M. L. H. Green, P. J. Knowles, *J. Chem. Soc. Perkin Trans. I,* 193 (1979).
[10] R. L. Cooper, M. L. H. Green, *J. Chem. Soc. (A),* 1155 (1967).
[11] C. C. Romão, Doctoral Thesis, Lisbon (1979).

RESUMO

Complexos metálicos com ligandos diazinas e 4,4'-bipiridilo.
Descreve-se a síntese e caracterização de complexos obtidos por reacção de [M(η-C$_5$H$_5$)$_2$X$_2$] (M = Mo, W ; X = halogéneo) ou [Mo(η-C$_5$H$_5$)$_2$HI] com os ligandos piridazina, pirimidina e 4,4'-bipiridilo.

SEBASTIÃO J. FORMOSINHO
CIRIACO M. T. MARTINS
ABÍLIO M. da SILVA
Departamento de Química
Universidade de Coimbra
3000 Coimbra

SOLVENT EFFECTS AS A DIAGNOSTIC TEST FOR RADIATIONLESS MECHANISMS

Oxygen and nitric oxide singlet and triplet quenching efficiencies of aromatic compounds in polar and nonpolar solvents are reported. Solvent effects depend on the electronic energy of the electronic states, but are only strong for triplet states of high electronic energy. An increase in solvent polarity increases the triplet quenching rate for O_2 and decreases the quenching rate for NO. The results are interpreted in terms of the weak and strong coupling situation of radiationless transitions and reveal that solvent effects can provide a test to distinguish between these two nonradiative cases.

1 — INTRODUCTION

Theories of radiationless transitions reveal that the coupling strength of the nuclear modes in electronic states determines the mechanism of nonradiative processes [1,2]. For small nuclear coordinate displacements (weak coupling case) radiationless transition rate constants decrease with an increase in the energy-gap of the electronic states, *i.e.*, follow a normal energy-gap law. In contrast, for strong coordinate displacements (strong coupling case), radiationless transitions follow an inverse energy-gap law [3]. The elucidation of nonradiative mechanisms is generally based on the electronic energy dependence of the nonradiative rates. However solvent polarity affects the electronic state energies and can also be employed as a tool to distinguish between weak and strong coupling situations.

Fig. 1 presents the potential energy curves of a diatomic oscillator in the ground and in an excited state for weak and strong coupling situations. Increasing solvent polarity is assumed to decrease the energy-gap between the excited and ground states, because, commonly, excited states have an higher charge-transfer character than ground states. For the weak coupling case fig. 1 shows that an increase in solvent polarity leads to a decrease on the barrier of energy and width of the oscillators and, consequently, increases the nonradiative rate constants [2]. For the strong coupling situation the opposite
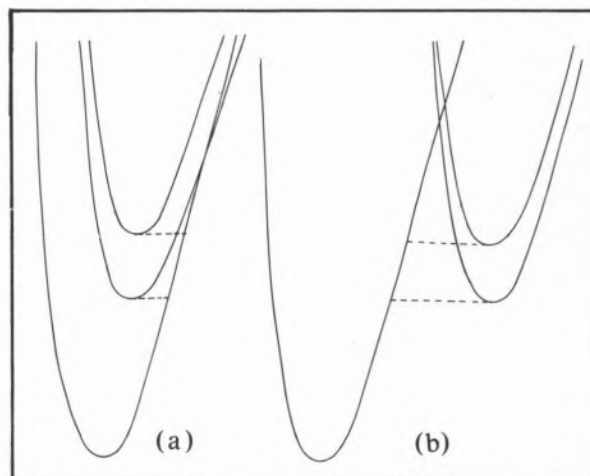
Fig. 1

Relative positions of the potential energy curves in the weak coupling (a) and strong coupling (b) situations

effect is observed since increasing solvent polarity increases the energy barrier and the barrier width Δx and decreases the nonradiative rates. This solvent effect can still be enhanced by an increase of the oscillator displacements with increasing polarity, particularly if the change in bond lengths between ground and excited states is associated with a transfer of charge. Therefore theory predicts opposite solvent effects on nonradiative rates for the weak and strong coupling cases and for the last situation the effect is expected to be of a larger magnitude.

2 — MECHANISMS OF OXYGEN AND NITRIC OXIDE QUENCHING OF AROMATIC MOLECULES

The rates of quenching of excited aromatic molecules by paramagnetic species can depend on molecular parameters [4,5] and this has been interpreted in terms of the following mechanism

$$M^* + Q \xrightleftharpoons[k_{-d}]{g_s\,k_d} (M.Q)^* \xrightarrow{k_c} \text{products}$$
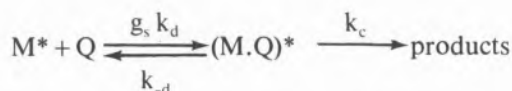
where $(M.Q)^*$ is a transient complex between the excited molecule M^* and the quencher Q via which overall spin could be conserved. The quenching rate is given by

$$k_q = g_s\,k_d \frac{k_c}{k_{-d} + k_c}$$

where g_s is a spin statistical factor, k_d the diffusion rate, k_{-d} the dissociation rate of the complex and k_c the rate of electronic relaxation (internal conversion) of the initially formed excited state of the quenching complex. Fig. 2 presents the relevant electronic states of the quenching complexes. The significant differences between the two quenchers, apart from the spin multiplicity factors, resides in the fact that O_2 has low lying electronic states that can be involved in the quenching process, whereas NO has no such states. The dependence of k_q on molecular parameters is attributed to the radiationless rate constant k_c, because k_d and k_{-d} depend on solvent viscosity, but are virtually independent of the hydrocarbon nature; k_c is weakly dependent on electronic matrix factors [3,6,7] and is strongly
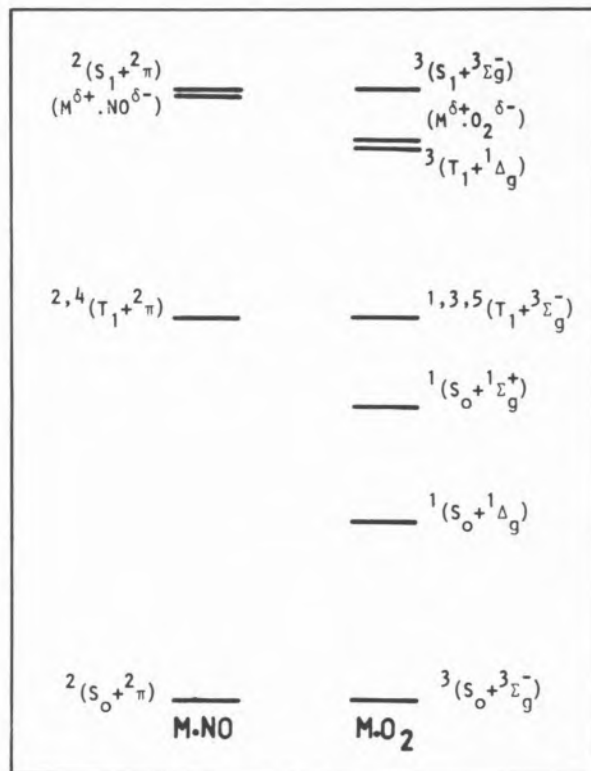
Fig. 2
Electronic energy states of the quenching complexes of aromatic molecules with NO and with O_2

affected by Franck-Condon factors of the radiationless conversions between the states of the quenching complexes.

When $k_c \gg k_{-d}$ ($k_{-d} \cong 10^{12}$ s^{-1}) the quenching rates are only controlled by diffusion and spin factors, but when $k_c \ll k_{-d}$ the quenching rates are proportional to k_c. Singlet quenching of aromatic molecules by O_2 and NO is diffusion controlled, since for both quenchers $g_s = 1$. Triplet states have quenching rate constants much smaller than $g_s\,k_d$. For O_2 the k_c rates are controlled by the Franck-Condon factors of CH stretching vibrations of the aromatic compounds which have a coordinate displacement of $R \cong 0$ and, consequently, are in the weak coupling situation. The same behaviour is found with NO quenching for triplet energies < 14500 cm^{-1}. However for higher energies k_c is controlled by the NO distension which suffers a strong displacement between ground and excited states and follows an inverse energy-gap law. Therefore quenching of aromatic triplets by paramagnetic species appears to be a good model system to investigate the use of solvent effects for probing radiationless mechanisms.

3 — SOLVENT EFFECTS IN SINGLET AND TRIPLET QUENCHING

Solvent effects arise through changes in viscosity and polarity, but only the last parameter influences the electronic states energies of the quenching complexes and is relevant for the present study. Consequently solvent effects are only considered for solvent of comparable macroscopic viscosities, η, but with different dielectric constants, ε. Previous studies on solvent effects in NO quenching considered such an effect as anomalous and no satisfactory interpretation was provided [5,7] because: i) no theoretical model for the interpretation of experimental data was available at the time [3] and ii) no reliable data for gas solubilities was available, at least in relative terms.

Here we report the fluorescence and triplet quenching efficiencies of several aromatic molecules by O_2 and NO in n- hexane and acetonitrile. Difficulties in finding literature solubility coefficients of the two gases in acetonitrile and the strong discrepancies (*ca.* 2 times) reported for the solubility of NO in n-hexane [5,8] have lead us to determine all the solubility coefficients at low pressures by gas chromatography [9]. The solubility values are presented in Table 1 together with solvent viscosities and dielectric constants.

The solvent effects for the singlet quenching have been determined by us through lifetime and Stern--Volmer measurements (Table 2) whereas the solvent effects for triplet quenching (Table 3) were estimated from the data of PORTER and coworkers [4,5] once corrected for the solubility coefficients of Table 1. The data reveal that solvent polarity has very little influence on singlet quenching, but for triplet states strong and opposite effects are observed for O_2 and NO at high triplet energies. For triplet energies below 15000 cm⁻¹ no solvent effect is found.

Charge-transfer states are located below the singlet states for oxygen [10]. Any increase in solvent polarity will increase the energy-gap between S_1 and CT states and should decrease the quenching rates. The small solvent effect observed for O_2 reveal a minor (*ca.* 10-15%) CT state contribution for the overall quenching process, in agreement with the findings of GIJZEMAN [7]. The coupling magnitude of two electronic states is proportional to the

Table 1
Gas Solubility Coefficients and Solvent Properties

Solvent	$\eta/cp^{a)}$	$\varepsilon^{a)}$	Gas solubility $s/10^{-5}$ mol 1^{-1} Torr^{-1}	
			$O_2{}^{b)}$	$NO^{b)}$
n-hexane	0.300	1.88	2.0	1.9
acetonitrile	0.325	37.5	1.1	1.2
acetone	0.304	20.7	—	$2.15^{c)}$

a) J. A. RIDDICK and W. B. BUNGER, «Organic Solvents — Physical Properties and Methods of Purification», 3ʳᵈ edn. in Techniques of Organic Chemistry, ed. A. Weissberger, vol. 2 (Wiley, Interscience, New York 1970).
b) Ref. [9].^{c} estimated from the data of ref. [5] corrected through the data of refs. [8] and [9].

Table 2
Solvent Effects for Singlet Quenching in Acetonitrile and n-Hexane

Compounds	E_{S_1}/cm^{-1}	$k_q(acet)/k_q(hex)$	
		O_2	NO
Naphthalene	32200	0.85	0.98
Pyrene	26900	0.9	1.0
Perylene	23000	0.75	0.95

Table 3
Solvent Effects for Triplet Quenching in Acetonitrile and in Hexane$^{a)}$

Compounds	E_T/cm^{-1}	$k_q(acet)/k_q(hex)$	
		O_2	NO
Chrysene	20 000	2.3	0.1
1,2-benzanthracene	16 500	—	0.15
3,4-benzpyrene	14 800	0.9	—
3,4:8,9-dibenzpyrene	12 000	—	$1.0^{b)}$

a) Data of refs. [4] and [5] corrected with the solubility coefficients of Table 1.
b) In acetone and hexane.

inverse square of the electronic energy-gap and, therefore, the absence of solvent effects for NO implies that its CT state is very far or is virtually isoenergetic with S_1. Since the NO affinity is higher, but not much different from the one of oxygen (NO 0.024 ev; O_2 0.44 ev [11]) the last hypothesis is the reasonable one.

In the triplet quenching only the highest triplet states ($>$ 15000 cm^{-1}) are sufficiently close to the CT states in order to possess any significant charge-transfer character. The relative positions of $^1(T_1 + {}^3\Sigma_g)$ and $^1(S_o + {}^1\Sigma_g)$ for O_2 and $^2(T_1 + {}^2\pi)$ and $^2(S_o + {}^2\pi)$ for NO are solvent dependent with the highest state shifting to lower energies with increasing polarity. The increase in the O_2 quenching rate of chrysene triplet corresponds to an energy stabilization of *ca.* 800 cm^{-1} from hexane to acetonitrile. With NO an even higher stabilization energy (*ca.* 950 cm^{-1}) is estimated at a constant R, but such an estimation is not consistent with the higher energy of the NO charge-transfer state. Acetonitrile seems to borrow some of its effects from an increase in the NO displacement, because an increase in the transfer of charge in the quenching complex increases the bond length of the NO moiety.

Althoug O_2 can suffer a transfer of charge similar to the one of NO, oxygen quenching does not present an inverse energy-gap behaviour. Two reasons can be invoked for such a situation: i) energy gaps between the electronic states in the quenching complexes are much smaller for O_2 than for NO and this favours the Franck-Condon factors of non-displaced oscillators such as the CH modes; ii) for the same amount of charge transfer the increase in O_2 bond length is smaller than in NO; in fact the relevant bond lengths O_2^- (0.126 nm) [12], O_2 (0.1207) and O_2^+ (0.1123) [13] reveal that the increase in bond length between O_2^- and O_2 is smaller than the one between O_2 and O_2^+, molecules isoelectronic with NO$^-$ and NO.

In conclusion the present results reveal that solvent effects for the weak and strong coupling situations of nonradiative transitions are of opposite signs and, when of a large magnitude provide an indication of the underlying radiationless mechanisms.

REFERENCES

[1] J. JORTNER, S. A. RICE, R. M. HOCHSTRASSER, *Adv. Photochem.*, 7, 149 (1969).

[2] S. J. FORMOSINHO, *J. C. S. Faraday II*, 70, 605 (1974).

[3] S. J. FORMOSINHO, *Mol. Photochem.*, 7, 13 (1976).

[4] O. L. J. GIJZEMAN, F. KAUFMAN, G. PORTER, *J. C. S. Faraday II*, 69, 708 (1973).

[5] O. L. J. GIJZEMAN, F. KAUFMAN, G. PORTER, *J. C. S. Faraday II*, 69, 727 (1973).

[6] O. L. J. GIJZEMAN, F. KAUFMAN, *J. C. S. Faraday II*, 69, 721 (1973).

[7] O. L. J. GIJZEMAN, *J. C. S. Faraday II*, 70, 1143 (1974).

[8] A. W. SHAW, A. J. VOSPER, *J. C. S. Faraday I*, 73, 1239 (1977).

[9] A. M. DA SILVA, S. J. FORMOSINHO, C. M. T. MARTINS, *J. Chromatogr. Science*, 18, 180 (1980).

[10] H. ISHIDA, H. TSUBOMURA, *J. Photochem.*, 2, 285 (1973/74).

[11] R. G. BROWN, D. PHILLIPS, *J. Photochem.*, 3, 337 (1975).

[12] «Handbook of Chemistry and Physics», Chemical Rubber Co, 52nd edn., 1972, F-181.

[13] G. HERZBERG, «Electronic Spectra of Diatomic Molecules», 2nd edn., Van Nostrand, New York, 1950.

SUMÁRIO

Efeitos de solvente na Análise dos Mecanismos de Transições Não-radiativas.

Estudam-se os efeitos de polaridade do solvente nas constantes cinéticas de supressão de singuletos e tripletos excitados de compostos aromáticos pelo oxigénio e pelo monóxido de azoto. O efeito de solvente depende da energia dos estados electrónicos e só é apreciável com tripletos de alta energia electrónica. Um aumento da polaridade do solvente aumenta as constantes de supressão pelo O_2 enquanto diminui as constantes de supressão pelo NO. Os resultados são interpretados com base nos mecanismos de acoplamento fraco e forte para transições não-radiativas, e revelam que noutros sistemas os efeitos do solvente podem ajudar a distinguir entre estes dois tipos de mecanismos.

ARMANDO J. L. POMBEIRO
MARIA FERNANDA N. N. CARVALHO

Centro de Quimica Estrutural
Complexo I
Instituto Superior Técnico
1000 Lisboa
Portugal

DIAZADIENE AND ISOCYANIDE CHLOROCOMPLEXES OF TUNGSTEN IN VARIOUS FORMAL OXIDATION STATES

A variety of tungsten chlorocomplexes with the diazabutadiene $N\widehat{}N = RN = CHCH = NR$ (where $R = 4 - C_6H_4OMe$) or the diamine $N\widehat{}N = Me_2NCH_2CH_2NMe_2$ as chelating or bridging ligands were prepared in a wide range of the metal oxidation state (from +5 to +2), from reactions of WCl_6 or $[WCl_4(PPh_3)_2]$.

Reaction of WCl_6 with $N\widehat{}N$, in the presence of zinc amalgam, yielded the W(V) species $[(WCl_5)_2(\mu - N\widehat{}N)]$ and the W(IV) complex $[WCl_4(N\widehat{}N)]$. Other W(IV) complexes, $[WCl_2(N\widehat{}N)_2]$ Cl_2 and $[|WCl_3(N\widehat{}N)|_2(\mu - N\widehat{}N)]$ Cl_2, were derived from substitution reactions of $[WCl_4(PPh_3)_2]$; a related molybdenum(III) species, $[|MoCl_3(N\widehat{}N)|_2(\mu - N\widehat{}N)]$, was formed from a similar reaction of $[MoCl_3(thf)_3]$ with $N\widehat{}N$.

Species in which the tungsten metal appears to be in a formal oxidation state of +3 were prepared from reduction of WCl_6 by zinc amalgam in the presence of an excess of $N\widehat{}N$: $[|WCl_2(N\widehat{}N)|_2(\mu - Cl)_2]$ and $[W(N\widehat{}N)_3]Cl_3$.

Further reduction to W(II) was also achieved in the following complexes: $[|WCl_2(N\widehat{}N)|_2(\mu - N\widehat{}N)_2]$ prepared from reduction of WCl_6 by zinc amalgam in the presence of $N\widehat{}N$; $[WCl_2(N\widehat{}N)_2]$ from reduction of $[WCl_4(PPh_3)_2]$ by magnesium metal in the presence of $N\widehat{}N$ {the analogous Mo(II) complex $[MoCl_2(N\widehat{}N)_2]$ was also prepared from reduction of $[MoCl_3(thf)_3]$ by sodium in the presence of $N\widehat{}N$}.

Methylisocyanide may also bind these metal sites and the W(IV) complex $[|WCl_4(CNMe)|_2(\mu - N\widehat{}N)]$ was prepared from reaction of the above mentioned species $[(WCl_5)_2(\mu - N\widehat{}N)]$ with an excess of CNMe. An isocyanide complex with the tungsten atom in a formal oxidation state of +2, $[WCl_2(CNMe)_2(N\widehat{}N)]$ was also prepared from the reaction of $[WCl_4(PPh_3)_2]$ with $N\widehat{}N$ in the presence of CNMe and sodium sand.

1 — INTRODUCTION

Diazadienes, unsaturated compounds formulated as $RN = C(R')C(R') = NR$, when ligating a metal atom, may exhibit various formal charges and different binding modes. This potential behaviour may provide the metal site with a high flexibility to adapt itself to the electronic and stereochemical requirements of other co-ligands to participate in a versatile chemistry.

When ligating a transition metal atom, diazadienes may behave as predominant σ donors but the bonding may also have a strong π component namely when the metal site is electron rich and an electronic acceptance of unfilled C-N π antibonding ligand orbitals occurs [1] from metal d filled orbitals.

The electron release and withdrawing abilities of the diazadienes may also be accounted for by VB representations such as those shown in fig. 1 which refer to a chelating ligand. Resonance forms (a) and (b) are the higher weighted ones when the diazadienes behave mainly as σ donors, whereas forms (c) and (d) account for the electron withdrawing ability of those ligands
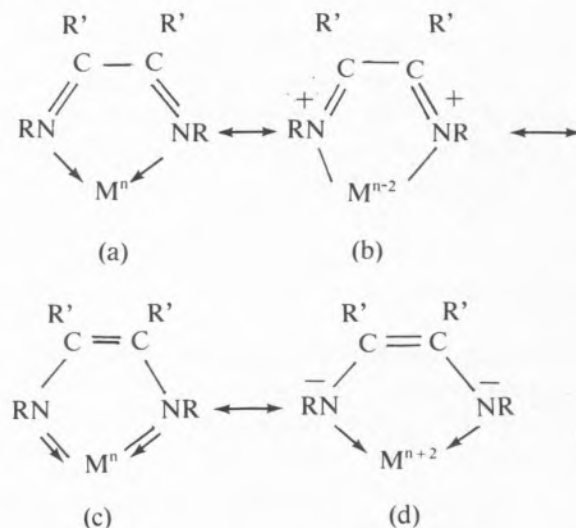
Fig. 1

VB representation of a chelating diazadiene ligand

The binding versatility of the diazadienes has already been ascertained in various compounds.

Hence, they may behave as σ monodentate ligands, through coordination via σ donation of the electron

pair located at one of the nitrogen atoms, as in the complexes [PdCl$_2$(DAB)$_2$] [2] and [M(CO)$_5$(DAB)], [3] where DAB is a diazobutadiene (diazadiene with R' = H) and M = Cr, Mo or W.

Diazabutadienes acting as σ,σ donors bridging two metal atoms are also known as in the complexes [{PtCl$_2$(PBu$_3$)}$_2$(μ−DAB)][4], and [{Rh(CO)$_2$Cl}$_2$ (μ−DAB)], [2] whereas a σ,σ chelating binding is common, being present, *e.g.*, in the complexes [M(CO)$_4$(DAB)] [1,5] (M = Cr,Mo or W).

Although a diazadiene is expected to be able to electronic π acceptance from an electron rich metal site, it may also be regarded, in some cases, as a π donor through the filled C-N π bonding orbital, as authenticated by the X-ray structure determination of [Fe$_2$(CO)$_6$(DAB)] where the DAB species behaves as a six-electron σ,π donor ligand [6].

Catalysis constitutes another recent aspect in the studies of diazadiene complexes, and, *e.g.*, [Ni(RN = CHCH = NR)$_2$] (R = CHPr$^i_2$) is a catalyst for the tetramerization of HC≡CX (where X = CH$_2$OH, CMe$_2$OH, CH$_2$OMe, CMe$_2$NH$_2$), [Fe(RN = CHCH = NR)$_2$] activated by AlEt$_3$ catalyses the dimerization of dienes, and the coordinatively unsaturated complex [Cr(RN = CHCH = NR)$_2$] or [V(RN = CHCH = NR)$_3$] with trialkylaluminium catalyses the tail-to-tail dimerization of isoprene [7].

Apart from the abovementioned importance of the diazadiene complexes, we are also interested on the fixation of isocyanides to transition metals and on the study of the reactivity of the derived species, in attempting to establish the experimental conditions which may be suitable for binding and activation of dinitrogen once the analogy of behaviour between these two species has been previously demonstrated [8].

In a previous paper [9], we have reported the products from the reactions of [MoCl$_3$(thf)$_3$] (which is a parent of *trans*-[Mo(N$_2$)$_2$(Ph$_2$PCH$_2$CH$_2$PPh$_2$)$_2$]) with diazadienes and isocyanides, and we wish now to present the results from the reactions of another dinitrogen complex precursor, [WCl$_4$(PPh$_3$)$_2$] (and of the parent WCl$_6$), with the diazabutadiene RN = CHCH = NR (where R = 4−C$_6$H$_4$OMe), the diamine Me$_2$NCH$_2$CH$_2$NMe$_2$ and the methylisocyanide.

2 — RESULTS

2.1 — REACTIONS OF [WCl$_4$(PPh$_3$)$_2$] WITH DIA-ZADIENE (N⌢N) OR DIAMINE (N⌢N)

2.1.1 COMPLEXES WITHOUT ISOCYANIDE

Once the dinitrogen complex *trans*-[W(N$_2$)$_2$(dppe)$_2$] (where dppe = Ph$_2$PCH$_2$CH$_2$PPh$_2$) is conveniently prepared [10] from [WCl$_4$(PPh$_3$)$_2$] according to scheme 1, we have started by attempting similar reactions using the diazabutadiene RN = CHCH = NR (N⌢N where R = 4−C$_6$H$_4$OMe) instead of the dppe species.

$$[WCl_4(PPh_3)_2] + dppe \xrightarrow[78°C]{toluene} [WCl_4(dppe)]$$

$$[WCl_4(dppe)] + dppe + 2Mg + 2N_2 \xrightarrow{thf}$$
$$\longrightarrow trans\text{-}[W(N_2)_2(dppe)_2] + 2MgCl_2$$
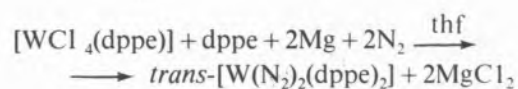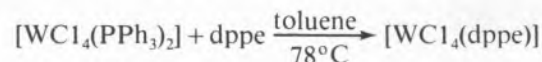
Scheme 1

Preparation of trans-[W(N$_2$)$_2$(dppe)$_2$]

Hence, from reaction of [WCl$_4$(PPh$_3$)$_2$] (**A**) with N⌢N, first in toluene and then in thf, under N$_2$, a species formulated as [WCl$_2$(N⌢N)$_2$]Cl$_2$ (**B**) was formed upon replacement (reaction 1) of the phosphine and chloride ligands by the diazabutadiene (used in a total amount corresponding to a molar ratio of 2.5:1 relative to the W metal).

$$[WCl_4(PPh_3)_2] + 2N⌢N \rightarrow [WCl_2(N⌢N)_2]Cl_2 + 2PPh_3$$
$$\quad (\textbf{A}) \qquad\qquad\qquad (\textbf{B}) \qquad\qquad\qquad (1)$$
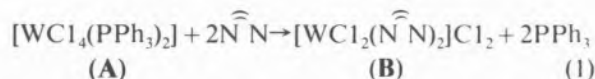
Moreover, in the presence of Mg, reduction also occurs and by using a smaller amount of diazabutadiene [2.0 excess relative to the starting species (**A**)], the complex [WCl$_2$(N⌢N)$_2$] (**C**) was obtained according to reaction (2).

$$[WCl_4(PPh_3)_2] + Mg \xrightarrow[45°C]{N⌢N, Toluene} [WCl_2(N⌢N)_2] +$$
$$\quad (\textbf{A}) \qquad\qquad\qquad\qquad (\textbf{C})$$
$$+ 2PPh_3 + MgCl_2 \qquad (2)$$
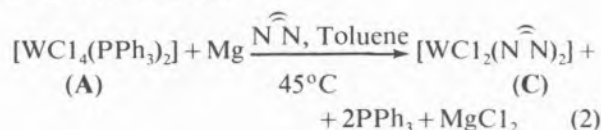
Complexes (**B**) and (**C**) have been formulated on the basis of microanalytical and infrared data and magnetic susceptibility measurements.

They display broad bands in the infrared spectrum at 240-300 cm^{-1} which are ascribed to ν(W-Cl), and two strong bands at *ca.* 1600 and 1500 cm^{-1} due to ν(C = N) of the ligating diazabutadiene, as it has been observed [9] in other diazabutadiene species such as [MoCl$_3$(CNMe)(N⌢N)] and

$[MoCl_2(CNMe)_2(N\widehat{}N)]$. Complex (C) is analogous to $[MoCl_2(N\widehat{}N)_2]$ (D), which was also prepared in the present work, upon reduction of $[MoCl_3(thf)_3]$ by sodium in the presence of $N\widehat{}N$ (equation 3). Species (D) has $\nu(\text{Mo-Cl})$ at 330 cm^{-1}, $\nu(C=N)$ at 1595 and 1493 cm^{-1}, and (B), (C) and (D) are paramagnetic with values of μ_{eff} which agree with two unpaired electrons as it may be expected for octahedral d^2 (in complex B) or d^4 (in complexes C and D) metal atoms.

$$[MoCl_3(thf)_3] + 2N\widehat{}N + Na \longrightarrow$$
$$\longrightarrow [MoCl_2(N\widehat{}N)_2] + NaCl + 3thf \quad (3)$$
$$\textbf{(D)}$$

Reactions of $[WCl_4(PPh_3)_2]$ (A) with diamine $Me_2NCH_2CH_2NMe_2$ ($N\widehat{}N$) have also been tried, and from a mixture of (A) with $N\widehat{}N$ (1:3) in toluene at 65°C, a species formulated as $[\{WCl_3(N\widehat{}N)\}_2$ $(\mu\text{-}N\widehat{}N)]Cl_2$, (E), was obtained (reaction 4). In its infrared spectrum, $\nu(\text{W-Cl})$ appears at 310 s, br and 345 wm, and strong and broad bands may also be seen at 2560 and 2450 cm^{-1}; similar bands have also been observed in other diamine complexes (see below) and they are suggested to be due to $\nu(\text{C-H})$ where the hydrogen atom is involved in hydrogen bond probably with a chlorine atom.

$$2[WCl_4(PPh_3)_2] + 3N\widehat{}N \xrightarrow[65°C]{\text{Toluene}}$$
$$[\{WCl_3(N\widehat{}N)\}_2(\mu\text{-}N\widehat{}N)]Cl_2 + 4PPh_3 \quad (4)$$
$$\textbf{(E)}$$

Complex (E) is paramagnetic and the value of μ_{eff} (2.5) agrees with an octahedral d^2 metal.

A molybdenum(III) species which is related to complex (E) was also prepared in the present study from reaction of $[MoCl_3(thf)_3]$ with the diamine $N\widehat{}N$ (1:3.5) in thf (reaction 5); its formulation as $[\{MoCl_3(N\widehat{}N)\}_2(\mu\text{-}N\widehat{}N)]$, (F), was also based on the elemental microanalytical and infrared data and on the value of μ_{eff}(3.6 B.M.).

$$2[MoCl_3(thf)_3] + 3N\widehat{}N \xrightarrow{\text{thf}}$$
$$[\{MoCl_3(N\widehat{}N)\}_2(\mu\text{-}N\widehat{}N)] + 6thf \quad (5)$$
$$\textbf{(F)}$$

In the infrared spectrum of complex (F), $\nu(\text{Mo-Cl})$ is observed at 300 and 275 cm^{-1}, whereas strong and broad bands at 2550 and 2440 cm^{-1} are also present as in the related species (E).

2.1.2 — ISOCYANIDE COMPLEXES

From reaction in thf of $[WCl_4(PPh_3)_2]$ with CNMe and the diamine $N\widehat{}N$ (in molar ratios of 1:4:2.2), in the presence of sodium metal, the tungsten(II) complex $[WCl_2(CNMe)_2(N\widehat{}N)]$, (G), was obtained according to reaction 6, *via* metal reduction and phosphine displacement.

$$[WCl_4(PPh_3)_2] + 2CNMe + N\widehat{}N + 2\,Na \xrightarrow{\text{thf}}$$
$$[WCl_2(CNMe)_2(N\widehat{}N)] + 2\,NaCl + 2PPh_3 \quad (6)$$
$$\textbf{(G)}$$

The characterization of complex (G) was based on the same techniques used for the previous species. Its infrared spectrum shows $\nu(\text{W-Cl})$ and $\nu(C\equiv N)$ of the coordinated isocyanide as broad and strong bands at 305 and 2150 cm^{-1}, respectively. The value of μ_{eff}, 2.7 B.M., agrees with a high spin d^4 metal site. This complex is analogous to the previously reported [9] $[MoCl_2(CNMe)_2(N\widehat{}N)]$, which exhibits $\nu(C\equiv N)$ at 2145 and 2130 cm^{-1} and $\nu(\text{Mo-Cl})$ at 305 cm^{-1}.

The two expected bands for $\nu(C\equiv N)$ are not observed probably due to their broadness and overlap. All the abovementioned reactions of $[WCl_4(PPh_3)_2]$ are summarized in the scheme 2.

2.2 — REACTIONS OF WCl₆ WITH DIAZADIENE OR DIAMINE

Tungsten hexachloride is the precursor for $[WCl_4(PPh_3)_2]$ (A) which is derived from the former upon reduction by zinc amalgam in CH_2Cl_2 in the presence of PPh$_3$ [10].

Once we are interested in the preparation of complexes of diazadienes which may be precursors for new dinitrogen complexes with these co-ligands, we have also investigated the reactivity of WCl$_6$ towards the diazabutadiene $N\widehat{}N$ and a related diamine $N\widehat{}N$ mentioned above, under reduction conditions which are similar to those used in the preparation of $[WCl_4(PPh_3)_2]$.

$$[WCl_2(N\overset{\frown}{N})_2]$$
$$\textbf{(C)}$$

$$\uparrow$$

$$(2) \quad \begin{array}{c} N\overset{\frown}{N} \\ \\ Mg \\ toluene \end{array}$$

$$[WCl_2(N\overset{\frown}{N})_2]Cl_2 \xleftarrow[N\overset{\frown}{N}]{(1)} [WCl_4(PPh_3)_2] \xrightarrow[N\overset{\frown}{N}]{(4)} [|WCl_3(N\overset{\frown}{N})|_2(\mu\text{-}N\overset{\frown}{N})]Cl_2$$

$$\textbf{(B)} \qquad \begin{array}{c} toluene \\ thf \end{array} \qquad \textbf{(A)} \qquad toluene \qquad \textbf{(E)}$$

$$(6) \quad \begin{array}{c} CNMe \\ \\ N\overset{\frown}{N} \\ \\ Na \\ \\ thf \end{array}$$

$$\downarrow$$

$$[WCl_2(CNMe)_2(N\overset{\frown}{N})]$$
$$\textbf{(G)}$$

Scheme 2

Reactions of [WCl$_4$(PPh$_3$)$_2$] with diazabutadiene (N$\overset{\frown}{N}$) or dia-
mine (N$\overset{\frown}{N}$) and methylisocyanide

Hence, from reaction in CH_2Cl_2 of WCl_6 with $N\overset{\frown}{N}$ in a molar ratio of 1:1.1 and in the presence of Zn/Hg, reduction of the metal occurs and the tungsten(V) complex, with bridging diazabutadiene, $[(WCl_5)_2(\mu\text{-}N\overset{\frown}{N})]$, **(H)**, was isolated after *ca.* 10h reaction (equation 7). This species was characterized on the basis of microanalytical and infrared data and of the magnetic properties. Bands in the infrared spectrum due to $\nu(C=N)$ of the diazabutadiene ligand are present at 1605, 1575 and 1500 cm^{-1}, whereas bands at 345 and 332 cm^{-1} are ascribed to $\nu(W\text{-}Cl)$. The value of $\mu_{eff}(1.4$ B.M.$)$ agrees with a d^1 metal centre.

$$2WCl_6 + N\overset{\frown}{N} \xrightarrow[-Cl^-]{Zn/Hg} [(WCl_5)_2(\mu\text{-}N\overset{\frown}{N})] \quad (7)$$
$$\textbf{(H)}$$
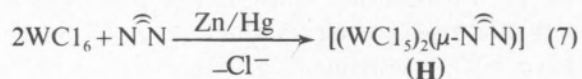
Complex **(H)** reacts with methylisocyanide (1:6) in thf at reflux, yielding the methylisocyanide tungsten(IV) species $[|WCl_4(CNMe)|_2(\mu\text{-}N\overset{\frown}{N})]$,

(I), which retains the bridging diazabutadiene ligand (reaction 8). In the infrared spectrum of this complex, $\nu(C\equiv N)$ of the coordinated isocyanide appears at 2220 cm^{-1}, well above the value encountered for free CNMe (*ca.* 2160 cm^{-1}) in

$$[(WCl_5)_2(\mu\text{-}N\overset{\frown}{N})] \xrightarrow[thf,reflux]{CNMe}$$
$$\textbf{(H)}$$

$$[|WCl_4(CNMe)|_2(\mu\text{-}N\overset{\frown}{N})] \qquad (8)$$
$$\textbf{(I)}$$
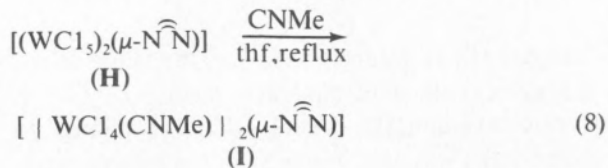
agreement with the expected predominance of the σ electronic donation (from the ligating isocyanide to the electron poor metal) over the π acceptance of that ligand. Bands at 1695 and 1630 cm^{-1} are also present and they are assigned to $\nu(C=N)$ of the ligating diazabutadiene; $\nu(W\text{-}Cl)$ appears at 305 and 290 cm^{-1}. Complex **(I)** is also paramagnetic and the value of μ_{eff}, 2.6 B.M., is in agreement with a high--spin d^2 metal centre.

Another species, tentatively formulated as $[WCl_4(N\overset{\frown}{\ }N)]$ or $[(WCl_4)_2(\mu\text{-}N\overset{\frown}{\ }N)_2]$, **(J)**, was isolated after 24 h reaction of WCl_6 with an excess (1.5:1) of the diazabutadiene, also in CH_2Cl_2 and in the presence of Zn/Hg (reaction 9). In the infrared spectrum $\nu(C=N)$ appears at 1600 and 1505 cm^{-1}, whereas ν(W-Cl) is observed at *ca.* 303 and 275 cm^{-1}

$$WCl_6 \xrightarrow[\text{--Cl}^-]{N\overset{\frown}{\ }N,\ Zn/Hg,\ CH_2Cl_2} [WCl_4(N\overset{\frown}{\ }N)] \quad (9)$$
$$\text{(J)}$$
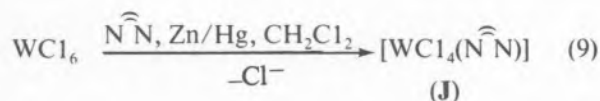
Species **(J)** is diamagnetic but the low solubility in the usual solvents precluded N.M.R. studies and molecular weight measurements, thus preventing the distinction between the two formulations.

Reactions of WCl_6 with the diamine $N\overset{\frown}{\ }N$ were also tried, and various reduced species with chelating or bridging diamine appear to be formed in the presence of zinc amalgam as a reducing agent.

Hence, two species formulated as $[|WCl_2(N\overset{\frown}{\ }N)|_2(\mu\text{-}N\overset{\frown}{\ }N)_2]$, **(K)**, and $[|WCl_2(N\overset{\frown}{\ }N)|_2(\mu\text{-}Cl)_2]$, **(L)**, have been isolated from the reaction mixture of WCl_6 with an excess of $N\overset{\frown}{\ }N$ (1:7.2) and Zn/Hg in CH_2Cl_2 (reaction 10).

$$WCl_6 \xrightarrow[\text{--Cl}^-]{N\overset{\frown}{\ }N, Zn/Hg, CH_2Cl_2} [|WCl_2(N\overset{\frown}{\ }N)|_2(\mu\text{--}N\overset{\frown}{\ }N)_2] +$$
$$\text{(K)}$$

$$+ [|WCl_2(N\overset{\frown}{\ }N)|_2(\mu\text{--}Cl)_2] \quad (10)$$
$$\text{(L)}$$
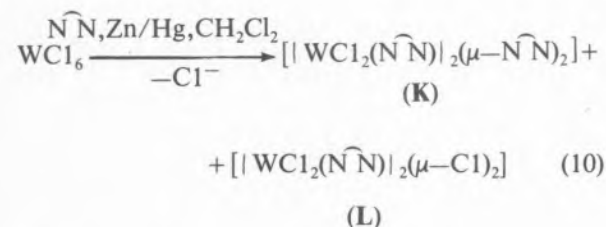
The infrared spectra of these complexes exhibit ν(W-Cl) as broad bands at 290 **(K)** and 280 cm^{-1} **(L)**. Strong and broad bands at *ca.* 2720 **(K)**, 2705 **(L)**, 2560 **(K,L)** and 2440 cm^{-1} **(K,L)** are also observed, as it has been mentioned above for the diamine complexes **(E)** and **(F)** and they are also assigned to ν(C-H...Cl) (see below).

Complex **(K)** is diamagnetic, whereas **(L)** is paramagnetic with $\mu_{eff} = 4.0$ B.M. in agreement with a high-spin d^3 metal centre, (the spin only value is 3.87 B.M.). The low solubility of complex **(K)** in the usual solvents precluded N.M.R. measurements.

If an excess of diamine is added to solid WCl_6, a vigorous reaction occurs and addition of a mixture of MeOH/CH_2Cl_2 followed by Zn/Hg, leads to the formation of a species which may be formulated as the tungsten(III) complex $[W(N\overset{\frown}{\ }N)_3]Cl_3$, **(M)** (reaction 11).

$$WCl_6 \xrightarrow[\text{--Cl}^-]{N\overset{\frown}{\ }N, MeOH/CH_2Cl_2, Zn/Hg} [W(N\overset{\frown}{\ }N)_3]Cl_3 \quad (11)$$
$$\text{(M)}$$
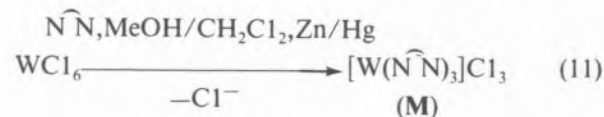
This species is paramagnetic with $\mu_{eff} = 3.5$ B.M., its infrared spectrum does not exhibit any band which could be assigned to ν(W-Cl), whereas broad bands are observed at 2620 s, 2570 s, 2450 s and 2410 sh. These bands are only partially replaced by others (also broad, at 2000, 1920 and 1845 cm^{-1}) by stirring for two days in a mixture of thf/D_2O. Hence they are not ascribed to ν(N-H) once in this case the H/D exchange would be very facile; we suggest they refer to ν(C-H) where the H atom is involved in hydrogen bonding [11] with a chlorine atom. Similar bonds were also observed in other diamine complexes **(E,F,K** and **L)** as reported above.

The abovementioned reactions of WCl_6 are summarized in scheme 3.

3 — FINAL REMARKS

The preparation of the complexes described in the present study is strongly dependent and very sensitive to the experimental conditions employed. Diazabutadiene or diamine appear to chelate or bridge tungsten atoms in a wide range of oxidation states [including the very unusual W(III) oxidation state] and methylisocyanide ligating W(IV) or W(II) metal sites exhibits in the infrared spectra $\nu(C\equiv N)$ at higher or only slightly lower values than in the free molecule. Hence, these centres are not able to bind dinitrogen, and lower metal oxidation states are undoubtly required for such [8,12].

However, the potential lability of these complexes which may be susceptible to variations in the metal oxidation state and to replacement and rearrangement of versatile ligands to different binding types, constitutes an interesting feature which may be worthwile to exploit namely in catalysis.

4 — EXPERIMENTAL

All the reactions were carried out under dinitrogen using dried and purified solvents by standard methods, unless otherwise stated.

Infrared spectra were recorded on a 577 or 457 Perkin Elmer Grating Infrared Spectrophotometer using Nujol mulls between caesium iodide plates.

Magnetic susceptibilities were measured using a Faraday balance.

WCl_6, $[WCl_4(PPh_3)_2]$[10] and $RN = CHCH = NR$ [13] (for $R = 4-C_6H_4OMe$) and CNMe[14] were prepared by published methods. The diamine $Me_2NCH_2CH_2NMe_2$ was purchased from BDH and used after purification by refluxing over KOH for 3h followed by distillation.

$[(WCl_5)_2(\mu-N\overset{\frown}{N})]$
(H)

$[WCl_4(N\overset{\frown}{N})]$
(J)[a]

CNMe(1:6) thf,reflux (8) (7)

$N\overset{\frown}{N}(1:1.1)$
Zn/Hg
CH_2Cl_2
10 h

(9) $N\overset{\frown}{N}(1:1.5)$
Zn/Hg
CH_2Cl_2
24 h

$[|WCl_4(CNMe)|_2(\mu-N\overset{\frown}{N})]$
(I)

WCl_6

(10) $N\overset{\frown}{N}(1:7.2)$
Zn/Hg
CH_2Cl_2

$N\overset{\frown}{N}(1:3.5)$
(11) Zn/Hg
$MeOH/CH_2Cl_2$

$[|WCl_2(N\overset{\frown}{N})|_2(\mu-N\overset{\frown}{N})_2]$
(K)
+

$[W(N\overset{\frown}{N})_3]Cl_3$
(M)

$[|WCl_2(N\overset{\frown}{N})|_2(\mu-Cl)_2]$
(L)
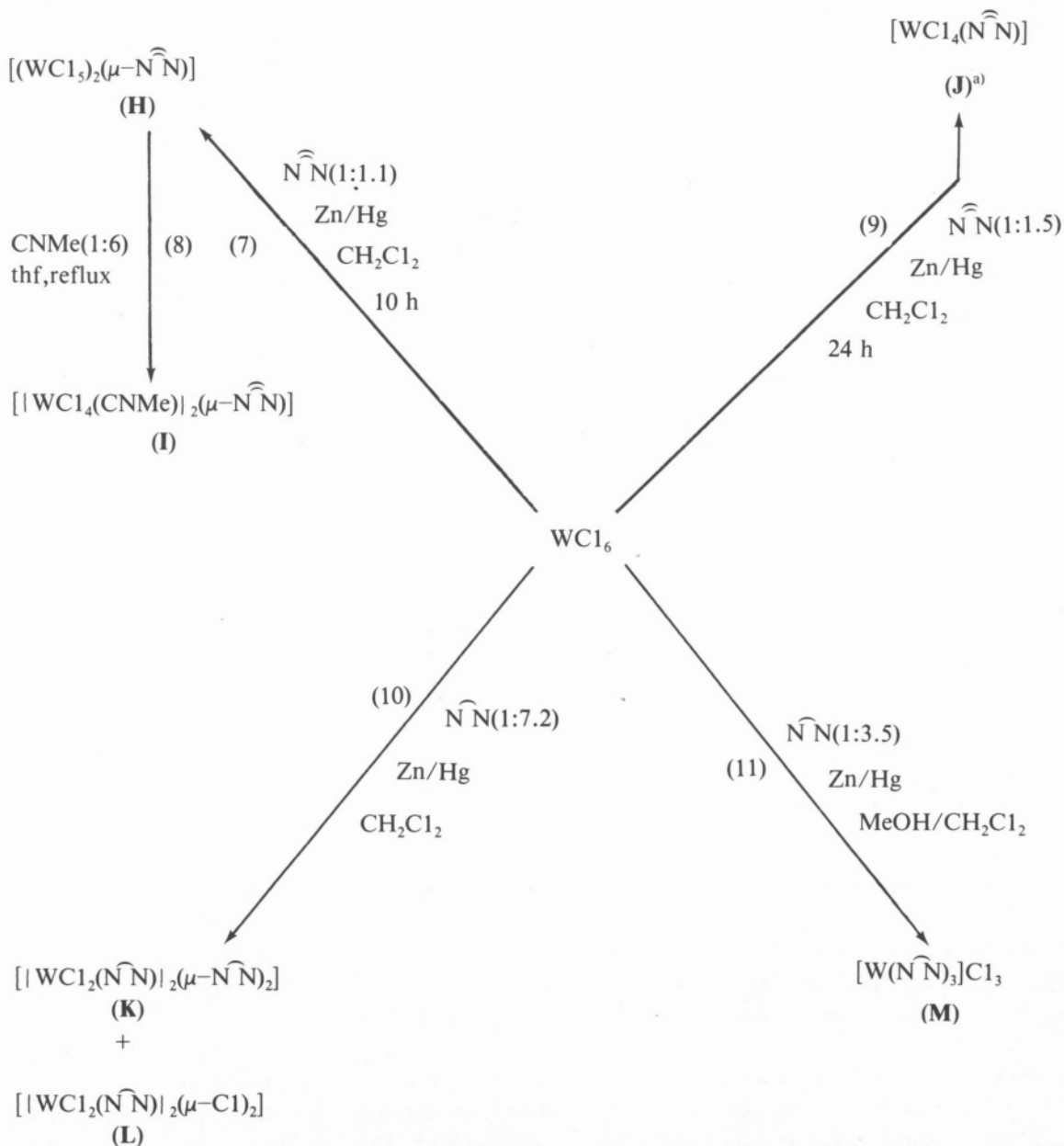
Scheme 3
Reactions of WCl_6 with diazabutadiene ($N\overset{\frown}{N}$) or diamine ($N\overset{\frown}{N}$)
in the presence of a reducing agent (Zn/Hg)

[a] $[(WCl_4)_2(\mu-N\overset{\frown}{N})_2]$ constitutes another possible formulation.

4.1 — REACTIONS OF [WCl$_4$(PPh$_3$)$_2$], (A).

4.1.1 — PREPARATION OF COMPLEXES WITHOUT THE ISOCYANIDE LIGAND.

Bis| 1,4−bis(4−methoxyphenyl)−1,4−diazabutadiene) | dicloro tungsten(II) dichloride, [WCl$_2$(RNCHCHNR)$_2$] Cl$_2$ (R = 4−MeOPh), (B)

Diazabutadiene (0.20 g, 0.75 mmol) was added to a suspension of [WCl$_4$(PPh$_3$)$_2$](0.50 g, 0.59 mmol) in toluene (8 ml) and the mixture was heated to *ca.* 60°C for 3h. The solid was filtered off the solution, washed by toluene and dissolved in thf (*ca.* 10 ml). The thf solution was filtered to solid diazabutadiene (0.20 g, 0.75 mmol) and left overnight at *ca.* 65°C with a reflux condenser. The solution was then filtered and complex (**B**) precipitated out as a dark brown solid by addition of diethylether and cooling (50 mg, *ca.* 10% yield).

Bis| 1,4−bis(4−methoxyphenyl)−1,4−diazabutadiene) | dichloro tungsten(II)[WCl$_2$(RNCHCHNR)$_2$] (R = 4−MeOPh), (C)

Diazabutadiene (N͡N) (0.128 g, 0.478 mmol) was added to a suspension of [WCl$_4$(PPh$_3$)$_2$] (0.203 g, 0.239 mmol) with an excess of magnesium in toluene (5 ml) and the mixture was heated to *ca.* 45°C and left stirring overnight.
The solution was then filtered and the very dark solid was washed by toluene. It was recrystallised from thf/ether affording the dark brown solid (**C**) (0.040 g, 0.050 mmol, 21% yield).

μ−(N,N,N',N'−tetramethyl−1,2−diaminoethane) bis{trichloro(N,N,N',N'−tetramethyl−1,2−diaminoethane)tungsten(IV)}dichloride, [\{WCl$_3$(Me$_2$NCH$_2$CH$_2$NMe$_2$)\}$_2$ (μ−Me$_2$NCH$_2$CH$_2$NMe$_2$)]Cl$_2$, (E)

The diamine N͡N (0.104 ml, 0.690 mmol) was added to a suspension of [WCl$_4$(PPh$_3$)$_2$] (0.196 g, 0.231 mmol) in toluene (*ca.* 25 ml) and the mixture was left stirred overnight at 65°C. The solution was filtered and the brown solid, (**E**), was washed by toluene (0.030 g, 0.060 mmol, 26% yield).

4.1.2 — PREPARATION OF COMPLEXES WITH THE ISO-CYANIDE LIGAND

Dichlorobis(methylisocyanide)(N,N,N',N'−tetrame-thyl−1,2−diamionethane) tungsten(II), [WCl$_2$(CNMe)$_2$(Me$_2$NCH$_2$CH$_2$NMe$_2$)], (G)

To a suspension of [WCl$_4$(PPh$_3$)$_2$] (0.214 g, 0.252 mmol) in thf (10 ml), sodium metal, methyl isocyanide (0.0474 ml, 1.0 mmol) and the diamine N͡N (0.0836 ml, 0.554 mmol) were added in this order. The solution was filtered after 1h, concentrated and crude complex (**G**) was obtained as a light green solid which was recrystallised from CH$_2$Cl$_2$//Et$_2$O (0.040 g, 0.074 mmol, 30% yield).

4.2 — REACTIONS OF WCl$_6$

Preparation of μ −[1,4−bis(4−methoxyphenyl)−1,4− −diazabutadiene] bis[pentachlorotungsten(V)], [(WCl$_5$)$_2$(μ−RNCHCHNR)] (R = 4−MeOPh), (H)

A solution of N͡N (0.37 g, 1.4 mmol) in CH$_2$Cl$_2$ (10 ml) and zinc amalgam (1.0 g) were added to a solution of WCl$_6$ (0.50 g, 1.3 mmol) in CH$_2$Cl$_2$ (15 ml). A dark brown suspension was formed which was left stirring overnight. The solution was filtered, concentrated under vacuo, and complex (**H**) precipitated as a dark brown solid (*ca.* 0.20 g, 32% yield) upon addition of ether and cooling at *ca.* −5°C. Decomposition occurred on attempted recrystallisation from CH$_2$Cl$_2$.

Preparation of μ−[1,4−bis(4−methoxyphenyl)−1,4− −diazabutadiene]bis[tetrachloro(methylisocyanide)tun-gsten(IV)], [\{WCl$_4$(CNMe)\}$_2$(μ−RNCHCHNR)] (R = 4−MeOPh), (I)

CNMe (0.090 ml, 1.9 mmol) was added to a suspension of complex (**H**) (0.30 g, 0.30 mmol) in thf (20 ml) and the mixture was refluxed for 2h. The resulting brown solid was then filtered off, recrystallised from CH$_2$Cl$_2$/Et$_2$O and dried under vacuum (**I**; 0.15 g, 60% yield).

Preparation of [1,4−bis(4−methoxyphenyl)−1,4− −diazabutadiene] tetrachlorotungsten(IV), [WCl$_4$(RNCHCHNR)] (R = 4−MeOPh), (J)

An excess of Zn/Hg (2.5 g) was added to a solution of WCl$_6$ (0.50 g, 1.3 mmol) and N͡N (0.50 g, 1.9 mmol) in CH$_2$Cl$_2$ (20 ml), and the mixture was stirred for 24 h. The resulting dark green solid with Zn/Hg was filtered off and the former was dissolved in thf; the resulting solution was filtered and a dark green solid (**J**, *ca.* 0.20 g, 37% yield) was obtained on concentration under vacuum, addition of diethylether and cooling to *ca.* −5°C.

Preparation of bis[μ—(N,N,N',N'—tetramethyl—1,2—
—diaminoethane)]bis[dichloro(N,N,N',N'—tetramethyl
—1,2—diaminoethane)tungsten(II)],
[\WCl₂(Me₂NCH₂CH₂NMe₂)}₂
(μ—Me₂NCH₂CH₂NMe₂)₂], (K), and di(μ—chloro)bis
[dichloro(N,N,N'N'—tetramethyl—1,2—diaminoethane)
tungsten(III)], [\WCl₂(Me₂NCH₂CH₂NMe₂)}₂(μ—Cl)₂], (L)

N͡N (2.0 ml, 13.3 mmol) was added to a solution of WCl₆(0.74 g, 1.9 mmol) in CH₂Cl₂ (15 ml), the mixture was stirred for 2 h and Zn/Hg (3 g) was then added. After 20 h the resulting greenish-brown solid was filtered off, washed with toluene, and dried under vacuum. Recrystallisation from CH₂Cl₂/Et₂O afforded complex (K) as a light brown solid (0.36 g, 40% yield).

The reaction mother liquor (filtered out the greenish-brown solid) was concentrated under vacuum and, upon addition of diethylether, a light brown solid separated out. It was filtered off, washed with toluene and dried under vacuum (L; 0.20 g, 26% yield).

Preparation of tris(N,N,N',N'—tetramethyl—1,2—
—diaminoethane) tungsten(III) trichloride,
[W(Me₂NCH₂CH₂NMe₂)₃]Cl₃, (M).

N͡N (2.0 ml, 13.3 mmol), solvent (CH₂Cl₂ and MeOH, 15 ml) and Zn/Hg (3 g) were added in this order to solid WCl₆ (1.5 g, 3.8 mmol) and the mixture was stirred for 2 h. The resulting light brown solid [complex(M)] was then filtered off,

washed with CH₂Cl₂ and dried under vacuum (*ca.* 1.4 g, 60% yield).

4.3 — REACTIONS OF [MoCl₃ (thf) ₃]

Preparation of bis[1,4—bis(4—methoxyphenyl)—1,4—
—diazabutadiene] dichloromolybdenum(II),
[MoCl₂(RNCHCHNR)₂](R=4—MeOPh), (D)

Sodium sand (0.10 g, 4.4 mmol) was added to a benzene (19 cm³) solution of N͡N (0.20 g, 0.74 mmol). The solution colour turned dark reddish-brown upon the addition of [MoCl₃(thf)₃] (0.15 g, 0.37 mmol) and, after a few minutes, a dark greenish suspension began to precipitate.

The suspension was left stirring overnight, the dark brown solution was then filtered, concentrated under vacuo, allowed to cool at *ca.* 5°C and complex (D) precipitated as a dark brown solid (0.14 g, 55% yield).

Preparation of μ—(N,N,N',N'—tetramethyl —1,2—
—diaminoethane)bis{trichloro(N,N,N'N'—tetramethyl—
—1,2—diaminoethane)molybdenum(III)},
[\MoCl₃(Me₂NCH₂CH₂NMe₂)}₂
(μ—Me₂NCH₂CH₂NMe₂)], (F)

Sodium sand (0.10 g, 4.4 mmol) was added to a thf (15 cm³) solution of [MoCl₃(thf)₃] (0.19 g, 0.46 mmol) and N͡N (0.25 ml, 1.7 mmol). The solution colour turned very dark brown. A very dark suspension started to form and after 2h the solution was filtered, concentrated *in vacuo*, and complex (F) precipitated as a brown solid (50 mg, 30% yield) upon addition of ether and cooling at *ca.*-10°C.

Table 1

Physical data for diazadiene or diamine complexes derived from [WCl₄(PPh₃)₂][a]

Complex	Colour	Infrared data[b]				μ_eff[c]	Microanalytical data[d]		
		ν(C≡N)	ν(C=N)	ν(W-Cl)	others	(B.M.)	%C	%H	%N
[WCl₂(N͡N)₂]Cl₂, (B)	Dark brown	—	1600 s,br 1500 s	240 w,br		3.0	37.6(37.1)	4.0(3.1)	7.7(7.5)
[WCl₂(N͡N)₂],C)	Dark brown	—	1590 s,br 1500 s,br	300 s,br		2.8	49.1(48.6)	4.0(4.1)	6.7(7.1)
[\WCl₃(N͡N)\₂(μ-N͡N)]Cl₂ (E)	Light brown	—	—	345 w,m 310 s,br	2560 m,br[e] 2450 s,br[e]	2.5	20.9(21.6)	4.4(4.8)	7.7(8.4)
[WCl₂(CNMe)₂(N͡N)], (G)[f]	Light green	2145 s	—	305 w,br		2.7	23.9(24.6)	4.5(4.5)	11.0(10.4)

[a] N͡N = (4-MeOPh)N = CHCH = N(4-MeOPh), N͡N = Me₂NCH₂CH₂NMe₂
[b] In Nujol mull. ν(C≡N) refers to ligating CNMe, whereas ν(C = N) refers to coordinated N͡N. [c] Values corrected for the diamagnetic contribution. [d] Calculated values in parenthesis. [e] Assigned to ν(C-H...Cl). [f] With CH₂Cl₂ of crystallisation.

Table 2
Physical data for diazadiene or diamine complexes derived from WCl_6[a]

Complex	Colour	Infrared data[b]				μ_{eff}[c] (B.M.)	Microanalytical data[d]		
		$\nu(C\equiv N)$	$\nu(C=N)$	$\nu(W\text{-}Cl)$	others		%C	%H	%N
$[(WCl_5)_2(\mu\text{-}N\frown N)]$, (**H**)[e]	Dark brown		1605 m,br 1575 m,br 1500 s,br	345 sh 332 s		1.4	21.0(20.3)	2.0(1.9)	3.0(2.6)
$[\{WCl_4(CNMe)\}_2(\mu\text{-}N\frown N)]$, (**I**)[f]	Brown	2220 m	1695 s 1630 s,br	305 sh 290 s,br		2.6	29.9(29.1)	3.3(3.1)	6.1(7.3)
$[WCl_4(N\frown N)]$, (**J**)[g]	Dark green		1600 s,br 1505 s,br	303 s,br 275 sh,br		—	30.0(30.1)	3.5(4.1)	3.3(2.7)
$[\{WCl_2(N\frown N)\}_2(\mu\text{-}N\frown N)_2]$, (**K**)	Light brown			290 s,br	2720 s[i] 2560 s[i] 2440 s[i]	—	30.6(29.9)	7.8(5.8)	10.6(11.6)
$[\{WCl_2(N\frown N)\}_2(\mu\text{-}Cl)_2]$, (**L**)[h]	Light brown			280 s,br	2705 s[i] 2560 s[i] 2440 s[i]	4.0	25.5(25.3)	5.9(4.5)	5.4(6.2)
$[W(N\frown N)_3]Cl_3$, (**M**)	Light brown				2620 s,br[i] 2570 s,br[i] 2450 s[i] 2410 sh[i]	3.5	34.7(34.1)	8.8(7.6)	13.1(13.3)

a), b), c), d) See notes a), b), c), d), for Table 1. [e] With $2CH_2Cl_2$ of crystallisation. [f] With thf of crystallisation. [g] With CH_2Cl_2 of crystallisation. [h] With $\frac{1}{2}C_6H_5CH_3$ of crystallization. [i] Ascribed to $\nu(C\text{-}H...Cl)$ (see text).

Table 3
Physical data for diazadiene and diamine complexes derived from $[MoCl_3(thf)_3]$[a]

Complex	Colour	Infrared data[b]			μ_{eff}[c] (B.M.)	Microanalytical data		
		$\nu(C=N)$	$\nu(Mo\text{-}Cl)$	others		%C	%H	%N
$[MoCl_2(N\frown N)_2]$, (**D**)	Dark brown	1595 m 1493 m,s	330 m		2.9	58.8(58.4)	4.7(4.9)	7.6(7.2)[d]
$[\{MoCl_3(N\frown N)\}_2(\mu\text{-}N\frown N)]$, (**F**)	Light brown	—	300 s 275 sh	2550 s,br[e] 2440 s,br[e]	3.6	29.0(28.7)	6.6(6.7)	10.9(11.2)

a), b), c) See notes a), b), c), for Table 1. [d] %Cl = 9.1(9.1). [e] Assigned to $\nu(C\text{-}H...Cl)$.

ACKNOWLEDGEMENTS

REFERENCES

[1] H. BOCK, H. TOM DIECK, *Chem. Ber.*, **100**, 228 (1967).

[2] H. VAN DER POEL, G. V. KOTEN, K. VRIEZE, *J. Organo-metallic Chem.*, **135**, C63 (1977).

[3] L. H. STAAL, D. J. STUFKENS, A. OSKAM, *Inorg. Chim. Acta*, **26**, 255 (1978).

[4] H. VAN DER POEL, G. V. KOTEN, K. VRIEZE, M. KOKKES, C. H. STAM, *J. Organometallic Chem.*, **175**, C21 (1979).

[5] H. Bock, H. tom Dieck, *Angew. Chem. Int. Ed. Engl.*, **5**, 521 (1966); H. tom Dieck, I. W. Renk, *Chem. Ber.*, **104**, 110 (1971); H. tom Dieck, I. W. Renk, *Chem. Ber.*, **105**, 1419 (1972).

[6] H. W. Frühauf, A. Landers, R. Goddard, C. Krüger, *Angew. Chem. Int. Ed. Engl.*, **17**, 64 (1978).

[7] H. tom Dieck, H. Bruder, K. Hellfeldt, A. Kinzel, J. Klaus, A. Lauer, B. Runge, M. Svoboda, *Proc. IX Intern. Conf. Organometallic Chem.*, S16, Dijon, France, 1979: H. tom Dieck, H. Bruder, *J. C. S. Chem. Comm.*, 24 (1977).

[8] A. J. L. Pombeiro, «Rections of Ligands Analogous to Dinitrogen in Dinitrogen-Binding Sites», *in* «New Trends in the Chemistry of Nitrogen Fixation», Ch.9, J. Chatt, L. M. C. Pina and R. L. Richards, eds., Academic Press, 1980.

[9] A. J. L. Pombeiro, R. L. Richards, *Transition Metal Chem.*, **6**, 255 (1981).

[10] B. Bell, J. Chatt, G. J. Leigh, *J. C. S. Dalton*, 2492 (1972).

[11] R. D. Green, «Hydrogen Bonding by C-H Groups», MacMillan, 1974.

[12] A. J. L. Pombeiro, «Preparation, Structure, Bonding and Reactivity of Dinitrogen Complexes», *in* «New Trends in the Chemistry of Nitrogen Fixation», Ch.6, J. Chatt, L. M. C. Pina and R. L. Richards, eds., Academic Press, 1980.

[13] H. tom Dieck, I. W. Renk, *Chem. Ber.*, **104**, 92 (1971).

[14] R. E. Schuster, J. E. Scott, J. Casanova, Jr., *Org. Synth.*, **46**, 75 (1966).

RESUMO

Clorocomplexos diazadiénicos e isonitrílicos de tungsténio em vários estados formais de oxidação.

Por reacções de WCl_6 ou $[WCl_4(PPh_3)_2]$ com o diazabutadieno $N\frown N = RN = CHCH = NR$ (sendo $R = 4-C_6H_4OMe$) ou a diamina $N\frown N = Me_2NCH_2CH_2NMe_2$ foi possível a preparação de vários clorocomplexos com estes ligandos (sob a forma quelante ou em ponte), apresentando-se o metal com estado formal de oxidação numa vasta gama (de $+5$ a $+2$).

As espécies $[(WCl_5)_2(\mu-N\frown N)]$, de $W(V)$, e $[WCl_4(N\frown N)]$, de $W(IV)$, foram obtidas por reacção de WCl_6 com $N\frown N$ na presença de amálgama de zinco, enquanto que os complexos de $W(IV)$, $[WCl_2(N\frown N)_2] Cl_2$ e $[\mid WCl_3(N\frown N)\mid_2(\mu-N\frown N)] Cl_2$ se formaram por reacções de substituição de $[WCl_4(PPh_3)_2]$; a espécie relacionável de molibdénio(III), $[\mid MoCl_3(N\frown N)\mid_2 (\mu-N\frown N)]$, foi obtida por reacção de $[MoCl_3(thf)_3]$ com $N\frown N$. Os compostos $[\mid WCl_2(N\frown N)\mid_2(\mu-Cl)_2]$ e $[W(N\frown N)_3] Cl_3$, de tungsténio(III), foram obtidos na redução de WCl_6 por amálgama de zinco na presença de um excesso de $N\frown N$.

Foi ainda obtida a redução a $W(II)$ nos complexos seguintes: $[\mid WCl_2(N\frown N)\mid_2(\mu-N\frown N)_2]$ preparado na redução de WCl_6 por amálgama de zinco na presença de $N\frown N$; $[WCl_2(N\frown N)_2]$ obtido na redução de $[WCl_4(PPh_3)_2]$ por magnésio na presença de $N\frown N \mid$ o complexo análogo de $Mo(II)$, $[MoCl_2(N\frown N)_2]$, foi também preparado por redução de $[MoCl_3(thf)_3]$ por sódio na presença de $N\frown N\mid$.

O metilisonitrilo pode também coordenar-se a estes centros metálicos, tendo o complexo de $W(IV)$, $[\mid WCl_4(CNMe)\mid_2 (\mu-N\frown N)]$, sido preparado na reacção de $[(WCl_5)_2(\mu-N\frown N)]$ com um excesso de $CNMe$. Foi também obtido um complexo isonitrílico de $W(II)$, $[WCl_2(CNMe)_2(N\frown N)]$, por reacção de $[WCl_4(PPh_3)_2]$ com $N\frown N$ na presença de $CNMe$ e areia de sódio.

32

M. JOAQUINA S. A. AMARAL TRIGO
M. ISABEL M. R. ESTEVES BARBEDO
M. ISABEL A. OLIVEIRA SANTOS
Centro de Investigação em Química
Faculdade de Ciências,
Universidade do Porto
4000 PORTO

ESTUDO DA SÍNTESE DE PÉPTIDOS SIMÉTRICOS, PROTEGIDOS, DE L-CISTINA E GLICINA

Descreve-se a síntese dos péptidos de L-cistina e glicina: N,N'-bis
(terc-butiloxicarbonil)-L-cistinil-bis (glicinato de etilo), N,N'-bis
(terc-butiloxicarbonil)-L-cistinil-bis(glicilglicinato de estilo) é
N,N'-bis*(terc-butiloxicarbonil-L-cistinil-bis(glicilglicilglicinato*
de etilo), pelos métodos de condensação da N,N'-dicicloexilcar-
bodiimida *e dos ésteres activados* o *e* p-nitrofenílicos.

No âmbito de um programa de síntese de péptidos cíclicos heterodéticos de L-cistina e glicina, começou-se por realizar um estudo preliminar de preparação de péptidos simples contendo aqueles aminoácidos, com o fim de seleccionar grupos de protecção e métodos de condensação.

Neste artigo descrevem-se os resultados obtidos nas experiências realizadas para a síntese de três péptidos simétricos, protegidos, de L-cistina e glicina de fórmula geral:

$$\begin{array}{c} \text{Boc-Cys-(Gly)}_n\text{-OEt} \\ | \\ \text{Boc-Cys-(Gly)}_n\text{-OEt} \end{array}$$
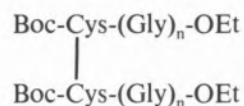
$$n = 1, 2 \text{ e } 3$$

Na síntese destes três péptidos usaram-se como «componente carboxílico» a N,N'-bis (*terc*-butiloxicarbonil)-L-cistina e como «componentes amino» os ésteres etílicos da glicina, da glicilglicina e da glicilglicilglicina, respectivamente para $n = 1$, 2 e 3. Utilizaram-se os métodos de condensação da N,N'-dicicloexilcarbodiimida e dos ésteres *para*-nitrofenílicos no caso dos três péptidos e, ainda, o método dos ésteres *orto*-nitrofenílicos no caso do péptido correspondente a $n = 1$.

Verificou-se que os rendimentos das reacções de condensação diminuem com o aumento do número de resíduos de glicina, especialmente, quando se passa de dois para três resíduos.

Nas condensações pelo método da N,N'-dicicloexilcarbodiimida verificou-se que a tendência para a formação de N-acilureias aumenta com a temperatura e com o número de resíduos de glicina; na purificação dos péptidos foi também difícil eliminar a contaminação da N,N'-dicicloexilureia. Em face destas dificuldades tentou-se a condensação pelo método dos ésteres nitrofenílicos que evita a presença dessas impurezas.

No entanto, só no caso do péptido correspondente a $n = 1$ o rendimento da condensação foi superior ao obtido pelo método da carbodiimida.

O método dos ésteres o-nitrofenílicos foi utilizado apenas no caso de $n = 1$, uma vez que se provou que não conduzia a melhores rendimentos que o dos ésteres p-nitrofenílicos.

No quadro seguinte apresenta-se um resumo dos resultados experimentais.

Quadro Resumo

Péptido	Método de condensação	Rendimento
[Boc-Çys-Gly-OEt]$_2$ p.f. 129-130°C [α]$_D^{24}$-112,5°(c 2,00 em MeOH)	N,N'-Dicicloexilcarbodiimida Ésteres p-nitrofenílicos Ésteres o-nitrofenílicos	56% 74% 56%
[Boc-Çys-(Gly)$_2$-OEt]$_2$ p.f. 120-122°C [α]$_D^{20}$-88,2°(c 2,00 em MeOH)	N,N'-Dicicloexilcarbodiimida Ésteres p-nitrofenílicos	42% 25%
[Boc-Çys-(Gly)$_3$-OEt]$_2$ p.f. 79-84°C	N,N'-Dicicloexilcarbodiimida Ésteres p-nitrofenílicos	5% 5%

PARTE EXPERIMENTAL

A pureza de todos os compostos foi confirmada por cromatografia em placa de Kieselgel 60 F$_{254}$ (Merck) nos quatro seguintes sistemas de solventes: clorofórmio-metanol (9:1), 1-butanol-ácido acético-água (4:1:5), piridina-ácido acético-água (1:2:2) e benzeno-clorofórmio-etanol(12:12:1). Os cromatogramas foram revelados pelo método ZIMIŃSKI e BOROWSKI [1] (com (NH$_4$)$_2$SO$_4$-H$_2$SO$_4$). As evaporações e concentrações foram efectuadas sob pressão reduzida em evaporador rotativo. Os extractos orgânicos foram secos sobre sulfato de magnésio anidro. O éter de petróleo usado refere-se à fracção p.e. 40-60°C. Os espectros de ressonância magnética nuclear foram registados a 33°C com espectrómetros Perkin--Elmer R32 90MHz e Varian 60 MHz. As microanálises foram efectuadas por Dr. Ilse Beetz (Kronach, Alemanha). As rotações ópticas foram medidas com um polarímetro Bellingham e Stanley Pepol 66.

N,N'-Bis(terc-butiloxicarbonil)-L-cistinato de bis(o--nitrofenilo)(I) [2].

Dissolveu-se N,N'-bis-Boc-L-cistina [3] (2,60g; 0,0059 mol) em acetato de etilo (43 ml). A esta solução arrefecida a −30°C, adicionou-se sucessivamente N,N'-dicicloexilcarbodiimida (2,43g; 0,0118 mol) em acetato de etilo (3 ml) e o-nitrofenol (1,65g; 0,0119 mol) dissolvido em acetato de etilo (3 ml). Deixou-se a mistura da reacção, com agitação mecânica, à temperatura de −20°C durante 48 horas e à temperatura ambiente durante 24 horas. Em seguida, filtrou-se a ureia e evaporou-se o filtrado, obtendo-se um óleo amarelado que cristalizou de acetato de etilo. Isolou-se 2,6g (64,7%) do éster de p.f. 140-144°C.

Por recristalização em acetato de etilo a ponto de fusão constante, obteve-se o N,N'-bis(terc-butiloxicarbonil)-L-cistinato de bis(o-nitrofenilo) (2,2g; 54,7%) de p.f. 145-150°C, [α]$_D^{24}$-162,7° (c 2,00 em MeOH), τ(CDCl$_3$) 1,87-2,01 (2H, d, C$_6$H$_4$); 2,25--2,82 (6H, complexo, C$_6$H$_4$); 4,45-4,75 (2H, d, NH); 4,95-5,30 (2H, complexo, CH); 6,38-6,94 (4H, complexo, CH$_2$); 8,43-8,80 (18H, s, Bu^t). (Encontrado: C−49,6; H−5,1; N−8,1; S−9,0. C$_{28}$H$_{34}$N$_4$O$_{12}$S$_2$ requer C−49,3; H−5,0; N−8,2; S−9,4%).

Cloreto de glicilglicilglicinato de etilo(II)

N-tritilglicina [4] foi condensada com cloreto de glicilglicinato de etilo [5] pelo método da N,N'-dicicloexilcarbodiimida, obtendo-se N-tritilglicilglicilglicinato de etilo (64%), p.f. 183-185,5°C (lit. [6] p.f. 185,5-186°C, preparado pelo método dos ésteres cianometílicos). O grupo tritilo foi removido por acção de HCl em etanol, obtendo-se o cloreto do tripéptido (81%), p.f. 208-209°C (decompondo-se desde 97°C), (lit. [7] p.f. 213-214°C com decomposição, obtido por reacção da 2-tio-5-tiazolidona com o cloreto de glicilglicinato de etilo na presença de trietilamina, seguida de acidificação).

N,N'-*Bis*(terc-*butiloxicarbonil*)-L-*cistinil-bis(glicinato de etilo)(III)*

A — Método da N,N'-dicicloexilcarbodiimida

A uma suspensão de N,N'-bis(terc-butiloxicarbonil)--L-cistina (4,40g; 0,01 mol) em diclorometano seco

(28 ml), arrefecida a 0°C e agitada magneticamente, adicionou-se DCCI (4,31g; 0,021 mol) em pequenas porções durante 25 minutos. Em seguida, juntou-se cloreto de glicinato de etilo [8] (2,80g; 0,02 mol) e trietilamina (2,02g; 0,02 mol). Deixou-se a mistura da reacção a 0°C durante 2 horas e à temperatura ambiente durante 65 horas. Filtrou-se a ureia e o cloreto de trietilamónio, adicionando-se ao filtrado ácido acético glacial (0,5 ml) a fim de eliminar os vestígios da DCCI. Após duas horas a 0°C filtrou-se a N,N'-dicicloexilureia, e o filtrado foi extraído, sucessivamente, com água, solução aquosa de ácido cítrico a 5%, solução aquosa de hidrogenocarbonato de sódio 1 M e água. A camada orgânica depois de seca (MgSO₄) foi evaporada e o resíduo obtido foi cristalizado de etanol dando 3,9g (63,9%) de composto de p.f. 126-127°C. O péptido assim obtido mostrou, por análise cromatográfica e de R.M.N., estar contaminado com N,N'-dicicloexilureia.

Dissolveu-se novamente o composto em acetona e, após 24 horas a 0°C, separou-se por filtração uma pequena quantidade de ureia. O filtrado foi evaporado à secura e o resíduo obtido foi submetido a várias cristalizações de etanol, obtendo-se o N,N'--bis(terc-butiloxicarbonil)-L-cistinil-bis(glicinato de etilo) (3,4g; 55,7%) de p.f. 129-130°C, $[\alpha]_D^{24}$-112,5° (c 2,00 em MeOH), $[\alpha]_D^{25}$-127,7° (c 0,40 em DMF), τ(CDCl₃) 1,80-2,10 (2H, t, NH); 4,30-4,60 (2H, d, NH); 4,90-5,30 (2H, complexo, CH); 5,60-6,30 (8H, complexo, CH₂); 6,70-7,17 (4H, d, SCH₂); 8,40-8,65 (18H, s, Buᵗ); 8,70-8,90 (6H, t, CH₃). (Encontrado: C-47,3; H-7,1; N-9,0; S-11,0. C₂₃H₄₂O₁₀N₄S₂ requer C-47,2; H-6,9; N-9,1; S-10,5%).

B — Método dos ésteres p-nitrofenílicos

A uma suspensão de cloreto de glicinato de etilo (0,56g; 0,004 mol) em diclorometano (20 ml), arrefecida num banho de acetona e neve carbónica e com agitação magnética, adicionou-se N,N'-bis(terc--butiloxicarbonil)-L-cistinato de bis(p-nitrofenilo) [9, 10] (1,37g; 0,002 mol) e trietilamina (0,40g; 0,004 mol) em diclorometano (10 ml).

Deixou-se então a mistura da reacção à temperatura ambiente, com agitação magnética, durante três dias. Em seguida extraiu-se a solução sucessivamente com água, solução aquosa de hidrogenocar-

bonato de sódio 1 M, ácido cítrico aquoso a 5% e solução aquosa saturada de cloreto de sódio. A camada orgânica, depois de seca (MgSO₄), foi evaporada à secura e o sólido obtido foi cristalizado de etanol, dando 0,9g (73,7%) do composto cristalino branco de p.f. 126-128°C.

Depois de uma recristalização de etanol e duas de acetato de etilo, o composto apresentava p.f. 129--130°C, $[\alpha]_D^{24}$-130,2° (c 0,50 em DMF), mostrando portanto ser idêntico ao N,N'-bis(terc-butiloxicarbonil)-L-cistinil-bis(glicinato de etilo) preparado pelo método da N,N'-dicicloexilcarbodiimida.

C — Método dos ésteres o-nitrofenílicos [2]

Efectuou-se a condensação do N,N'-bis(terc-butiloxicarbonil)-L-cistinato de bis(o-nitrofenilo) com o cloreto de glicinato de etilo, em condições de reacção idênticas às referidas para o composto III, método B. Obteve-se o péptido com o rendimento de 55,8% de p.f. 125-129°C, $[\alpha]_D^{24}$-133,5° (c 0,40 em DMF).

N,N'-Bis(terc-$butiloxicarbonil$-L-$cistinil$-bis(glicil-glicinato de etilo)(IV)

A — Método da N,N'-dicicloexilcarbodiimida

Este péptido foi preparado em condições análogas às referidas para o péptido III — método A. A purificação do composto foi conseguida por trituração do resíduo obtido com éter de petróleo seguida de três recristalizações de acetato de etilo. O rendimento da reacção foi de 42% de péptido puro de p.f. 120-122°C e $[\alpha]_D^{20}$-88,2° (c 2,00 em MeOH). τ[(CD₃)₂SO] 1,70-2,10 (4H, t, NH); 2,71-3,10 (2H, d, NH); 5,68-5,98 (4H, complexo, OCH₂); 5,98--6,30 (19H, complexo, CH e NCH₂); 6,50-6,89 (4H, d, SCH₂); 8,45-8,60 (18H, s, Buᵗ); 8,60-8,85 (6H, t, CH₃). (Encontrado: C—46,4; H—6,7; N—11,6; S—8,9. C₂₈H₄₈O₁₂N₆S₂ requer C—46,8; H—6,8; N—10,9; S—8,9%).

B — Método dos ésteres p-nitrofenílicos

Efectuou-se a condensação do N,N'-bis(terc-butiloxicarbonil)-L-cistinato de bis(p-nitrofenilo) com o cloreto de glicilglicinato de etilo, em condições de reacção idênticas às referidas para o composto III, método B.

Após cinco recristalizações de acetato de etilo obteve-se 25% do péptido puro, que por cromatografia e ponto de fusão mostrou ser idêntico ao péptido N,N'-bis(terc-butiloxicarbonil)-L-cistinil-bis((glicilglicinato de etilo) preparado pelo método da DCCI.

N,N'-*Bis(terc-butiloxicarbonil)-L-cistinil-bis(glicilglicilglicinato de etilo)(V)*

A — Método da N,N'-dicicloexilcarbodiimida

Realizou-se a condensação da N,N'-bis(terc-butiloxicarbonil)-L-cistina com o cloreto de glicilglicilglicinato de etilo nas condições referidas para o composto III, método A. Dado ter-se manifestado uma grande tendência para a formação de N-acilureia efectuou-se então a reacção a − 15°C durante quatro dias e à temperatura ambiente durante mais dois dias. Mesmo assim, o sólido obtido mostrava-se muito contaminado e resistiu a todas as tentativas de purificação por cristalização. Recorreu-se então à técnica de cromatografia em coluna para efectuar a separação dos componentes da mistura. O sólido obtido (1,3g) foi dissolvido em clorofórmio (3 ml) e aplicado a uma coluna de gel de sílica (<0,08 mm da Merck) (25g) de diâmetro interno 1,7 cm, correspondendo a um comprimento de cerca de 25 cm de enchimento. Usou-se pressão de azoto aplicada no topo da coluna para se conseguir uma velocidade de eluição conveniente.

Usaram-se na separação os seguintes solventes, sucessivamente:

a) Clorofórmio (550 ml) que separou os vestígios de ureia.

b) Clorofórmio-etanol (90:5) (160 ml) que permitiu separar as contaminações de $R_f(1) = 0,74$; 0,57 e 0,53.

c) Clorofórmio-etanol (90:10) (420 ml) que separou um composto de $R_f(1) = 0,47$ e vestígios de $R_f(1) = 0,99$; 0,81 e 0,53.

d) Clorofórmio-etanol (80:20) (70 ml) que separou o que nos pareceu ser o péptido (0,22g; 5,2%), de p.f. 79-84°C, $R_f(1) = 0,42$.

O péptido foi analisado por espectrometria de R.M.N. $\tau[(CD_3)_2SO]$ 1,70-2,07 (6H, complexo, NH); 2,80-3,10 (2H, d, NH); 5,60-6,00 (4H, q, OCH_2); 6,00-6,42 (14H, complexo, CH e NCH_2); 6,75-7,22 (4H, d, SCH_2); 8,50-8,95 (25H,

complexo, Bu^t e CH_3). (Encontrado: C-45,6; H-6,6; N-11,9; S-7,5. $C_{32}H_{54}O_{14}N_8S_2$ requer C-45,8; H-6,5; N-12,4; S-7,6%).

B — Método do ésteres p-nitrofenílicos

A condensação do N,N'-bis(terc-butiloxicarbonil-L--cistinato de bis(p-nitrofenilo) com o cloreto de glicilglicilglicinato de etilo foi realizada de modo idêntico ao descrito para o péptido III, método B.
O resíduo obtido mostrou-se muito contaminado tendo sido submetido a cromatografia em coluna de gel de sílica, de acordo com o processo usado na experiência anterior.
Isolou-se apenas 4,5% de composto idêntico ao péptido descrito nessa mesma experiência.

BIBLIOGRAFIA

[1] T. ZIMIŃSKI, E. BOROWSKI, *J. Chromatog.*, **23**, 480(1966).
[2] M. M. da R. DIAS, Seminário em Síntese Peptídica, Ano lectivo 1973/74, Faculdade de Ciências do Porto, Laboratório de Química, Porto, 1974.
[3] J. J. FERRARO, *Biochem. Prep.*, **13**, 39 (1971).
[4] G. AMIARD, R. HEYMÈS, L. VELLUZ, *Bull. Soc. chim. France*, 191 (1955).
[5] H. F. SCHOTT, J. B. LARKIN, L. B. ROCKLAND, M. S. DUNN, *J. Org. Chem.*, **12**, 490 (1947).
[6] R. SCHWYZER, B. ISELIN, W. RITTEL, P. SIEBER, *Helv. Chim. Acta.*, **39**, 872 (1956).
[7] A. H. COOK, A. L. LEVY, *J. Chem. Soc.*, 646 (1950).
[8] F. O. dos S. P. SERRÃO, «Síntese de Péptidos Assimétricos, Protegidos, da L-Cistina», Dissertação para doutoramento, Porto, 1960, pág. 194.
[9] E. ENGELS, «Diplomarbeit Tech. Hochschule», Aachen (1967).
[10] W. LUNKENHEIMER, H. ZAHN, *Annalen,* **740**, 1 (1970).

ABSTRACT

The syntheses of the peptides, N,N'-bis(t-butyloxycarbonyl)-L--cystinyl-bis(glycine ethyl ester), N,N'-bis(t-butyloxycarbonyl)-L--cystinyl-bis(glycylglycine ethyl ester) and N,N'-bis(t-bytyloxy-carbonyl)-L-cystinyl-bis(glycylglycylglycine ethyl ester) by using the N,N'-dicycloexylcarbodiimide, the o-and p-nitrophenyl esters condensation methods are described.

M. A. MORSI

Department of Chemistry
Faculty of Science
Elmansoura University
Elmansoura — Egypt

H. M. FAHMY
M. H. ELNAGDI
M. ABDEL AZZAM

Department of Chemistry
Faculty of Science
Cairo University
Egypt

EFFECT OF RING TYPE ON IONIZATION OF THE HYDRAZONO LINKAGE IN AQUEOUS MEDIA

The acid-base equilibria for a series of hydrazones in ethanolic aqueous media is reported and discussed through correlation of polarographic and potentiometric data.

1 — INTRODUCTION

It was generally accepted up till this last decade that phenylhydrazones are inactive in alkaline media. This inactivity was rationalized for by assuming hydrolysis of this linkage, or to the lack of hydrogen ions in these media which are considered a prerequisite for the reduction sequence and the general scheme suggested by LUND [1] for their electroreduction was followed. However, recently the results of several comprehensive papers showed [2,3,4], that in contrast to previously reported behaviour of these compounds, they may be reduced in both acid and alkaline media respectively depending on the degree of ionization of the NH of their $-C=N=NH$ linkage [5].

In connection, we report the polarographic and potentiometric data for compounds **I**, **II** and **III**

I, $R_1 = CN$ $R_2 =$
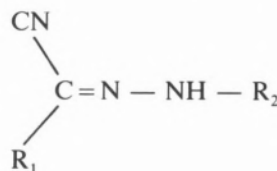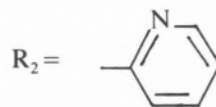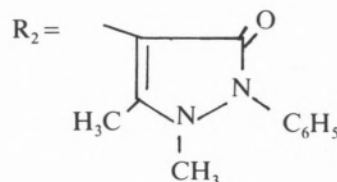
II, $R_1 = CN$ $R_2 =$

III, $R_1 = COOC_2H_5$ $R_2 =$
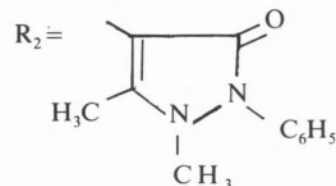
IV, $R_1 = CN$ $R_2 =$
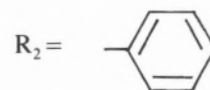
2 — EXPERIMENTAL

2.1 — ORGANIC SYNTHESES

Diazotized 4-aminoantipyrine (prepared from 0.1 mole of 4-amino antipyrine and the appropriate

quantities of concentrated hydrochloric acid and NaNO₂ as has been previously described [6] was added to a solution of 0.1 mole of malononitrile (**II**) or ethylcyano acetate (**III**) in ethanol (100 ml) containing sodium acetate (10.0 g). The solid product formed on standing was filtered and crystallized from ethanol.

The pyridin-3-yl azo derivative (**I**) was prepared by coupling diazotized 3-aminopyridine with malononitrile utilizing similar procedure.

The obtained compounds gave correct spectral data (IR, H¹NMR and MS) in excellent agreement with the proposed structures. These data together with their chemistry will be published in a separate communication now in preparation.

2.2 — POLAROGRAPHIC MEASUREMENTS

2.2.1 — APPARATUS

Polarograms were recorded with a pen type recorder E506 polarograph-Metrohm-Switzerland product. The capillary possessed the following characteristics in H_2O open circuit: $t = 5.1$ s/drop, $m = 1.49$ mg. s⁻¹ for $h = 40$ cm.

2.2.2 — SOLUTION

10^{-3}M stock solutions were prepared by dissolving an accurately weighed quantity of material in the appropriate volume of absolute ethanol. Britton-Robinson modified universal buffers [7] were used as supporting electrolyte.

2.2.3 — MEASUREMENTS

All experiments were carried at $25° \pm 2°C$; the half-wave potentials were measured graphically and expressed *versus* SCE with an accuracy of ± 0.005V.

2.2.4 — PROCEDURE

16 ml of buffer solution and 2 ml of ethanol were introduced into the polarographic cell. The mixture was then deaerated with H_2 gas for 12 minutes. 2 ml of 10^{-3} M depolarizer was then introduced into the cell so that the final concentration was 10^{-4} M in 20 ml of 20% (v/v) ethanolic buffer.

2.3 — DETERMINATION OF THE ACID DISSOCIATION CONSTANT

Potentiometric titrations were carried out using an electronically controlled syringe burette, Electroburex type in conjunction with automatic recording TAT-5 unit (Solea Tacussel-France) accurate to ± 0.01 pH unit. The pK_a values were conventionally calculated [8] from the registered graphs obtained by titrating a 10^{-3} M solution (30 ml; 1:4 $C_2H_5OH + H_2O$) of each compound.

3 — RESULTS AND DISCUSSION

The polarographic behaviour of compounds **I-III** are illustrated graphically in fig. 1, by **I**. As is clear the shift of $E_{1/2}$ with increase of pH is described by a straight line. At pH 9, $E_{1/2}$ is independent of any variation in pH. The i_1–pH plot shows a deep well defined dissociation curve. pK value (apparent
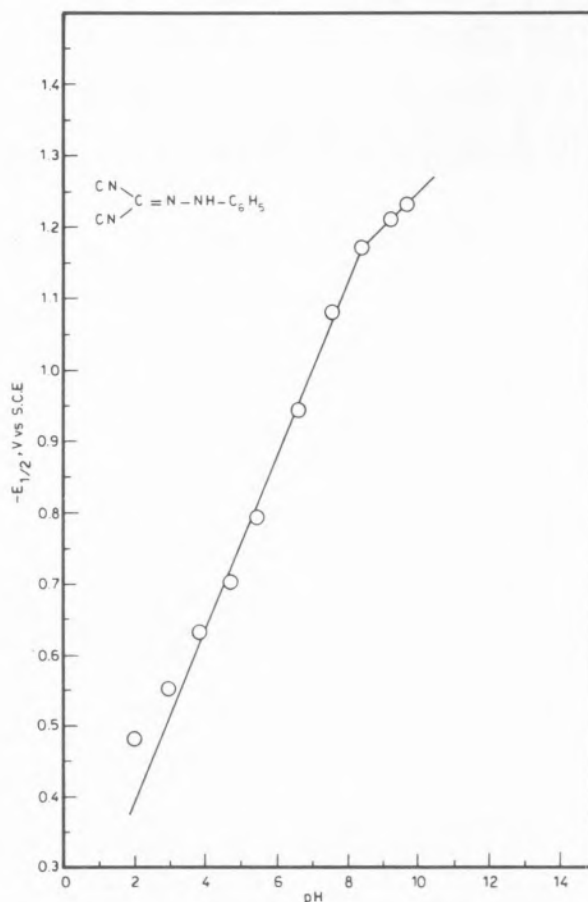
Fig. 1
$E_{1/2}$ — pH relation for compound **I**

dissociation constant) obtained from the i_l-pH plot, as the value of pH at $i_{lim}/2$, is in good agreement with that obtained by the intersection of the two segments of the $E_{1/2}$-pH plot [9]. The obtained dissociation curves assigned two main points whether these are strong acids or hydrolysed in alkaline media. Thus at this stage it was found mandatory to calculate the pK_a of such compounds which we assumed by similarity to arylhydrazonomesoxalonitrile [5] IV to be due to the ionization of NH of the hydrazonic linkage according to

$$\underset{CN}{\overset{CN}{\diagdown}}C=N-NH-R \rightleftharpoons \underset{CN}{\overset{CN}{\diagdown}}C=N-\overline{N}-R+H^+$$
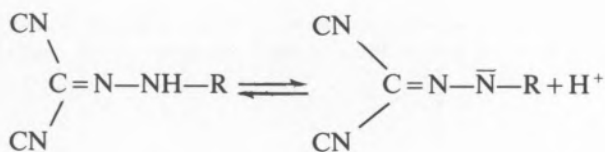
That these compounds are polarographically inert in alkaline medium is due to the fact that the negative charge is distributed over the whole molecule in a way that prevents further reduction. This type of behaviour is analogous to those of monobasic acids [10] and is represented by the following acid-base equilibrium,

$$HA \underset{k_r}{\overset{k_d}{\rightleftharpoons}} H^+ + A^- \qquad (1)$$

where the ratio k_d/k_r equals to K'.

From the difference between the polarographic and potentiometric pK's it is possible to calculate the value of the rate constant k_r using the following equation

$$\log k_r = 2 \ pK' - pK_1 - 2 \log 0.886 - \log t$$

and from k_r values one may obtain the appropriate theoretical curve using the following relation [10]

$$\frac{i_{HA}}{i_d} = \frac{0.886 \, (\frac{k_r t_1}{K_1})^{1/2} \, [H^+]}{1 + 0.886 \, (\frac{k_r t_1}{K_1})^{1/2} \, [H^+]}$$

From fig. 2 it is obvious that the theoretical curve is superimposed on the experimental results indicating that these compounds behave as acids with one ionizable center. At this point it was found
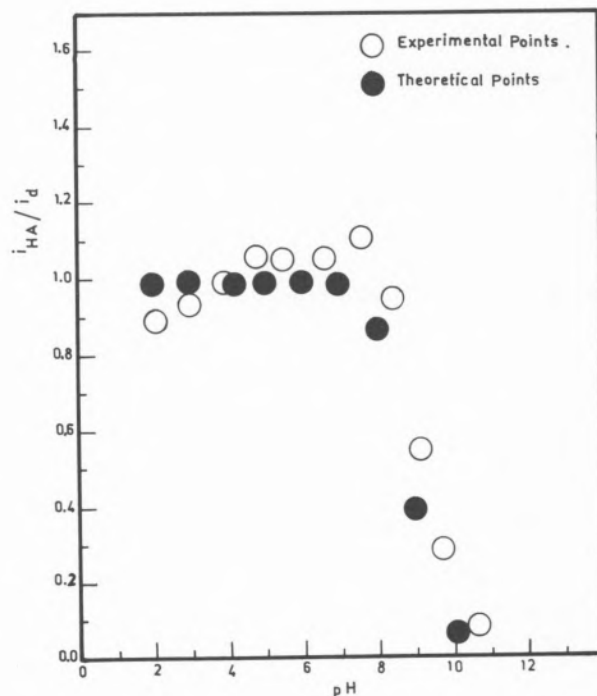
Fig. 2
Theoretical and experimental pH dependence of the limiting current i_{HA}/i_Avs. pH

worthwhile to investigate the effect of ring substitution on the ionization process. As is clear the variation of ring structure has no effect on the ionization of the NH group as reflected from the more or less constant values of pK_a and pK' of the compounds I, II and IV compiled in table 1 while when the substitution is in the carbon of the —C = N — NH linkage, compound III, the pK_a and pK' changed significantly indicating that substitution on the carbon of the hydrazone —C = N — NH — linkage has a straightforward effect on the ionization process in such molecules.

Table 1

Compound	$E_{1/2}$ *vs* pH (mV/pH)	pK	pK_a	$K_r/$ $mol^{-1}sec^{-1}$	k_d/sec^{-1}
I	$E_{1/2} = -0.160 - 0.117$ pH	9.20	6.00	9.84×10^{11}	9.84×10^5
II	$E_{1/2} = -0.305 - 0.098$ pH	9.20	5.90	7.82×10^{11}	9.84×10^5
III	$E_{1/2} = -0.235 - 0.101$ pH	10.10	7.20	3.92×10^{12}	2.47×10^5
IV*	$E_{1/2} = -0.570 - 0.076$ pH	9.20	6.23	4.90×10^{11}	2.90×10^5

* Data obtained for **IV** in 40% by volume ethanolic Britton-Robinson buffers [5].

REFERENCES

[1] H. LUND, *Acta Chem. Scand.*, **13**, 249 (1959).

[2] H. M. FAHMY, M. H. ELNAGDI, *J. Electroanal. Chimica Acta*, **23**, 255 (1978).

[3] M. H. ELNAGDI, H. M. FAHMY, *J. Electroanal. Chem.*, **84**, 149 (1977).

[4] H. M. FAHMY, M. H. ELNAGDI, *Electrochimica Acta*, **23**, 255 (1978).

[5] M. H. ELNAGDI, H. M. FAHMY, M. A. MORSI, *J. Electroanal. Chem.*, **68**, 237 (1976).

[6] G. T. MORGAN, J. REILLY, *J. Chem. Soc.*, **103**, 808 (1913).

[7] H. T. S. BRITTON, «Hydrogen Ions», Volume 1, Chapman and Hall, p. 365, 1955: *J. Chem. Soc.*, **458**, 1456 (1931).

[8] W. M. CLARK, «The Determination of Hydrogen Ion» Bailliers, Tindalad Cox; London, 3rd ed., pp. 22 and 528 (1928).

]9] J. KOUTECKY, *Collect. Czech. Chem. Commun.*, **18**, 587 (1953).

[10] P. ZUMAN, «The elucidation of organic electrode processes». Academic Press, London, Chapter 2, pp. 20-74 (1969).

RESUMO

Efeito do tipo de anel na ionização de hidrazonas em soluções aquosas.

Os equilíbrios ácido-base de uma série de hidrazonas em soluções em água + etanol são estudados por meio de polarografia e potenciometria.

V. M. JARDIM-BARRETO
J. J. C. TEIXEIRA-DIAS

University Chemical Laboratory
3000 Coimbra, Portugal

A FORCE FIELD CALCULATION AND VIBRATIONAL ANALYSIS OF METHYL ACETATE

Carboxylic esters present a number of difficulties in a force field calculation as the number of experimental data (fundamental frequencies) is generally insufficient to fully determine the calculated force constants. These include a large number of important interactions as the vibrational modes are strongly delocalized over the carbon-oxygen skeleton. Since little quantitative information concerning the assignments of the carbon-oxygen skeletal modes is yet available, we report in this work a force field refinement and a normal coordinates calculation for methyl acetate using previously published frequencies.

1 — INTRODUCTION

Besides the mathematical difficulties which can arise in the force constant refinement procedure and are described and discussed in [1], the calculation of force constants in large molecules (molecules for which it is not possible to accumulate as many independent experimental data as force constants included in the potential function) relies very much on (i) well known geometrical parameters; (ii) complete and secured vibrational assignments of all fundamental modes and (iii) the possibility of transferring, from chemically similar species, well established force constants.

In order to obtain a unique molecular force field, the observed frequencies of a suficient number of isotopically labelled species have to be included in the calculation and simultaneously processed through the least squares refinement procedure. Besides increasing the computation time, this procedure has to be exercised with care for the reasons stated in [2]. In fact, the least squares force field refinement minimizes the weighted sum of the squares of the residual deviations $\delta\lambda_i = \lambda_i^{calc} - \lambda_i^{obs}$, where the vibrational eigenvalues λ_i are directly proportional to the squares of the harmonic frequencies ($\lambda_i \propto \omega_i^2$) and the summation extends over the deviations of the available experimental frequencies for the isotopically labelled species. Now, the observed values of λ_i are usually taken directly from the anharmonic experimental frequencies and include anharmonic corrections which may lead to conflicting consistent errors in the least squares refinement in so far as they are not conform to the product rule relations which are normally built in the programs. In particular, the inclusion of both CH and CD stretchings bring in large anharmonic corrections and may prevent from obtaining a converged least squares solution.

In this paper we present a calculation of a force field for the methyl acetate molecule and discuss the results on the light of existing experimental data on several deuterated species as well as of previously established assignments. Our primary objective is not to obtain a unique force field for the methyl acetate molecule but to simply present a set of force constants which can be used as a set of spectroscopically useful parameters for a quantitive assignment of the skeletal modes of the ester group in basic agreement

with previously established empirical assignments [3,4]. Starting with a previously determined force field for the ester group [5] we proceeded with a refinement for the CH_3COOCH_3 isotopic species. The resulting force field allows a good fitting of the ester group frequencies and conforms to the previously established assignments for methyl acetate [3,4,6]. The subsequent calculation of harmonic frequencies for the deuterated species shows a good fitting of the skeletal observed frequencies and further confirms the existence of large and conflicting anharmonic errors if CH_3 and CD_3 stretching and angular deformation frequencies are inclued in the refinement [2,7].

The type of approximate force field we adopt in these calculations is the simplified general valence force field. This form of the general valence force field contains a reduced number of interaction constants compatible with a good fit of the vibrational fundamental frequencies. While the arbitrariness in choosing force constants is reduced in a Urey-Bradley type of force field, the frequency fit is frequently not as good and the interaction constants often keep features of an arbitrary nature [8 and references therein]. We have decided to use the more powerful general valence force field. However, under the above mentioned conditions, the calculated force fields cannot claim uniqueness, thus loosing, to some extent, the useful feature of transferability among chemically related compounds. Under these circumstances, the physical meaning of the force constants is partially lost and they restrict themselves to the role of spectroscopic parameters which simply enable us to interpret the vibrational spectra.

2 — RESULTS AND DISCUSSION

The computer programs used to perform the normal coordinates analysis were adapted to a Univac Sigma 5 computer system from [9], and consist of three programs: CART which converts molecular structural parameters to cartesian coordinates; GMAT which sets up the kinetic energy matrix and FPERT which calculates and refines the force constants using the least squares method.

The conformation chosen for methyl acetate was based on the structure of methyl formate [10] whose carbon-oxygen skeleton is planar, with the methyl group of the methoxyl moiety *cis* with respect to the carbonyl oxygen [10,11]. Both methyl groups were assumed to have tetrahedral angles and the CH bond length was fixed at the value indicated in [10]. A list of these parameters is shown in Table 1.

Table 2 shows the definition of internal coordinates for methyl acetate. Apart from the usual changes in bond lengths and bond angles we have included three torsion coordinates around the C-C, C-O and O-C bonds and an out-of-plane wagging coordinate for $C=O$ [12].

Before starting the calculation of force constants it is necessary to eliminate any redundant coordinates. In the case of methyl acetate, the internal coordi-

s-cis
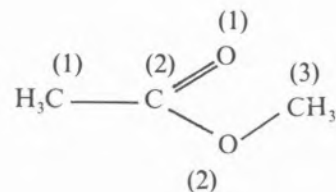
Fig. 1

The s-cis conformation of methyl acetate

Table 1

Geometrical parameters for methyl acetate [10]*

Bond lengths in $\overset{\circ}{A}$:

C_1-C_2	1.515
C_2-O_1	1.200
C_2-O_2	1.334
O_2-C_3	1.437
C -H	1.086

Bond angles in degrees:

$\sphericalangle C_1C_2O_1$	124.83
$\sphericalangle C_1C_2O_2$	110.30
$\sphericalangle O_1C_2O_2$	124.87
$\sphericalangle C_2O_2C_3$	114.78
$\sphericalangle HCH = \sphericalangle \ HC_1C_2 = \sphericalangle HC_3O_2$	109.47

* Nomenclature as in fig. 1.

Table 2
Definition of internal coordinates *

Skeleton:	CH_3-C:
$r_1 = \Delta(C_1C_2)$	$s_i = \Delta(C_1\text{-}H_i)$
$r_2 = \Delta(C_2\text{-}O_1)$	$\alpha_i = \Delta(\sphericalangle H_jC_1H_k)\, j,k \neq i$
$r_3 = \Delta(C_2\text{-}O_2)$	$\beta_i = \Delta(\sphericalangle H_iC_1C_2)$
$r_4 = \Delta(O_2\text{-}C_3)$	$\tau(C_1C_2) = $ torsion around C_1C_2
$\varepsilon = \Delta(\sphericalangle C_1C_2O_1)$	CH_3-O:
$\gamma = \Delta(\sphericalangle O_1C_2X_2)$	$s_i^! = \Delta(C_3\text{-}H_i)$
$\delta = \Delta(\sphericalangle C_1C_2O_2)$	$\alpha_i^! = \Delta(\sphericalangle H_jC_3H_k)\, j,k \neq i$
$\omega = \Delta(\sphericalangle C_2O_2C_3)$	$\beta_i^! = \Delta(\sphericalangle H_iC_3X_2)$
$\tau(C_2O_2) = $ torsion around C_2O_2	$\tau(O_2C_3) = $ torsion around O_2C_3
$\zeta = $ Out-of-plane of O_1	

* Atoms numbering as in fig. 1.

nates we have defined exceed the number of vibrational degrees of freedom $(3N-6 = 27)$ in three. One can separate the redundant coordinates by taking linear combinations of the above mentioned bending coordinates so that three of them correspond to the sums of the bond angle changes around the atom centres where three or more bonds are coincident (these sums are identically zero). Table 3 shows the new set of internal coodinates grouped in a vector array S. In this system of coordinates, all the diagonal and off-diagonal force constants which involve any identically zero S coordinate are not included in the force field as they refer to non--existent coordinates. If any of these zero force constants were transformed back to the initial set of internal coordinates (R), one would obtain linear re-

lationships among the $F_{R_iR_j}$ force constants. Hence, by eliminating the redundant coordinates we no longer need to artificially add those constraints into the force field refinement.

Another remark about the definition of our S coordinates is necessary as we did not use the molecular symetry group (C_s) and preferred instead the highest local symmetry coordinates consistent with the methyl group $(C_{3v}$ symmetry). While the particular choice of any linear and orthogonal transformation among the basis coordinates is irrelevant as regards to the calculated eigenvalues and to the information contained in the final PED matrix, our seems to be justified as we are mainly fitting vibrational frequencies taken from condensed phases spectra and both methyl groups should be considered, for that purpose, to be axially symmetric around the C-C and O-C bonds. In fact, the barrier to internal rotation of the methyl group in the methoxyl moiety was found to be approximately 1.2 kcal/mole [10,4] and the value for the potential barrier around the C-methyl bond should even be smaller judging by its value in acetic acid (0.5 kcal/mole) [13] from which it should not differ much, anyway. Moreover, the primary objective of this work is to vibrationally analyse the carbon-oxygen skeleton of the molecule rather than to accurately reproduce the observed vibrational frequencies of the entire molecule, let alone the torsional motions occurring at low frequencies [14,15].

Since all the symmetrically identical elements of the

Table 3
Definition of a new set of internal coordinates and their approximate description (*)

Skeleton		CH_3—C		CH_3—O	
$S_1 = r_1$	s	$S_8 = (1/\sqrt{3})(s_1+s_2+s_3)$	ss	$S_{16} = (1/\sqrt{3})(s_1^!+s_2^!+s_3^!)$	ss
$S_2 = r_2$	s	$S_9 = (1/\sqrt{6})(2s_1-s_2-s_3)$	as	$S_{17} = (1/\sqrt{6})(2s_1^!-s_2^!-s_3^!)$	as
$S_3 = r_3$	s	$S_{10} = (1/\sqrt{2})(s_2-s_3)$	as	$S_{18} = (1/\sqrt{2})(s_2^!-s_3^!)$	as
$S_4 = r_4$	s	$S_{11} = (1/\sqrt{6})(\alpha_1+\alpha_2+\alpha_3-\beta_1-\beta_2-\beta_3)$	sb	$S_{19} = (1/\sqrt{6})(\alpha_1^!+\alpha_2^!+\alpha_3^!-\beta_1^!-\beta_2^!-\beta_3^!)$	sb
$S_5 = (1/\sqrt{6})(2\gamma-\varepsilon-\delta)$	b	$S_{12} = (1/\sqrt{6})(2\alpha_1-\alpha_2-\alpha_3)$	ab	$S_{20} = (1/\sqrt{6})(2\alpha_1^!-\alpha_2^!-\alpha_3^!)$	ab
$S_6 = (1/\sqrt{2})(\delta-\varepsilon)$	b	$S_{13} = (1/\sqrt{6})(2\beta_1-\beta_2-\beta_3)$	r	$S_{21} = (1/\sqrt{6})(2\beta_1^!-\beta_2^!-\beta_3^!)$	r
$S_7 = \omega$	b	$S_{14} = (1/\sqrt{2})(\alpha_2-\alpha_3)$	ab	$S_{22} = (1/\sqrt{2})(\alpha_2^!-\alpha_3^!)$	ab
$S_{25} = \tau(C_2O_2)$	t	$S_{15} = (1/\sqrt{2})(\beta_2-\beta_3)$	r	$S_{23} = (1/\sqrt{2})(\beta_2^!-\beta_3^!)$	r
$S_{27} = \zeta$	ω	$S_{24} = \tau(C_1C_2)$	t	$S_{26} = \tau(O_2C_3)$	t

(*) s = stretch; b = bend; t = torsion; w = wag; r = rock; whenever two letters are used the first stands for «symmetric» (s) or«antisymmetric» (a).
As the numbering of the coordinates is arbitrary, we follow the sequence set up for the computer calculation where the torsion and the out-of--plane coordinates were numbered last. However, for the purpose of this calculation, the skeletal and methyl coordinates are herein grouped under different headings.

F matrix must be changed in the same manner during the refinement, it is convenient to store the force field as a linear array of force constants ϕ and build the F matrix from the elements of ϕ by means of matrices Z, according to

$$F = \Sigma_i \, \phi_i Z^i,$$

where ϕ_i is the ith element of ϕ and Z^i is the ith Z matrix which specifies the positions of the element ϕ_i in the final F matrix [16]. Besides all the off-diagonal elements relative to the in-plane coordinates of the carbon-oxygen skeleton, we have also included the off-diagonal interactions $F_{S_1 S_{11}}$ and $F_{S_4 S_{19}}$. This corresponds to having ignored in [8] the off-diagonal interactions which are not consistent with the hypothesis of free internal rotations of the methyl groups. The simplicity of our force field as regards to the alkyl groups and, in particular, to the interaction elements coupling the ester and alkyl groups should not significantly affect the conclusions withdrawn for the ester group vibrations.

Table 4
Calculated valence force constants for methyl acetate

Diagonal force constants Skeleton		Off-diagonal force constants Skeleton-skeleton interactions	
(1,1)	4.0060	(1,2)	0.3875
(2,2)	11.5364	(1,3)	0.4140
(3,3)	6.2762	(1,4)	0.2137
(4,4)	5.4504	(1,5)	-0.4341
(5,5)	1.1682	(1,6)	-0.0878
(6,6)	1.0027	(1,7)	0.2183
(7,7)	0.6185	(2,3)	0.4840
(25,25)	0.6236	(2,4)	-0.0312
(27,27)	0.3589	(2,5)	0.2253
CH₃-C		(2,6)	-0.3498
		(2,7)	-0.1819
(8,8)	4.9781	(3,4)	0.3885
(9,9) = (10,10)	4.7804	(3,5)	0.2859
(11,11)	0.5450	(3,6)	0.1701
(12,12) = (14,14)	0.5092	(3,7)	-0.1472
(13,13) = (15,15)	0.6727	(4,5)	-0.2461
(24,24)	0.0716	(4,6)	0.0816
		(4,7)	0.2254
CH₃-O		(5,6)	0.1444
(16,16)	5.0447	(5,7)	0.0375
(17,17) = (18,18)	4.9088	(6,7)	0.1370
(19,19)	0.5690		
(20,20) = (22,22)	0.4577	Skeleton-methyl interactions	
(21,21) = (23,23)	1.1013	(1,11)	-0.1729
(26,26)	0.0029	(4,19)	-0.1667

Table 5
Observed and calculated frequencies (cm⁻¹) and approximate potential energy distribution for CH₃COOCH₃ (*)

ν_{obs} [4]	ν_{cal}	Potential energy distribution
3040	3040	$S_{17}(73), S_{18}(26)$
—	3040	$S_{17}(26), S_{18}(73)$
3000	3000	$S_9(99)$
—	2999	$S_{10}(99)$
2961	2961	$S_{16}(100)$
2940	2940	$S_8(100)$
1771	1771	$S_2(83), S_3(15)$
1467	1481	$S_{23}(44), S_{20}(36), S_{21}(15)$
1459	1471	$S_{21}(43), S_{22}(42), S_{23}(14)$
1446	1456	$S_{12}(66), S_{14}(22)$
1439	1439	$S_{19}(89), S_4(19)$
1439	1431	$S_{14}(69), S_{12}(23)$
1378	1378	$S_{11}(98)$
1275	1277	$S_{20}(35), S_3(34), S_1(10)$
1246	1220	$S_{22}(57), S_{21}(30), S_{23}(10)$
1194	1185	$S_{20}(28), S_{23}(22), S_3(18), S_5(13), S_1(12)$
1058	1058	$S_4(65), S_{13}(17)$
1058	1057	$S_{15}(86)$
976	978	$S_{13}(60), S_4(13), S_1(10)$
842	840	$S_1(50), S_3(14), S_5(18)$
634	633	$S_5(51), S_1(14)$
525	529	$S_{27}(77), S_{25}(12)$
427	427	$S_6(66)$
295	317	$S_{25}(82), S_{27}(11)$
203	202	$S_7(86), S_6(18), S_5(11)$ b)
—	189	$S_{24}(86)$
40 a)	40	$S_{26}(100)$

(*) PED contributions less than 10% were ignored.

a) From [15].

b) The off-diagonal element $S_6 S_7$ has a large negative contribution (-14%).

The calculated valence force constants are reported in Table 4 and the observed and calculated frequencies and their potential energy distribution for CH₃COOCH₃ are shown in Table 5. The conclusions from the potential energy distribution are summarised in the assignments given in Table 6 for the skeletal modes of all the isotopic labelled species. Comparision of the results reported in [5] with those of Table 5 reveals the importance of including the methyl vibrational modes for the study of the skeletal modes. In fact, there is an appreciable distribution of potential energy among the methyl and skeletal modes in a large number of vibrations despite the fact that the force constants of the methyl groups are restricted to diagonal elements with only two off-diagonal elements

Table 6
Calculated frequencies (cm^{-1}) and vibrational assignments for the skeletal modes
of CH$_3$COOCH$_3$ and its deuterated species

CH$_3$COOCH$_3$	CH$_3$COOCD$_3$	CD$_3$COOCH$_3$	CD$_3$COOCD$_3$	
1771	1770	1767	1766	C = O stretching
1277	1276	1276	1274	C-O stretching
1058	— a)	1040	— a)	O-CH$_3$ stretching
840	809	805	791	C-C stretching
633	624	588	582	O = C-O bend
529	528	486	486	C = O out-of-plane wag
427	416	396	385	CH$_3$-C in-plane wag
317	293	309	285	Torsion around C-O
202	189	198	182	C-O-C bend
189	186	138	138	Torsion around C-C
40	30	40	29	Torsion around O-CH$_3$

a) For these isotopic species a strong mixture of O-CH$_3$ stretching and umbrella motion ($\tilde{>}$ 40%) raises these frequencies to 1225 cm^{-1}
(CH$_3$COOCD$_3$) and 1223 cm^{-1} (CD$_3$COOCD$_3$).

coupling the skeleton and methyl vibrational coordinates. The assignments of Table 5 and 6 agree in general terms with those of Table 5 in [4], in particular for the skeletal modes which have a large number of force constants. However, it should be mentioned that the assignments of the CH$_3$-C and CH$_3$-O stretching in [4] should be interchanged as they do not agree either with the intensity features described in the text and shown in Tables 1-4 of the same paper or with the assignments reported in [3] and [6]. Taking this correction into consideration then the assignments shown in Table 6 show general agreement with those of [4] with the exception of the calculated frequency at 1277 cm^{-1} which deviates markedly from the observed value at 1246 cm^{-1} empirically assigned to the C-O stretching mode [3,4, 6]. Among the skeletal deformation modes, the observed bands at 295 cm^{-1} and 203 cm^{-1} [4] have been assigned to the torsion around the C-O bond and the C-O-C bend, respectively, although these assignments may still have some degree of uncertainty.

Having restricted this calculation to the methyl acetate molecule with a reduced number of interaction constants compatible with a good fit of the vibrational fundamental frequencies, the resulting force field cannot claim uniqueness, thus loosing, to some extent, the feature of transferability among chemical related compounds. While this aspect of a force field calculation is not decisive on its quality, it is useful on the descritive and chemical point of view and has been recently considered in [17] for a

series of molecules containing C = O groups, including pyruvic acid, acetone, acetic acid, methyl acetate, formic acid and methyl formate.

Ackowledgements

REFERENCES

[1] J. ALDOUS, I. M. MILLS, *Sprectrochim. Acta,* **18,** 1073 (1962); *ibid,* **19,** 1567 (1963).

[2] K. G. KIDD, H. H. MANTSCH, *J. Molec. Spectrosc.,* **85,** 375 (1981).

[3] J. K. WILMSHURST, *J. Molec. Spectrosc.,* **1,** 201 (1957).

[4] W. O. GEORGE, T. E. HOUSTON, W. C. HARRIS, *Spectrochim. Acta,* **30A,** 1035 (1974).

[5] P. MATZKE, O. CHACÓN, C. ANDRADE, *J. Molec. Structure,* **9,** 255 (1971).

[6] R. M. MORAVIE, J. CORSET, *J. Molec. Structure,* **30,** 113 (1976).

[7] G. E. HANSEN, D. M. DENNISON, *J. Chem. Phys.,* **20,** 313 (1952).

[8] H. SUSI, J. R. SCHERER, *Spectrochim. Acta,* **25A,** 1243, (1969).

[9] H. Fuhrer, V. B. Kartha, K. G. Kidd, P. J. Krueger, H. H. Mantsch, *National Research Council of Canada Bulletin* N.º 15, (1976).

[10] R. F. Curl, Jr., *J. Chem. Phys.*, **30**, 1529 (1959).

[11] W. C. Harris, D. A. Coe, W. O. George, *Spectrochim. Acta,* **32A**, 1 (1976).

[12] J. C. Decius, *J. Chem. Phys.*, **17**, 1315 (1949).

[13] W. J. Tabor, *J. Chem. Phys.*, **27**, 974 (1957).

[14] T. Miyazawa, *Bul. Chem. Soc. Jp.*, **34**, 691 (1961).

[15] E. Knözinger, *Ber. Bunsenges. Physik. Chem.*, **78**, 1199 (1974).

[16] I. W. Levin, R. A. R. Pearce, in *Vibrational Spectra and Structure,* 101, 1975, (J. R. Durig, ed.).

[17] H. Hollenstein, Hs. H. Gunthard, *J. Molec. Spectrosc.*, **84**, 457 (1980).

RESUMO

Cálculo de constantes de força e análise vibracional do acetato de metilo.

Os ésteres carboxílicos apresentam um certo número de dificuldades no cálculo das suas constantes de força devido ao facto do número de dados experimentais (frequências fundamentais) ser geralmente insuficiente para determinar completamente as constantes de força a calcular. Estas incluem um grande número de interacções importantes dado que os modos vibracionais estão fortemente deslocalizados no grupo éster. Este trabalho surge em virtude de apenas existir reduzida informação quantitativa relativa aos modos vibracionais dos ésteres carboxílicos e descreve uma optimização de constantes de força e um cálculo de coordenadas normais para a molécula de acetato de metilo partindo das frequências previamente publicadas.

M. A. FORTES

Centro de Mecânica e Materiais (CEMUL)
Departamento de Metalurgia
Instituto Superior Técnico
1000 Lisboa

ALTERNATIVE EQUILIBRIUM CONFIGURATIONS OF THE INTERFACE BETWEEN TWO FLUIDS IN CONTACT WITH SOLIDS

A cylindrically symmetric system comprising two immiscible fluids placed between two identical parallel plates is analysed for the possible equilibrium configurations of the fluid interface. The configurations include bridges, attached «drops» and isolated «drops» and multiply connected combinations of these. After determining the geometrical properties and the Helmholtz energy of each configuration, the stability of the various configurations is discussed and the transitions between them, as the stability limits are overshoot, are predicted.

1 — INTRODUCTION

The equilibrium shape of the interface between two immiscible fluids acted by externally applied fields is the solution of Young-Laplace differential equation [1,2] that satisfies the specific conditions of each particular problem. Usually these conditions are the given volume of the fluid enclosed by the interface and boundary conditions for the interface. Two types of boundary conditions can be distinguished: i) geometrical and ii) contact angle conditions. Examples of the first type are the boundary conditions at the apex and at the line of contact of a drop hanging from a tube of given radius. Contact angle conditions appear, for example, in liquid bridges between two spheres or two indefinite plates and in drops hanging from a ceiling. These latter conditions are in fact necessary for equilibrium [2] but are generally introduced as boundary conditions for the interface.

Particularly when solid bodies of a given geometry are present, there may be alternative equilibrium configurations for the fluid interface, each with specific boundary conditions. It is also possible *(e.g.,* in pendent drops [3]) that more than one equilibrium configuration is compatible with the imposed conditions (volume and boundary conditions). As the geometrical parameters of the system (that is, the position of the solid bodies or the volume of fluid, if this regarded as a variable parameter) are allowed to change, it generally happens that a particular set of boundary conditions can only be fulfilled for values of the parameters within a certain interval.

Problems on equilibrium shapes of interfaces are usually discussed for a particular type of boundary conditions, without allowance for alternative conditions *(e.g.,* [3-7]). But an actual two fluid system comprising solids of a given geometry may frequently admit multiple equilibrium configurations, each with specific boundary conditions. This possibility may change the stability limits of a particular type of configuration [8]. In addition, no attention is generally given to the change in configuration that necessarily occurs when the geometrical parameters overshoot the permissible interval for a particular set of boundary conditions. This is essentially a dynamical problem but, as will be shown,

predictions on the final configuration can be made based on equilibrium properties.

This paper contains a detailed study of the alternative configurations of the interface between two fluids bounded by two identical plates symmetrically placed. To make the calculations easiest, a cylindrically symmetric geometry is assumed, in the absence of applied fields. The cross-section of the fluid interface is then circular, provided the fluid interfacial tension, γ, is independent of position in the interface [2]. The contact angle, θ_c, of fluid 1 with the plates (in presence of fluid 2) will be taken as a characteristic of the system, and is given by Young's equation [1,2]

$$\cos\theta_c = \frac{\gamma_2 - \gamma_1}{\gamma} \qquad (1)$$

where γ_1, γ_2 are the solid-fluid interfacial tensions. It will be assumed that the ratio in the second term of equation (1) is in the interval [-1,1], so that θ_c has a well defined value.

The system to be studied is not easy to reproduce experimentally, but the approach developed can also be applied to more common situations, particularly to axially symmetric interfaces in a gravitational field [9], and to predict the distribution of liquid in wetted powders such as those used in liquid phase sintering [10].

2 — ALTERNATIVE EQUILIBRIUM CONFIGURATIONS

The fluid enclosed by the interface and plates will be denoted by fluid 1. The other fluid, 2, is the surrounding fluid. Only configurations with fluid 2 as the surrounding fluid will be considered. The volumes of both fluids are fixed. If allowance is made for the fragmentation of fluid 1 in several non-connected volumes, a large variety of configurations will be possible. We shall consider at this stage the «elementary» configurations, which can be classified into three groups: bridges, attached drops and isolated drops or i-drops. Examples are given in fig. 1. In the first two cases, the interface may contact the plates either at their edge or within the plates. These two configurations will be termed r- and θ_c- configurations, respectively. Therefore, the elementary configurations are: r-brides, θ_c-brid-
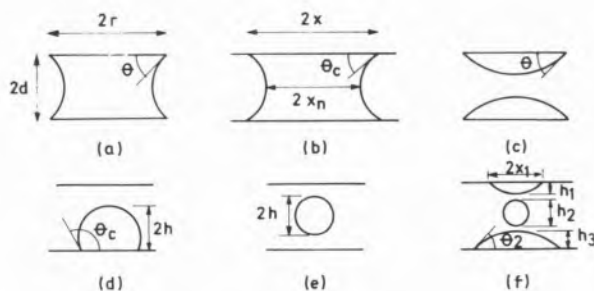
Fig. 1

Different types of equilibrium configurations with cylindrical symmetry: a) r-bridge; b) θ_c-bridge; c) two equal attached r-drops; d) one attached θ_c-drop; e) one isolated or i-drop; f) triply connected configuration with two θ_c-drops and an i-drop symmetrically placed

ges, r-drops, θ_c-drops and i-drops. We shall discuss in greater detail bridge configurations and triply connected configurations comprising two attached drops and an i-drop placed as shown in fig. 1f. Multiply connected θ_c-bridges and more complex configurations will not be treated explicity.

3 — GEOMETRICAL PARAMETERS, HELMHOLTZ ENERGY AND FORCE OF ADHESION

Let 2V be the volume of fluid 1 per unit length of the system, θ_c its contact angle with the plates, 2r and 2d, respectively, the plate width and separation. We calculate, for each of the configurations referred to above, the width 2x of the interface at the plates (in θ_c-configurations), the total heigth 2h perpendicular to the plates (for drops) and the Helmholtz energy 2A per unit length of the system. This is the sum of the energies of the fluid interface and solid interfaces [11]. Since V, r, and the γ's are fixed, it is sufficient, for comparative purposes, to compute the quantity (cf. eq. (1)

$$A^* = \frac{A}{2\gamma V^{\frac{1}{2}}} - \frac{\gamma_2}{\gamma}\frac{r}{V^{\frac{1}{2}}} = \frac{L}{2V^{\frac{1}{2}}} - \frac{x}{V^{\frac{1}{2}}}\cos\theta \quad (2)$$

where 2L is the total length of the fluid interface profile. For a given system A* increases linearly with A. In the following equations θ designates the angle between the interface and the plates measured at the line of contact. Clearly $\theta = \theta_c$ in θ_c-configurations (e.g. figs. 1b, d), and x = r in r-configurations (fig. 1a, c).

BRIDGES

The main equations are ($2x_n$ is the neck width, fig. 1b)

$$\frac{d}{V^{1/2}} = \frac{d}{x} \cdot \frac{x}{V^{1/2}} =$$

$$= \frac{d}{x} \left[2\frac{d}{x} + \left(\frac{d}{x}\right)^2 \left(tg\theta - \frac{\pi/2-\theta}{\cos^2\theta}\right) \right]^{-1/2} \quad (3)$$

$$A^* = \frac{d}{V^{1/2}} \left(\frac{\pi/2-\theta}{\cos^2\theta} - \frac{x}{d}\right)\cos\theta \quad (4)$$

$$\frac{x_n}{d} = \frac{x}{d} - \frac{1-\sin\theta}{\cos\theta} \quad (5)$$

DROP CONFIGURATIONS

θ_1, θ_2 are the angles of the attached drops with each plate and $2x_1$, $2x_2$ are their widths at the plates (fig. 1f); f_1, f_2, f_3 are the volume fractions of fluid 1 in the two attached drops and in the i-drop, respectively. In particular $f_3 = 1$ indicates an i-drop and $f_1 = f_2 = 1/2$ two equal attached drops. The total height $2h = h_1 + h_2 + h_3$, see fig. 1f. The main equations are:

$$\frac{x_1}{V^{1/2}} = \sqrt{2f_1}\,\lambda(\theta_1) \qquad \frac{x_2}{V^{1/2}} = \sqrt{2f_2}\,\lambda(\theta_2) \quad (6)$$

$$\frac{h}{V^{1/2}} = \frac{1}{\sqrt{2}} \left[\sqrt{f_1}\,\Psi(\theta_1) + \sqrt{f_2}\,\Psi(\theta_2) + 2\sqrt{f_3/\pi}\right] \quad (7)$$

$$A^* = \frac{1}{2\sqrt{2}} \left\{ \sqrt{f_1}\phi(\theta_1) + \sqrt{f_2}\phi(\theta_2) + 2\sqrt{\pi f_3} - \right.$$

$$-2\cos\theta_c[\sqrt{f_1}\,\lambda(\theta_1) + \sqrt{f_2}\lambda(\theta_2)] \quad (8)$$

with

$$\lambda(\theta) = \left(\frac{\theta}{\sin^2\theta} - ctg\theta\right)^{-1/2} \quad (9a)$$

$$\Psi(\theta) = \frac{1-\cos\theta}{\sin\theta}\lambda(\theta) \quad (9b)$$

$$\phi(\theta) = \frac{2\theta}{\sin\theta}\lambda(\theta) \quad (9c)$$

Fig. 2 shows plots of $x/V^{1/2}$ as function of $d/V^{1/2}$ in bridges, for various values of θ. Also shown (dotted lines) are curves of $x/V^{1/2}$ as a function of $h/V^{1/2}$ for one and two equal attached drops and the value of $h/V^{1/2}$ of an i-drop. Fig. 3 shows the limits of geometrical possibility of bridges and drops, as a function of θ. The limiting curves for bridges correspond to $x_n = 0$ when $\theta < \pi/2$ and to $x = 0$ when $\theta > \pi/2$. Bridges with a given θ are possible for values of $d/V^{1/2}$ smaller than the one given
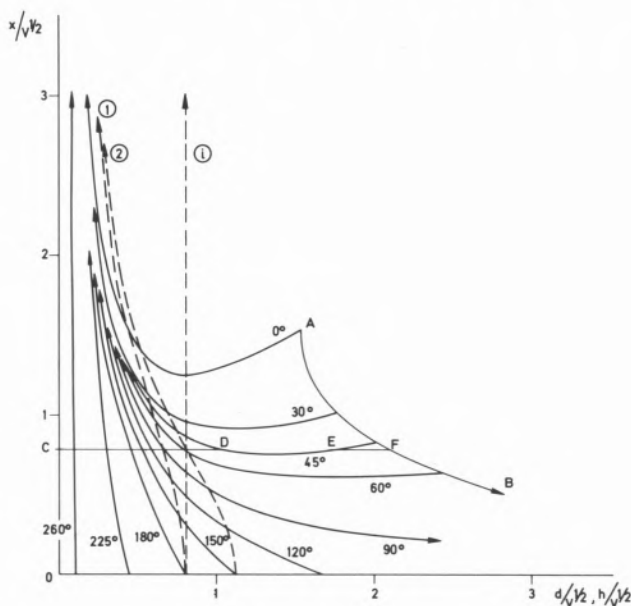

Fig. 2

Full lines give the bridge width, 2x, at the plates as a function of plate separation, 2d, for various values of θ. Dotted lines give the width of one (1) and two (2) attached drops and of one i-drop (i) as a function of the total height 2h of the drops. The line AFB marks the limit of possible bridge configurations. CDEF indicates the path of a bridge for $r/V^{1/2} = 0.78$ and and $\theta_c = 45°$. An arrow means that a curve continues

by the curves. The limiting curves for drops correspond to $h = d$. Each drop configuration (one or two equal drops or one i-drop) is possible for values of $d/V^{1/2}$ larger than those given by the curves of fig. 3. All the necessary information on the geometrical parameters of the various configurations can be obtained from figs. 2 and 3.
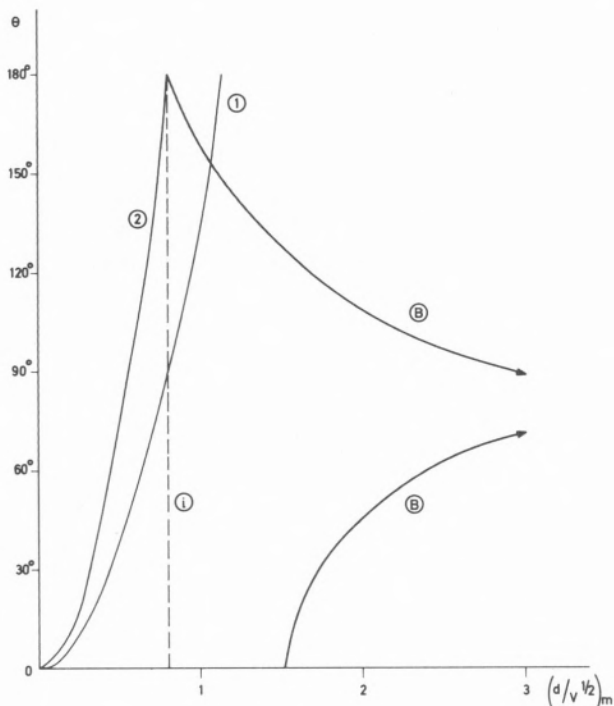
Fig. 3

Limiting values of $d/V^{1/2}$ as a function of θ for bridges (B), one attached drop (1) and two identical attached drops (2). Also marked is the limiting $d/V^{1/2}$ for one i-drop (i). Bridges and drops are possible for values of $d/V^{1/2}$ smaller and larger, respectively, than those in the limiting curves

The force of adhesion, F, due to a bridge can be determined from the rate of change of the Helmholtz energy with plate separation

$$F\acute{o}d = \delta A \tag{10}$$

As will be shown in more detail elsewhere [12] this gives for the force the following expression

$$\frac{F}{2\gamma} = \frac{x}{d}\cos\theta + \sin\theta \tag{11}$$

or

$$\frac{F}{\gamma} = \frac{V}{d^2}\cos\theta + \sin\theta + \frac{\pi/_2-\theta}{\cos\theta} \tag{12}$$

Equation (11) contains the usual two terms [13,14] due respectively to the pressure difference across the interface and to the fluid interfacial tension acting

as a force on the plates. Fig. 4 shows examples of the variation of F with plate separation in r- and θ_c--bridges.
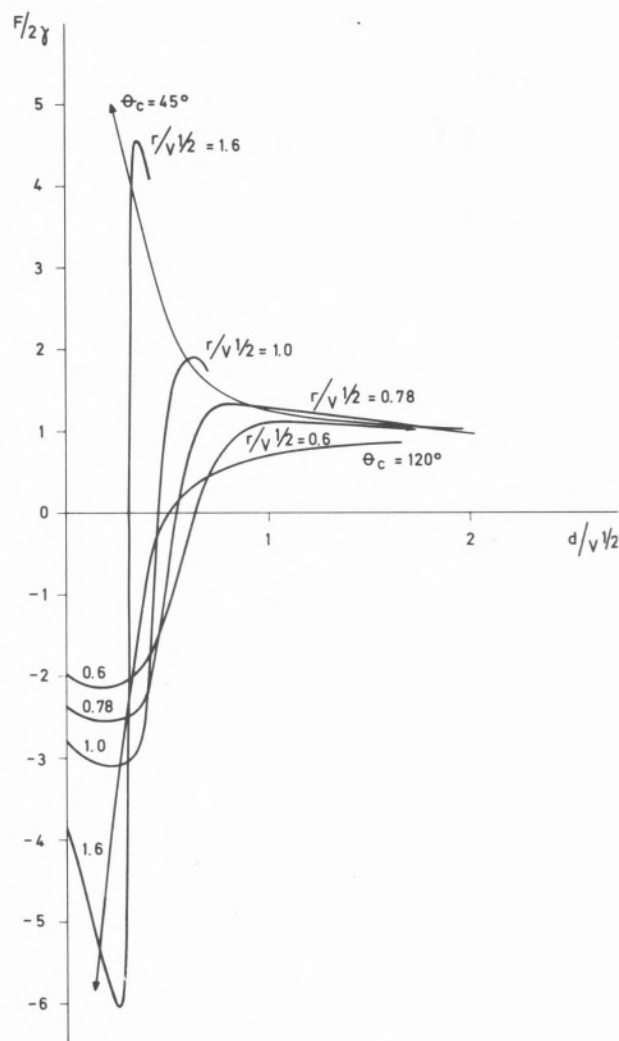
Fig. 4

The force of adhesion in θ_c-and r-bridges, as a function of plate separation, for various values of θ_c and $r/V^{1/2}$. The curves for $\theta_c = 45°$ and $r/V^{1/2} = 0.78$ intersect at two points. The curve for $r/V^{1/2} = 0.6$ is not shown complete

4 — STABILITY

Each type of configuration has a range of geometrical possibility which can be determined from the equations of the previous section. It is now necessary to find out whether each configuration is stable or unstable. As will be shown, some r-configura-

tions are unstable relative to θ_c-configurations. We discuss first the stability of bridge configurations. For given $r/V^{1/2}$ and θ_c there may be, as fig. 2 shows, intervals of $d/V^{1/2}$ where r- and θ_c-bridges are both possible. In these intervals it is x < r for θ_c-bridges and $\theta < \theta_c$ for r-bridges. For example, for $r/V^{1/2} = 0.78$ and $\theta_c = 45°$ both bridges are possible in the interval of $d/V^{1/2}$ between D and E in fig. 2. Outside this interval only the r- configuration is geometrically possible.

In the intervals of $d/V^{1/2}$ where the two bridge configurations are geometrically possible, calculation of A* shows that the θ_c-bridge always has a smaller Helmholtz energy than the r-bridge. This can also be seen in the examples of fig. 4. The force F is always larger for the r-bridge in the interval of coexistence: equation (10) then shows that its energy is larger. Consider now a r-bridge for a value of $d/V^{1/2}$ just above the smallest value for which the two configurations occur. If the r- bridge is slightly perturbed so as to produce a θ_c-bridge, the Helmholtz energy decreases. The r- bridge is therefore unstable.

If $d/V^{1/2}$ is increased from a value small enough for the bridge to be of the r-type, three possibilities can be distinguished: a) the bridge remains in the r- configuration until it breaks; b) the bridge changes to a θ_c- bridge at a critical separation and remains in this configuration until it breaks; c) the bridge changes to a θ_c-bridge and then again to the r- configuration. For example, for $\theta_c = 30°$ the three cases occur respectively for $r/V^{1/2} < 0.92$, for $r/V^{1/2}$ in the interval 0.92 -1.00 and for $r/V^{1/2} > 1.00$. For $\theta_c > 90°$ it is always case b) that occurs.

Similar conclusions can be drawn as regards the stability of attached drops. When both r- and θ_c- -drop configurations are possible, it is always the r-configuration that has larger A* and is therefore unstable. All other drop configurations are likely to be stable. In conclusion, all geometrically possible configurations (including those with any number of θ_c-bridges, θ_c-drops and i-drops) are stable, except the r-configurations when an alternative θ_c-configuration of the same type can occur.

We end this section with a brief discussion of the configurations that may be expected when $\zeta = (\gamma_2 - \gamma_1)/\gamma$ is not the interval [-1,1]. In such cases no θ_c-configurations are possible, but r-configurations can occur. For $\zeta > 1$, a geometrically possible

r-configuration will always be stable. In the case of r-bridges, as the value $\theta = 0$ is reached and d is further increased, it is expected that a special type of θ-bridge will take its place. This bridge ends within the plates with $\theta = 0$ but is prolonged to the edge of the plates by a thin layer of fluid. For this configuration there is no solid-fluid 2 interface. It is easily shown that in this case the force of adhesion has the same value as for a true θ_c-bridge with $\theta_c = 0$. For $\zeta < -1$, r-drops are likely to be unstable. Stable configurations that may occur in this case are r-drops and r-bridges with $\theta > 180°$. For separations larger than the one corresponding to $\theta = 180°$, a special type of θ_c-bridge, analogous to the one described above but without solid-fluid 1 interface, may be a stable configuration.

5 — TRANSITIONS BETWEEN EQUILIBRIUM CONFIGURATIONS

When the limit of existence of any of the stable configurations is reached and the plate separation is slightly changed to a value outside the range of stability, the system will irreversibly change to another equilibrium configuration. Note that the variable parameter is $d/V^{1/2}$ so that the discussion also applies to transitions due to volume variations. Kinetic energy is produced in the transition, and the problem is essentially a dynamical one. If the transition is at constant temperature (in addition to constant volume) and if a negligeable amount of mechanical work is put on the system to cause the transition, the final configuration must have a smaller A* thant the original one.

In fig. 5 are compared the Helmholtz energies, A*, of the following configurations: r- and θ_c-bridges, one and two equal attached drops and one i-drop. Only the stable bridge configurations are represented in fig. 5, but both r and θ_c-attached drops are considered, although r-drops are unstable relative to θ_c-drops. Other configurations have also been studied and their A* values calculated, but they are not indicated in fig. 5. The following conclusions can be drawn from these results.

i) Simply connected configurations of a given type (i.e., bridges, attached drops and i-drops) always have a smaller A* than multiply connected configurations of the same type.
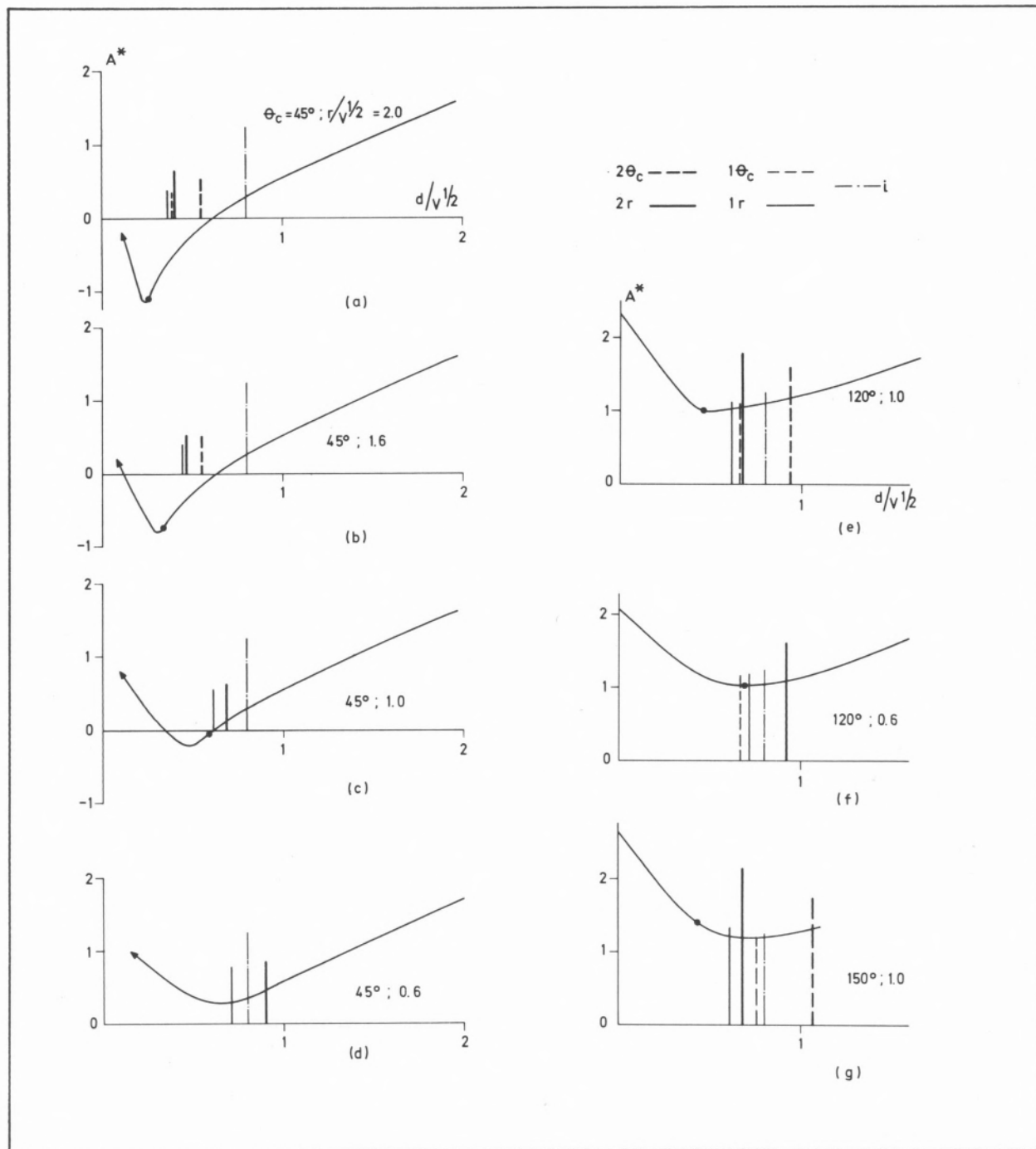
Fig. 5

Helmoltz energy, A*, as a function of plate separation, d/V^{1/2}, for various configurations and different values of contact angle, θ_c, and plate width, r/V^{1/2}. The curves give A* for bridges. The dot indicates the transition between r-and θ_c-bridge configurations. In (d) only the r-bridge occurs. The other configurations included are: one r-drop (——); two equal r-drops (—); one θ_c-drop (---); two equal θ_c-drops(— —); one i-drop (—.—.). Some of these configurations cannot occur in specific cases

ii) Considering only simply connected configurations (*i.e.,* one bridge, one attached drop, one i-drop) and values of d/V^{1/2} for which two or three of such configurations are possible, the A* for one attached drop is always smaller than that for an i-drop; the A* for the bridge may be larger or smaller than the A* for any of the two other configurations.

iii) The A* for two equal attached drops is larger than the A* for one i-drop when $\theta_c > 90°$ and *vice--versa*.

When the limiting $d/V^{1/2}$ for a stable configuration of the types considered in fig. 5 is slightly over-shoot, the new configuration cannot be predicted from the values of A* exclusively, since there are in general various alternative possibilities. However, some final configurations can be rulled out. For example, a θ_c-bridge with $\theta_c \lesssim 130°$ cannot give two attached drops (cf. fig. 4g).

The final configurations may even depend on the way $d/V^{1/2}$ is changed from its limiting value. If the two plates are moved in the same way, it is expected that a symmetric configuration will give rise to another symmetric configuration. However, if only one plate is displaced, for example, the final configuration may not be the same. A θ_c-bridge with $\theta_c > 90°$ illustrates this point. Depending on the way d is increased behyond the limiting value, either an i-drop or one attached drop may result.

Expected transitions for a symmetrical displacement of the plates are schematically shown in fig. 6. The following are the main conclusions.
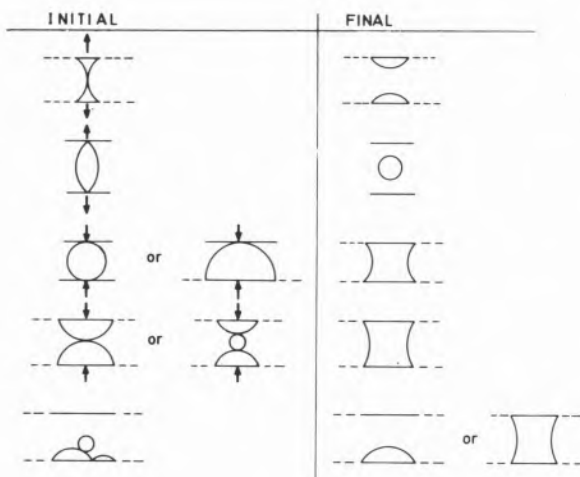

Fig. 6

Examples of irreversible transitions at the limit of stability of various initial configurations. The plates are moved in the same way, indicated by the arrows, to produce the transitions. The dotted lines indicate that either r- or θ_c-configurations may be considered

i) For bridges with $\theta_c < 90°$, two equal attached drops will result (either r- or θ_c-drops); if $\theta_c > 90°$, an i-drop will result.

ii) For one or two attached drops, or for an i-drop (or other conbinations such as in fig. 6), a bridge (r or θ_c) is expected to form.

Finally, when two volumes in a multiply connected configuration come in contact as a result of a displacement of the volumes, not necessarily associated with a displacement of the plates, they coalesce to produce a simply connected volume.

REFERENCES

[1] A. W. ADAMSON, «Physical Chemistry of Surfaces», 3rd ed., Wiley (Interscience), New York, 1976.

[2] M. A. FORTES, *Phys. Chem. Liquids,* **9**, 285 (1980).

[3] E. A. BOUCHER, M. J. B. EVANS, H. J. KENT, *Proc. Roy. Soc. London,* **A349**, 81 (1976).

[4] R. D. GILLETTE, D. C. DYSON, *Chem. Eng.* **2**, 44 (1971).

[5] J. F. PADDAY, A. R. PITT, R. M. PASHLEY, *J. Chem. Soc. Faraday I,* **10**, 1919 (1975).

[6] F. M. ORR, L. E. SCRIVEN, A. P. RIVAS, *J. Fluid Mech.* **67**, 723 (1975).

[7] E. PITTS, *J. Fluid Mech.* **63**, 487 (1974).

[8] E. A. BOUCHER, H. J. KENT, *J. Colloid Interface Sci.* **67**, 10 (1978).

[9] M. A. FORTES, ROSA M. MIRANDA, to be published.

[10] W. J. HUPPMANN, H. RIEGER, *Acta Met.* **23**, 965 (1975).

[11] R. E. JOHNSON, R. H. DETTRE, *Advanc. Chem. Ser.* **43**, 112 (1964).

[12] M. A. FORTES, IV Encontro Anual da S. P. Quimica, 1981; to be published.

[13] R. B. HEADY, J. W. CAHN, *Met. Trans.* **1**, 185 (1970).

[14] K. HOTTA, K. TAKEDA, K. IINOVA, *Powder Techn.* **10**, 231 (1974).

RESUMO

Configurações alternativas da interface entre dois fluidos em contacto com sólidos.

Faz-se um estudo comparativo das diversas configurações de equilíbrio (com simetria axial) que pode assumir a interface entre dois fluidos imiscíveis, colocados entre duas placas paralelas e idênticas. As configurações possíveis são: pontes líquidas, «gotas» cativas e «gotas» isoladas e combinações não-conexas destas. Com base em cálculos das propriedades geométricas e da energia de Helmholtz, discute-se a estabilidade de cada configuração e prevê-se as transições que ocorrem quando o limite de estabilidade de uma delas é ultrapassado.

THE TIME EVOLUTION OF ENERGY DONOR INTENSITIES WHEN THERE IS A TRANSIENT TERM

J. C. CONTE
J. M. G. MARTINHO

Centro de Quimica Fisica Molecular
Complexo I
Instituto Superior Técnico
1000 LISBOA

When excimer forming molecules Y are dissolved in an inert solvent at appropriate molar concentration c_Y in the presence of another fluorescent species Z, molar concentration c_Z and the system is excited with electromagnetic radiation of intensity I_O (einstein $l^{-1} s^{-1}$) the reactions that can take place are well known [1].

If the excitation takes the form of a δ-pulse the differential equations that describe the time evolution of the monomer and the excimer intensities of the donor Y are easily obtained. For the case where the rate constants for energy transfer from the excited monomer of Y and excimer (k_{ZY}^m and k_{ZY}^d respectively) are both able to transfer its energy to the acceptor Z and are assumed to present a transient term [2], they have the general form

$$k = \frac{4\pi DN}{1000} R_{eff} \left[1 + \frac{R_{eff}}{\sqrt{\pi Dt}} \right] \qquad (1)$$

that is

$$k_{ZY}^m = k_{ZY}^{mo} \left[1 + \frac{\sigma_m}{\sqrt{\pi Dt}} \right] = k_{ZY}^{mo} + At^{-1/2} \qquad (2)$$

$$k_{ZY}^d = k_{ZY}^{do} \left[1 + \frac{\sigma_d}{\sqrt{\pi Dt}} \right] = k_{ZY}^{do} + Bt^{-1/2} \qquad (3)$$

Then the general differential equations for the time evolution of monomer and excimer intensities when the solution is excited by a δ-pulse are

$$\frac{d}{dt}[M_Y^*] = k_{MDY}[D_Y^*] - k_{DMY}[M_Y^*]c_Y - k_{ZY}^{mo}[M_Y^*]c_Z -$$
$$- k_{MY}[M_Y^*] - At^{-1/2}[M_Y^*]c_Z \qquad (4)$$

$$\frac{d}{dt}[D_Y^*] = k_{DMY}[M_Y^*]c_Y - k_{MDY}[D_Y^*] - k_{ZY}^{do}[D_Y^*]c_Z -$$
$$- k_{DY}[D_Y^*] - Bt^{-1/2}[D_Y^*]c_Z \qquad (5)$$

The analysis of these equations is obviouly important since, as it is well known, accurate means of obtaining the time evolution of $[M_Y^*]$ and $[D_Y^*]$ are

available and also because they offer a means of studying the theories of the energy transfer, since they include the rate constants for this transfer in a form such as the different theories can be checked. Their complete integration, however, and to the present Author's knowledge, has not yet been achieved.

It is the purpose of this note to present the resolution of these equations in a particular case, as well as to the case where there is no acceptor in a novel way involving matricial calculus and to show how this can be extended to the general case. These considerations will be presented soon in future publications.

If we denote by x and y respectively, the concentrations of excited species $[M_Y^*]$ and $[D_Y^*]$ respectively we can write equations (4) and (5) above in the more appropriate form

$$\frac{d}{dt}x = A_x x + B_x y + C_x t^{-1/2} x \qquad (6)$$

$$\frac{d}{dt}y = A_y y + B_y x + C_y t^{-1/2} y \qquad (7)$$

where x and y are functions of t and A_x, B_x, C_x, A_y, B_y, C_y are independent of x, y and t.

Let us consider the simple case where there is no acceptor. Then we are reduced to the well known case of the monomer-excimer equilibrium

$$\frac{d}{dt}x = A_x x + B_x y \qquad (8)$$

$$\frac{d}{dt}y = A_y y + B_y x \qquad (9)$$

Although the solution of these equations is well known [3] it is introduced here to present it in a different way as an introduction to the general case. If we define a vector

$$\mathbf{X} = \begin{bmatrix} x \\ y \end{bmatrix} \qquad (10)$$

and the matrix

$$A = \begin{bmatrix} A_x & B_x \\ B_y & A_y \end{bmatrix} \qquad (11)$$

The equations (8) and (9) above can be written in a matrix form as

$$\frac{d}{dt}\mathbf{X} = A\mathbf{X} \qquad (12)$$

which can be easily integrated giving

$$\mathbf{X} = \text{EXP}(At)\ \mathbf{X}_O \qquad (13)$$

where $\text{EXP}(At)$ is the exponential function and $\mathbf{X}_O$ is the vector $\mathbf{X}$ for the initial conditions at $t = 0$

$$\mathbf{X}_O = \begin{bmatrix} x_O \\ y_O \end{bmatrix} \qquad (14)$$

Now it is known [4] that according to Sylvester's expansion theorem

$$\text{EXP}(At) = \sum_{i=1}^{n} \text{EXP}(\lambda_i t)\ F_i \qquad (15)$$

with

$$F_i = \sum_{\substack{j=1 \\ j \neq i}}^{n} \frac{A - \lambda_j I}{\lambda_i - \lambda_j} \qquad (16)$$

where I is the unit matrix and λ_i the eigenvalues of the matrix A.

According to the usual notation the eigenvalues of A are

$$\lambda \pm = \frac{(A_x + A_y) + \sqrt{(A_x - A_y)^2 + 4B_x B_y}}{2} \qquad (17)$$

and since they are intrinsically negative it is usual practice to define the quantities

$$\lambda_{1,2} = -\lambda \pm \qquad (18)$$

then by substitution we may write

$$\text{EXP}(At) = F_1 \text{EXP}(-\lambda_1 t) + F_2 \text{EXP}(-\lambda_2 t) \qquad (19)$$

with

$$F_1 = \frac{A + \lambda_2 I}{\lambda_2 - \lambda_1} \qquad (20)$$

$$F_2 = \frac{A + \lambda_1 I}{\lambda_2 - \lambda_1} \qquad (21)$$

Now if we write down the matrices A and I we get

$$F_1 = \frac{1}{\lambda_2 - \lambda_1} \begin{bmatrix} A_x + \lambda_2 & B_x \\ B_y & A_y + \lambda_2 \end{bmatrix} \qquad (22)$$

$$F_2 = \frac{1}{\lambda_2 - \lambda_1} \begin{bmatrix} A_x + \lambda_1 & B_x \\ B_y & A_y + \lambda_1 \end{bmatrix} \qquad (23)$$

Since there is no excimer present for $t = 0$, we way write, from (14)

$$\begin{bmatrix} x \\ y \end{bmatrix} = EXP(At) \begin{bmatrix} x_0 \\ 0 \end{bmatrix} \qquad (24)$$

and so, from (19) (22) (23) and (24)

$$x = x_0 \frac{A_x + \lambda_2}{\lambda_2 - \lambda_1} EXP(-\lambda_1 t) - x_0 \frac{A_x + \lambda_1}{\lambda_2 - \lambda_1} EXP(-\lambda_2 t) \qquad (25)$$

$$y = x_0 \frac{B_y}{\lambda_2 - \lambda_1} \left[EXP(-\lambda_1 t) - EXP(-\lambda_2 t) \right] \qquad (26)$$

which is the known result [3].

It is precisely the elegance of the method and its formal simplicity that has offered indication that it could be applied with success to some other more complicated cases in the domain of the study of energy transfer measurements.
Let us consider, in fact, equations (6) (7) again and let us make the substitution

$$\tau = t^{1/2} \qquad (27)$$

and then

$$\frac{d}{d\tau} x = 2A_x \tau x + 2B_x \tau y + 2C_x x \qquad (28)$$

$$\frac{d}{d\tau} y = 2A_y \tau y + 2B_y \tau x + 2C_y y \qquad (29)$$

In the matrix form we have have now

$$\frac{d}{d\tau} \mathbf{X} = (2A\tau + 2C) \mathbf{X} \qquad (30)$$

where $\mathbf{X}$ is the vector (10), A the matrix (11) and C a new matrix defined as

$$C = \begin{bmatrix} C_x & 0 \\ 0 & C_y \end{bmatrix} \qquad (31)$$

The first and very important factor to note is that the matrices A and C do not commute. In fact

$$AC - CA = (C_x - C_y) \begin{bmatrix} 0 & -B_x \\ B_y & 0 \end{bmatrix} \qquad (32)$$

It is precisely the fact that A and C do not commute that prevents us to integrate equation (30) as if it was a linear differential equation. However its simple form opens way to a simple treatment based in a series expansion and also as a infinit product which will be the subject of future publications.
From the foregoing considerations there is however one case where the complete integration is possible. It is obviously seen from (32) that A and C commute if

$$C_x = C_y = C_0 \qquad (33)$$

Then we may write, from (30)

$$\mathbf{X} = EXP(A\tau^2 + 2C\tau)\mathbf{X}_0 \qquad (34)$$

The reason why this is possible is that since A and C commute [5] we may write

$$EXP(A\tau^2 + 2C\tau) = EXP(A\tau^2) \cdot EXP(2C\tau) \qquad (35)$$

It will be left to future publications the full discussion of this case as well as the general cases. An example will be however given here to show how the solution (34) can be developed. For this it is necessary to use the expansion

$$EXP(P) = \sum_{k=0}^{\infty} \frac{P^k}{k!} \qquad (36)$$

Then if we use (36) we may write

$$\mathbf{X} = EXP(At + 2Ct^{1/2}) \, \mathbf{X}_o \qquad (37)$$

with

$$EXP(At + 2Ct^{1/2}) = \sum_{k=0}^{\infty} \frac{(At + 2Ct^{1/2})^k}{k!} \qquad (38)$$

an expression which is valid for any square matrix [4] although (37) is only valid if A and C commute. Now although the evaluation of (38) is straightforward it is rather cumbersome since it involves successive powers of the matrices A and C. We will present another way of dealing with the problem which can easily be tackled by the usual calculator processes.

We denote by $\lambda_{\pm}(t)$ the eigenvalues of the matrix $A(t) = At + 2Ct^{1/2}$ and define the quantities

$$\lambda_{1,2}(t) = -\lambda_{\pm}(t)$$

It must be stressed that although the quantities $\lambda_{\pm}(t)$ are similar to (18) they are not the same. They include the factor t as well as C_x and C_y in the present case.

If S and S^{-1} are the matrices that can lead $A(t)$ to the diagonal form

$$A'(t) = S^{-1} A(t) S = \begin{bmatrix} -\lambda_1(t) & 0 \\ 0 & -\lambda_2(t) \end{bmatrix} \qquad (39)$$

i.e.

$$A(t) = S \begin{bmatrix} -\lambda_1(t) & 0 \\ 0 & -\lambda_2(t) \end{bmatrix} S^{-1} \qquad (40)$$

Now from

$$EXP(At) = \sum_{k=0}^{\infty} \frac{[A(t)]^k}{k!}$$

$$= \sum_{k=0}^{\infty} \frac{1}{k!} \left\{ S \begin{bmatrix} -\lambda_1(t) & 0 \\ 0 & -\lambda_2(t) \end{bmatrix} S^{-1} \right\}^k$$

$$= \sum_{k=0}^{\infty} \frac{1}{k!} S \begin{bmatrix} -\lambda_1(t) & 0 \\ 0 & -\lambda_2(t) \end{bmatrix}^k S^{-1}$$

$$= S \begin{bmatrix} \sum_{k=0}^{\infty} \frac{[-\lambda_1(t)]^k}{k!} & 0 \\ 0 & \sum_{k=0}^{\infty} \frac{[-\lambda_2(t)]^k}{k!} \end{bmatrix} S^{-1}$$

$$= S \begin{bmatrix} EXP(-\lambda_1(t)) & 0 \\ 0 & EXP(-\lambda_2(t)) \end{bmatrix} S^{-1} \qquad (41)$$

It goes beyond the scope of the present note to develop more fully these considerations. It may be added at this stage however that the matrices S (and S^{-1}) are easily obtained from the eigenvalues of $A(t)$. If we consider the eigenvalue equation

$$A\mathbf{U}_{\pm} = \lambda_{\pm} \mathbf{U}_{\pm} \qquad (42)$$

in the form

$$\begin{bmatrix} a_{11} & a_{12} \\ a_{21} & a_{22} \end{bmatrix} \begin{bmatrix} 1 \\ \alpha_{\pm} \end{bmatrix} = \lambda_{\pm} \begin{bmatrix} 1 \\ \alpha_{\pm} \end{bmatrix} \qquad (43)$$

it will be found that

$$S = \begin{bmatrix} 1 & 1 \\ \alpha_{+} & \alpha_{-} \end{bmatrix} \qquad (44)$$

$$S^{-1} = \frac{1}{\alpha_{-} - \alpha_{+}} \begin{bmatrix} \alpha_{-} & -1 \\ -\alpha_{+} & +1 \end{bmatrix} \qquad (45)$$

Important relationships as

$$a_{11}-\lambda_{\pm} = -a_{12}\alpha_{\pm} \qquad (46)$$

$$a_{21}-\alpha_{\pm}\lambda_{\pm} = -a_{22}\lambda_{\pm} \qquad (47)$$

are easily derived which can be used to obtain S and S^{-1} from the (also easily obtained) eigenvalues of the matrix $A(t)$.

Then

$$\alpha_{\pm} = \frac{\lambda_{\pm}-a_{11}}{a_{12}} \qquad (48)$$

By substituion into (44) and (45) and then into (40) the expression for $EXP(At)$ is obtained. Then

$$\mathbf{X} = \begin{bmatrix} x \\ y \end{bmatrix} = EXP(At) \begin{bmatrix} x_o \\ 0 \end{bmatrix} \qquad (49)$$

Finally we get the solution

$$x = x_o[F_1 EXP(-\lambda_1 t)-F_2 EXP(-\lambda_2 t)] EXP(2C_o t^{1/2}) \quad (50)$$

$$y = x_o F_3[EXP(-\lambda_1 t)-EXP(-\lambda_2 t)] EXP(2C_o t^{1/2}) \qquad (51)$$

which obviously reduces to (25) and (26) when $c_z = 0$ and is the solution of (28) and (29) under conditions (33).

Numerical applications will be left to future publications.

REFERENCES

[1] J. C. CONTE, *Rev. Port. Quím.*, **11**, 169(1969).

[2] W. R. WARE, T. L. NEMZEK, *Chem. Phys. Letters,* **23**, 557 (1973)

[3] J. B. BIRKS, «Photophysics of Aromatic Molecules», Wiley — Interscience (1970), page 304.

[4] B. P. LATHI — «Signals, Systems and Controls», Intext Educational Publ., N. Y. (1974), page 501.

[5] T. APOSTOL, «Calculus», vol. I, Blaisdell Publ. Co., London, 1967.

ABSTRACT

The equations which give the time variation of the fluorescence emission intensities of an excimeric energy donor are analysed in the case where a transient term for the energy transfer rate constants has to be considered. A matricial method is proposed to solve the differential equations. A particular case is studied where a rigorous solution is achieved.

RESUMO

Evolução no tempo das intensidades de um doador de energia quando há um termo transiente

Analisam-se as equações que traduzem a variação no tempo da intensidade de emissão de fluorescência de um doador excimérico de energia no caso de haver necessidade de considerar que as constantes de transferência contêm termos transientes. Propõe-se um método Matricial para a resolução das respectivas equações diferenciais. No caso considerado o método conduz a uma solução rigorosa.